Shapes and shape transformations of vesicles induced by their adhesion to rigid surfaces

Ph.D. thesis

Jeel Raval

(2022, Warsaw)

Thesis submitted for the degree

of

Doctor of Philosophy

in the field

Chemical Sciences

titled

"Shapes and shape transformations of vesicles induced by their adhesion to rigid surfaces"

submitted by

Jeel Linesh Raval

Under the Supervision of

Prof. dr. hab. Wojciech Góźdź, IPC PAS, Warsaw, Poland

and

Prof. ddr. Aleš Iglič, UL, Ljubljana, Slovenia

The thesis was prepared within the International Ph.D. Studies

of the

Institute of Physical Chemistry of the Polish Academy of Sciences, ul. Kasprzaka 44/52, 01-224 Warszawa

(March 2022)

Acknowledgements

My interest in Physics grew from my school days, and it cemented when I finally decided to pursue it during my bachelor years and further on. I knew that Ph.D. was a part of the process to develop as a researcher but never really knew I would be there. Fast-forward, and here I am, writing a thesis about my research project. This journey of a couple of years, however, had a tumultuous start: from moving into a new country away from family, to working on a project on which my knowledge was scarce. But, the positive environment created by my supervisor, Prof.Góźdź and which was reflected in my very first meeting with him, has gone a long way. This journey had it's highs and lows all along. But, I am glad to have reached this point where I am able to write down my sincere thanks to the people who have supported me on this journey which has culminated into this thesis. I would like to extend my sincere gratitude to the following people:

And starting from my research supervisors,

Prof. Wojciech Góźdź, I have always found support from you, right from accepting me into this Ph.D. program to your continued guidance and advice through my research. You have always been open to discussions and ideas, and I have learnt a lot about the "how's" of research from your insightful questions and through our discussions. These discussions have been a guiding light all along and have groomed me into a better version of myself as a researcher. Thank you so much. I will always be thankful to you for your time and patience in guiding me whenever I needed help and just as you always say, "have fun with what you are doing", I would like to say that it has always been fun to discuss physics with you.

Prof. Aleš Iglič, although my time at the University of Ljubljana was pretty short and mired by Covid, it was still a delightful learning experience through our initial group discussions in the lab, which then continued on virtually due to the pandemic. Thank you for your continued guidance. Right from helping me settle down in Ljubljana to integrating me in your lab which let me experience the wonderful environment of the group. This has contributed to many exciting scientific discussions and fun excursions. A special thank-you to Prof. Veronika Kralj-Iglič for our lab discussions and kindly hosting candid meet-ups with the group during the pandemic, which made my stay in Ljubljana more memorable.

I would also like to sincerely thank Prof. Kołos for his invaluable advice on my presentation skills and for his minute and detailed corrections to my presentations

which have helped me immensely.

I would also like to thank my colleagues from my group in Warsaw – Svyatoslav (Slavko), Horacio, Carolina, Gabriel, and colleagues from my group in Ljubljana – Luka in particular from whom I have learnt a lot, Marko for greatly helping me through my stay there, Mitja, Darja, Zala and Niharika. It was lively to be a part of our group.

I would like to extend my thanks to our administration department and in particular Aleksandra Kapuścińska-Bernatek, Patrycja Nitoń, Agnieszka Tadrzak, Joanna Wiszniowska, Edyta Słojewska and Eliasz Fijołek for always helping with any query and problems that arose.

To my dear friend and my only personal support here in Warsaw, Ashmita. This time has been much more enjoyable with you. Thank you for being through the thick and thin with me, for listening to all my problems – and just evaporating them through your positivity. The best partner in crime and the fun explorer. Our trips will always be a beautiful memory to cherish for years to come.

And now to the people who are my strength and solace – my lovely family. You are the reason I am here. I am seeing the world, standing on your shoulders. Thank you for always supporting me with everything that I wanted to achieve. You have shown me to dream freely and have given me free reins to achieve them. My dreams were not just mine, the moment I said them, they became ours. It has always been this collective effort that has reached me here. Your love is my biggest strength, and I am so thankful for being a part of your lives.

Funding

This research is part of a project that has received funding from the European Union's Horizon 2020 research and innovation programme under the Marie Skłodowska-Curie grant No. 711859.

,

Scientific work funded from the financial resources for science in the years 2017-2022 awarded by the Polish Ministry of Science and Higher Education for the implementation of an international co-financed project.

Declaration of originality

I hereby declare that the research included within this thesis was carried out by myself or with support by others included in the acknowledgements.

I state that I have exercised care to ensure that the work is original and contains no previously published material or written by another person, except where citations have been made in the text. To the best of my knowledge, the content provided here does not violate any copyrights.

I accept that the Polish Academy of Sciences has the right to use plagiarism detection software to ensure the thesis's legitimacy.

I certify that no part of my thesis has been or will be submitted for obtaining a degree or diploma by the Institute of Physical Chemistry, Polish Academy of Sciences, or any other educational institution.

This thesis's copyright rests with the author, and no information derived from it may be published without the author's consent.

Warsaw, March 2022.

.....

(signature)

Dedicated to my loving parents and grand-parents who have always been my greatest support and strength throughout.

Abstract

Adhesion of cells and extracellular vesicles (EVs) is ubiquitous in nature and plays an important biological role in the functioning and sustenance of cells and the multicellular organism as a whole. Shape transformations of cells, for example, as observed during the fission and fusion processes, or during the morphological changes in the red blood cell (RBC) structure while passing through the capillaries, or during the interaction of cell with it's environment, etc., are crucial to their functions. Thus, the biological importance of adhesion and shape transformation makes it imperative to probe for adhesion-induced shape changes of cells. Cell membranes are complex and diverse structures with complex mechanisms of shape regulation, but a relatively simple elastic theory has been found to be successful in describing red blood cell shape and their transformations. In the thesis, we use a theoretical approach to study shape transformations using a simple vesicle model system that can effectively describe the necessary characteristics of a cell membrane.

In the thesis, we primarily study the shape transformations of lipid vesicles with spherical topology induced by their adhesion to a flat surface. The aim is to investigate the shapes of vesicles stabilized by adhesion and study the shape transformations between different classes of vesicles. Apart from the study of vesicle where the vesicle membrane is composed of a single kind of membrane component (single component vesicle), we also investigate the adhesion of vesicle systems where the vesicle membrane is composed of two kinds of membrane components (multi-component vesicle), and the membrane components are characterized by their intrinsic spontaneous curvatures. Experiments have suggested that the lateral distribution of membrane components can influence the shape of the vesicle, and conversely, the shape of the membrane can induce lateral segregation, with the components migrating to the membrane regions which are more favourable to their intrinsic curvature. The main aim here is to further our understanding of this hypothesis – which assumes a coupling between the shape and the lateral distribution of components under the context of adhesion. We study the vesicle system within the spontaneous curvature model and numerically minimize the energy functional to obtain the equilibrium shapes and the distribution of the components simultaneously. We have performed a detailed study of the shape transformations between vesicles adhered to a flat surface. It was shown that the most stable configuration of an adhered vesicle with the membrane composed of a single kind of component and characterized by a relatively small spontaneous curvature was oblate with the increase in adhesion. This situation can be more complex

with the multi-component vesicle membrane, where there is an extra degree of freedom in the form of a non-homogeneous lateral distribution of components over the vesicle surface. From the calculations, it followed that budding can be induced by adhesion, and even a slight change in adhesion strength was found to be enough to promote or suppress it. It has been shown that an increase in spontaneous curvature of the vesicle membrane could encourage an easy adhesion of vesicles and that this effect was different in concave oblate vesicles (vesicles that curve inwards on their surface) than in the convex oblate vesicles (vesicles that curve outwards on their surface). The relationship between the shape and the corresponding lateral distribution of membrane components of the adhered vesicles has been investigated, and it has been shown that a budded vesicle like a pear-shaped vesicle can support the mixing of components, and a non-budded vesicle shape like oblate can support lateral segregation of membrane components. Our calculations have suggested that an increase in adhesion can promote both mixing and segregation of components, and this depends strongly on the shape of the vesicle under adhesion. Similar behaviour was observed when the vesicles were elongated by growing inner microtubule or when the vesicle volume was changed by the change of trans-membrane osmotic pressure [1].

Abstrakt

Adhezja komórek biologicznych i pęcherzyków lipidowych jest powszechnym zjawiskiem w przyrodzie i odgrywa ważną rolę w funkcjonowaniu komórek biologicznych i wielokomórkowych organizmów. Zmiany kształtu komórek biologicznych obserwowane podczas ich łączenia się lub rozszczepienia, czy zmiany morfologiczne w krwinkach czerwonych podczas ich przepływu przez naczynia krwionośne, czy podczas oddziaływania komórki z jej otoczeniem są kluczowe dla ich normalnego funkcjonowania. Ze względu na dużą wagę zmian morfologicznych podczas adhezji niezmiernie ważne jest dogłębne poznanie i zrozumienie tego zjawiska. Membrany biologiczne są złożonymi i różnorodnymi strukturami ze złożonymi mechanizmami stosowanymi do regulowani ich kształtu. Pomimo to można opisać kształty transformacje tak złożonych obiektów biologicznych jak czerwone krwinki przez stosunkowo prostą teorię opartą na elastyczności membran lipidowych. W pracy zbadano metodami teoretycznymi właściwości pęcherzyków lipidowych oraz ich transformacje stosując matematyczny model pęcherzyków lipidowych. Zbadano przede wszystkim przekształcenia pęcherzyków lipidowych o sferycznej topologii indukowane przez ich przyleganie do płaskiej powierzchni. Celem było zbadanie kształtów pęcherzyków ustabilizowanych przez adhezję a także zbadanie możliwych transformacji pomiędzy różnymi klasami pęcherzyków przylegających do płaskich podłoży. Badane były zarówno pęcherzyki jednoskładnikowe jak i wieloskładnikowe, gdzie składniki membrany były scharakteryzowane przez ich spontaniczne krzywizny. Zgodnie za badaniami eksperymentalnymi można założyć, że rozkład składników w membranach lipidowych wpływa na kształt membrany oraz kształt membrany może indukować segregację składników w taki sposób, że składniki migrują do obszarów membrany o podobnej krzywiźnie do spontanicznej krzywizny danego składnika. Głównym celem było zbadanie tej hipotezy w kontekście adhezji przy założeniu powiązania kształtu pęcherzyków i rozkładu składników w membranie tworzącej ściany pęcherzyka. Obliczenia zostały przeprowadzone w ramach rozszerzonego modelu funkcjonału Helfricha ze spontaniczną krzywizną. Funkcjonał był minimalizowany numerycznie, a wynikiem minimalizacji były funkcje opisujące kształt pęcherzyka i rozkład składników w membranie tworzącej ściany pęcherzyka. Przeprowadzono szczegółową analizę transformacji kształtów pęcherzyków przylegających do płaskich podłoży. Pokazano, że najbardziej stabilne konfiguracje przylegających jednoskładnikowych pęcherzyków o relatywnie małej spontanicznej krzywiźnie miały spłaszczony kształt. Stabilizacji sprzyjał wzrost potencjału przyciągającego podłoża. W przypadku pęcherzyków

wieloskładnikowych zmiany kształtu pęcherzyków spowodowane przyleganiem do podłoża mogą powodować niejednorodny rozkład składników w membranie tworzącej ściany pęcherzyka. Przeprowadzone obliczenia wskazywały na możliwość występowania wielu ciekawych zjawisk fizycznych w układach, w których pęcherzyki lipidowe przylegały do płaskich podłoży. W szczególności pokazano, że zmieniając nieznacznie właściwości podłoża można doprowadzić do pączkowania pęcherzyka. Pokazano, że niewielka zmiana spontanicznej krzywizny pęcherzyka ułatwia jego przyleganie do podłoża. Efekt ten inaczej przebiega dla pęcherzyków wklęsłych a inaczej dla wypukłych. Zbadano zależność pomiędzy kształtem pęcherzyków przylegających do podłoża i rozkładem składników. Pokazano, że w zmieniając właściwości podłoża możliwe jest indukowanie zarówno mieszania się jak i rozmieszania się składników w pęcherzykach. Kształt pęcherzyka decydował o tym czy składniki ulegały mieszaniu czy rozmieszaniu. Podobne zachowanie było zaobserwowane w pęcherzykach zmieniających kształt pod wpływem rosnących wewnątrz mikrotubuli lub zmian objętości spowodowanych przez zmianę ciśnienia osmotycznego [1].

Contents

List of Figures

Chapter 1

Introduction

This chapter presents a brief introduction to the membrane structure and it's properties. It introduces the reader to the theory of adhesion and the importance of adhesion and shape transformations in biological cells. The mechanism of segregation which allows for the lateral redistribution of components in the multi-component membranes has also been explained.

1.1 Phospholipid membranes

Membranes play a crucial role in the biology of cells. They divide the cell space into sub-spaces or compartments of different compositions, and the outer layer to these compartments and organelles is made of the bilayer membrane [2]. Membranes can accommodate different proteins and therefore play an important role in the biochemical reactions of the cells. Although the biological membranes are extremely soft structures but they are resistant against disruption, and it is this stability that gives a protective outer shell to the cells [3].

Phospholipids are the fundamental building blocks of a cell membrane. They are amphiphilic molecules that consist of two hydrophobic fatty acid chains and a phosphate-containing hydrophilic head group [4]. Our model system membrane is a bilayer structure comprising of two monolayers where each monolayer is made out of such amphiphilic molecules. When amphiphilic molecules are dispersed in a polar solvent like water, they self-assemble spontaneously to form aggregates like vesicles called liposomes which are closed structures with the hydrophilic heads in contact with water and the hydrophobic tails embedded in the bilayer membrane of the vesicle, or they could also aggregate to form bilayer structures which involve a large edge free energy, etc. Due to the hydrophobic nature of the tail, whenever a hydrophobic molecule comes in contact with water, it disrupts the H-bonding between the surrounding water molecules. To compensate for the loss in H-bonds on disruption, the surrounding water molecules now form ice-like cage structures which act as cavities to accommodate the hydrophobic molecule. This rearrangement of water molecules around the hydrophobe, however, causes the entropy of the surrounding water molecules to re-

duce [5], and to counter this effect, the lipid molecules aggregate to lower the free energy of the system [6]. The critical length of the tail, the representative surface area occupied by the amphiphile, and the volume occupied by the hydrophobic part of the amphiphile determine the structure of the aggregate that it can form [7–9].

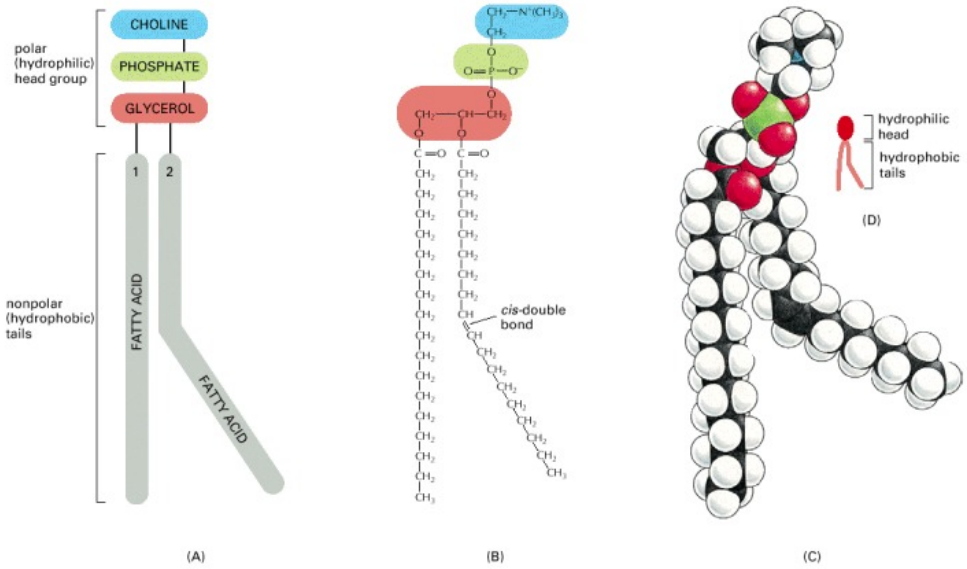

Figure 1.1: Schematic of a phospholipid molecule is shown with it's hydrophobic and hydrophilic parts. It acts as a fundamental building block of the bilayer membrane. Image credit: The original image is taken from the ref. [10].

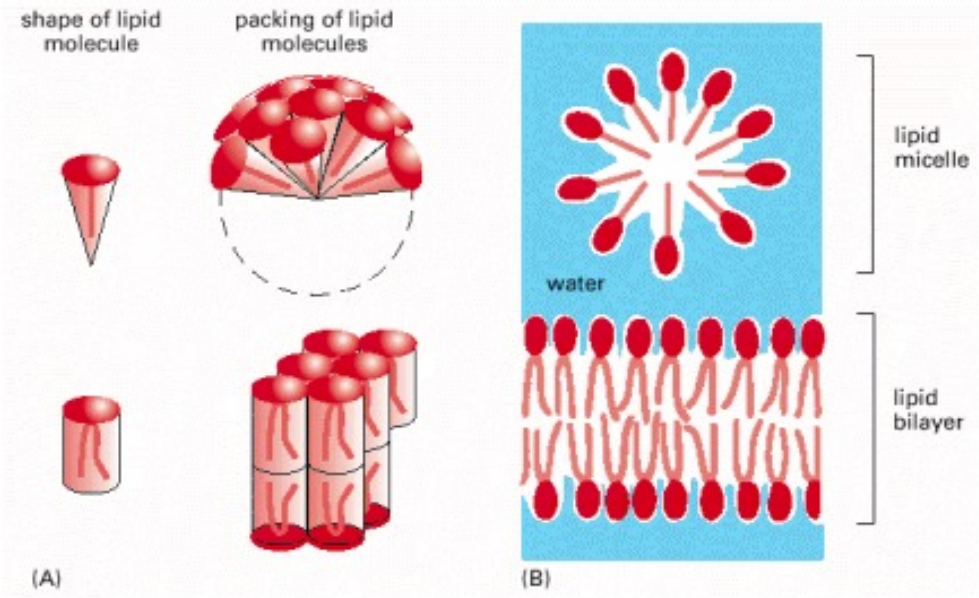

Figure 1.2: The self assembly of lipid molecules to form either a lipid micelle or a lipid bilayer depending on their shape is shown. Cylinder shaped lipids form a bilayer while the wedge shaped lipids form micelles. Image credit: The original image is taken from the ref. [10].

Biologically, shape transformations of the membrane play an important role – for e.g., in the formation of small buds on the plasma membrane of the cell during

the process of exo- or endocytosis (see Fig. 1.3 which shows the budding transition observed in giant phospholipid vesicle systems on the increase in temperature), or during the formation of thin nanotubes [11] which connect the parent cell to the daughter cell and are useful for transporting material through it, like for e.g., in the red blood cells. These shape transformations are also useful in the locomotion of the cell [2], while the shape of drug carriers can play an important role in their adhesion to the target site and thereby in the drug delivery process. Shape transformations can also help characterize diseases like Sickle cell anaemia, Alzheimers, etc. See refs. [12–14] for further reading on the importance of shapes and shape transformations of cells in nature.

The biological membranes comprise of many different kinds of lipids, other amphiphiles, and membrane proteins which are embedded in the bilayer and contribute towards the functional properties of the bio-membrane [16]. The lipid compositions in the two monolayers are generally very different from each other, and this kind of lipid asymmetry is also functionally important [10]. Oftentimes there is a polymeric network anchored to the membrane, which further ensures structural stability to the biological membranes. The artificial vesicle (devoid of polymeric network), in comparison, is however a model system which can provide us useful insight into the mechanisms that govern such complex bio-membranes [16].

The thickness of the membranes is about a few nanometers, but the size of the vesicle can go up to 100 micrometers [16]. Thus membranes can be regarded as 2D structures embedded in three-dimensional (3D) space when studied in length scales much bigger than the bilayer thickness. Membranes are extremely soft structures, and this is revealed by the thermally excited shape fluctuations which can be visible under a microscope [16]. Such shape transitions can therefore be physically observed by changing the temperature, or osmotic conditions [16]. The fluidity of bio-membranes is an important characteristic and it is the reason behind the large variety of shapes found [17]. Lipid molecules can laterally diffuse freely within the plane of the membrane, can undergo flip-flops (rarely) between the two monolayers, and can undergo rotation about it's axis which can all contribute to the fluidity of the membrane. Membranes can therefore change their local composition due to lateral redistribution of different kinds of lipid molecules, and intra-membrane domains can be formed [17]. The configurations of the membrane are however different from interfaces as they are not dictated by surface tension which is why there is a large variety of non-spherical shapes [16]. Theoretically, the shape deformations are found to depend on fluid-elastic parameters called the spontaneous curvature that describes the preferred curvature of the membrane and the bending rigidity of the membrane that describes the resistance

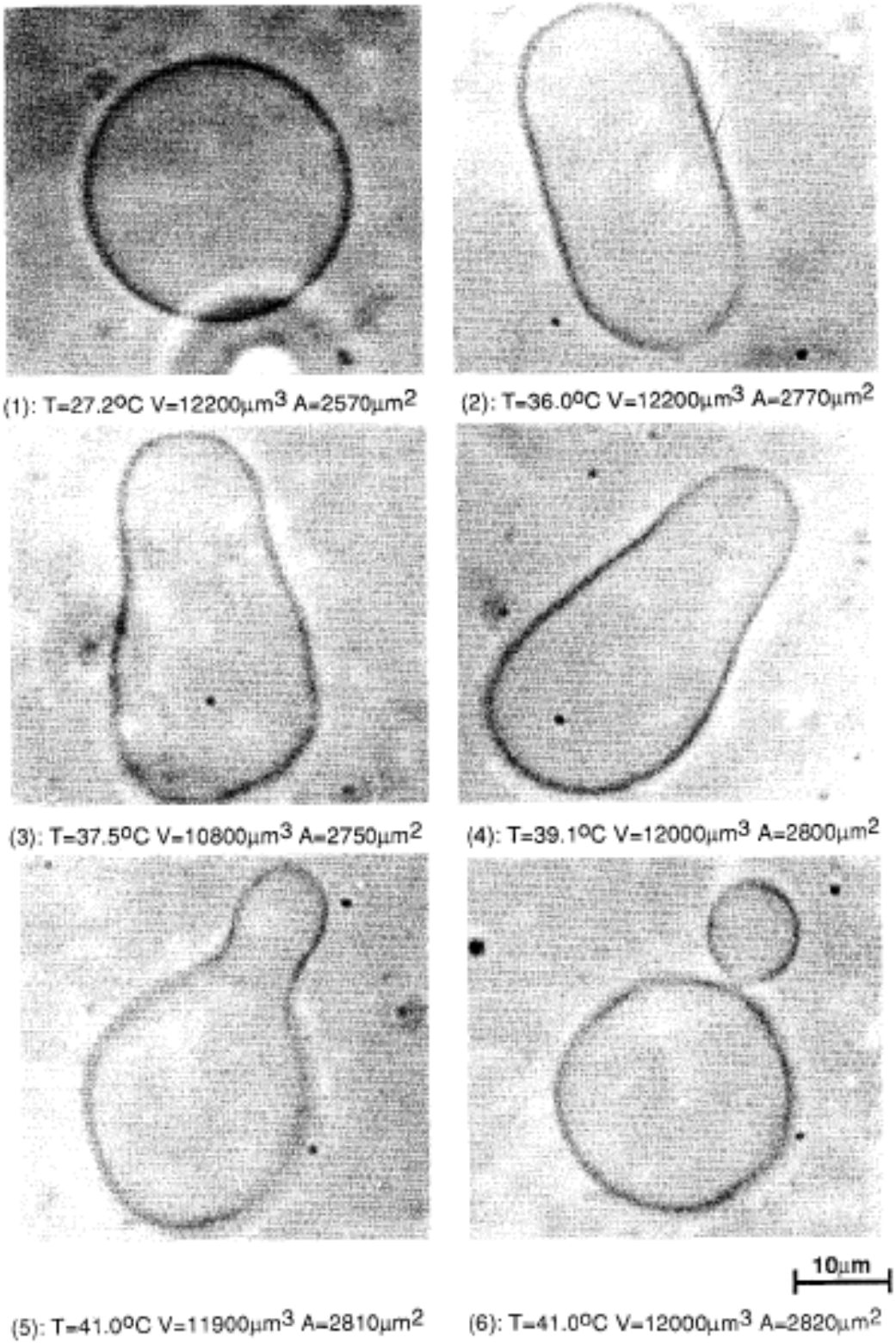

Figure 1.3: Budding transition is shown on increasing the temperature from 27.2, 36.0, 37.5, 39.1, 41.0 to 41.0 °C from left to right and top to bottom. Image credit: Originally taken from Käs and Sackmann 1991 [15, 16].

of the membrane in bending away from it's preferred curvature [17] (for our choice of model as explained in chapter 2).

From the chemistry and thermodynamics point of view, the bilayer membranes can exist in various phases and undergo phase transitions between these phases depending upon the composition of the membrane and the temperature. The temperature about which this transition occurs depends on the length and state of saturation of the hydrocarbon chains [10]. The biological membranes are mostly found in the liquid crystalline or the fluid phase (L_α phase), also called as a liquid-disordered phase which is found at a higher temperature, whereas, at a lower temperature, the bilayer undergoes a main transition to a 2D gel phase (L_β phase) [16]. Phospholipids in the presence of a high concentration of cholesterol can also form a liquid-ordered phase (L_o) where the hydrocarbon chains are more ordered, although the membrane still maintains it's fluidity [18–20]. In the gel phase, cholesterol is found to disrupt the ordering of the hydrocarbon chains [20]. The (L_o) represents kind of a mixed-phase between the L_α phase and the L_β phase [20]. The transition between the phases is shown in Fig. 1.4. A bilayer membrane with a mixture of two types of lipid components can be found in a coexistence phase that comprises a fluid and a gel phase. However, a bilayer can also be in a phase that comprises of two coexisting fluid phases like a coexistence of liquid-ordered and liquid-disordered phases. Such coexisting fluid phases are found in a system, for example, that contains a mixture of phospholipids and cholesterol [21, 22]. From the many different types of lipids that constitute the biological membranes, the sphingolipids tend to have longer and saturated hydrocarbon chains, and because of this, the attractive forces between the adjacent molecules can be strong enough that they can be held tightly together to form small microdomains or lipid rafts [10]. Lipid rafts are therefore thought to be the phase-separated regions within the fluid bilayer where due to the concentration of the molecules of longer and saturated chains, the thickness of rafts is larger than the rest of the bilayer [10].

The constraints that we have considered in our model section are a reflection of the physical properties of the studied system (vesicle). Due to the hydrophobic tails of the lipid bilayer, the lipid molecules do not practically dissolve in a polar solvent like water, and, therefore the number of lipid molecules within the bilayer remain constant. This ensures that the surface area of the vesicle remains constant and can adjust to its optimal value at a constant temperature. Also, the volume enclosed by the vesicle can be assumed to be a constant. This is because the bending energy is only capable of balancing small osmotic pressure differences generated due to the presence of impermeable molecules like large ions and sugar molecules that are

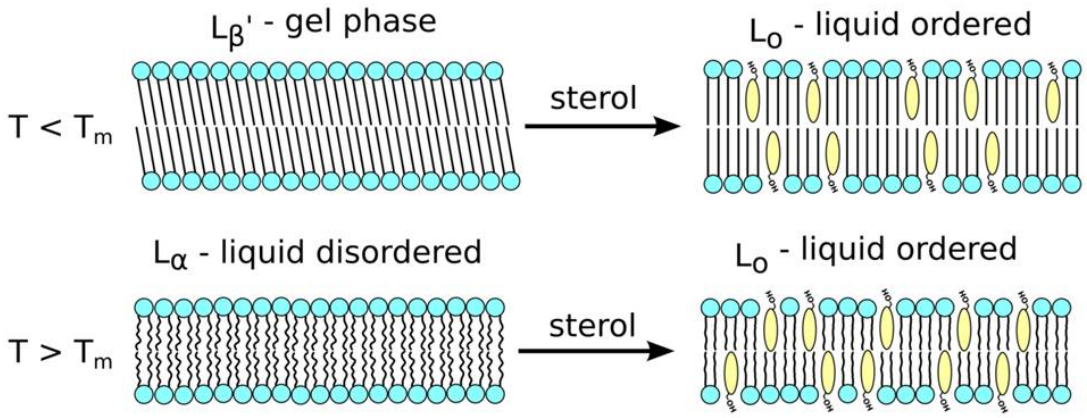

Figure 1.4: The different phases of a biological membrane and the transition between them as a function of temperature is shown. The effect of the presence of sterol molecules on the phases is also shown. Image credit: Originally taken from the University of California Davis: Biophysics 241 - Membrane Biology notes [23].

inevitably present in the aqueous solution at low concentrations due to impurities. Thus, as a good approximation, the volume can be considered to be constrained at the value for which the osmotic pressure becomes zero [16]. Both these constraints of constant surface area and volume are considered in chapter 2 later.

Fig. 1.5 shows the shapes obtained experimentally using giant phospholipid vesicles which are reminiscent of some interesting shape transition sequences. For e.g., the shapes from 1 to 4 describe the shape transition of a red blood cell [24, 25] from the disc shape on the far right of the row to the cup shape on the far left. Shapes 8 and 12-15 show the budded structures which have a narrow neck connecting two spheres and are similar to the structures observed during endocytosis and exocytosis.

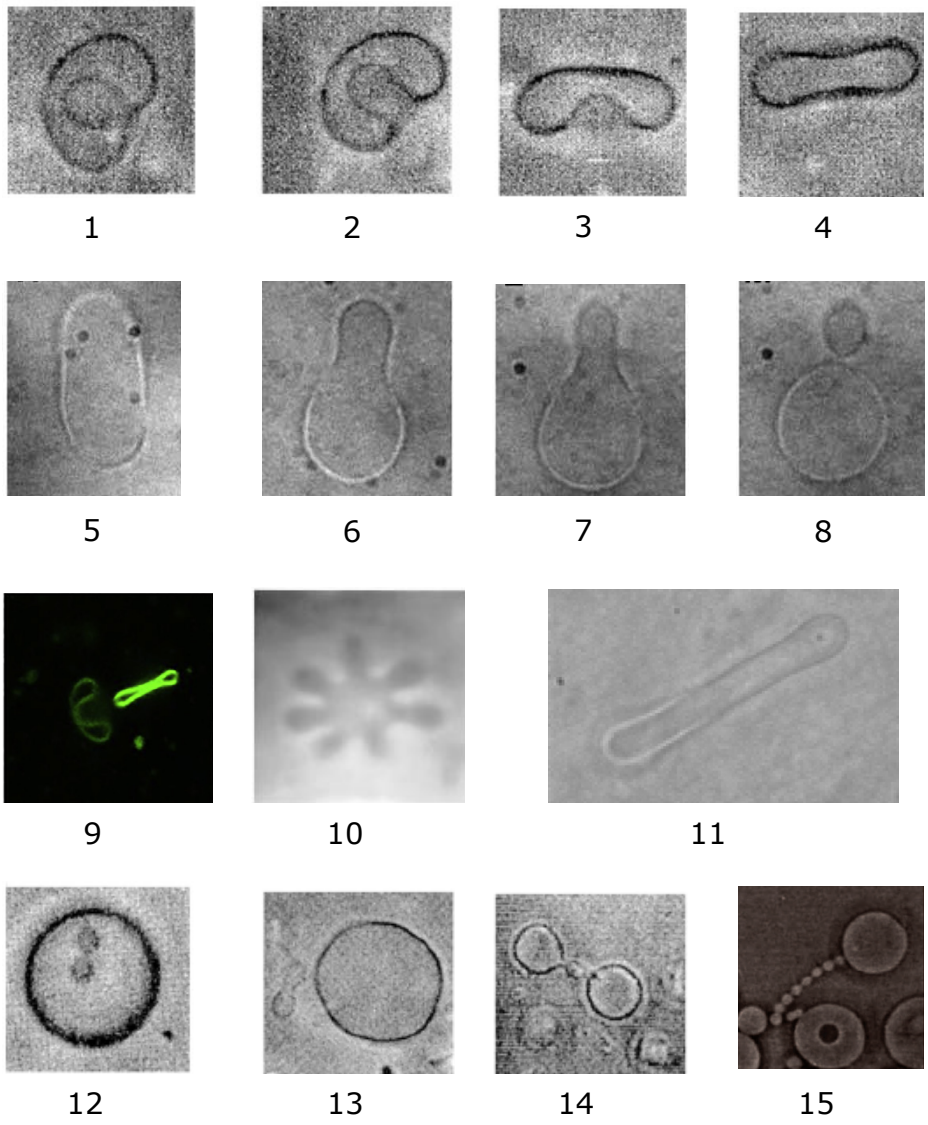

Figure 1.5: Experimental determination of shapes of giant phospholipid vesicles with different microscopy techniques. In the first row are three shapes belonging to the cup-shape class (1–3) and a shape belonging to the disc-shape class (4). In the second row are shapes belonging to the prolate (5) and pear-shape (6–8) classes. In the third row, the first two shapes have a relatively small value of the vesicle reduced volume. Shape 9 shows a codocyte on the left and a torocyte on the right, shape 10 is a starfish, and shape 11 is a cylindrical shape. The fourth row shows shapes characterized by narrow necks connecting nearly spherical vesicle parts. Shape 12 has two invaginated spheres within a large sphere. Shape 13 is composed of a large sphere and two small evaginated spheres. Shape 14 has a small sphere in between two large spheres, whereas shape 15 has (in addition to a large mother sphere) eight small spheres connected to it in a row. [25] Image credits: Image is assembled by taking shapes from different references: shapes 1–4, 12, and 13 (originally from Käs and Sackmann, 1991) [15, 25], 5–8 (B. Mavčič et al., 2004) [26], 9 (Drab et al., 2021) [27], 10 (W. Wintz et al., 1996) [28], 11 (A. Iglič et al., 1999) [29], 14 (originally from Farge and Devaux, 1992) [25, 30], 15 (Veronika Kralj-Iglič, 2012) [31].

1.2 Adhesion of vesicles and biological cells

The adhesion of cells is biologically relevant. It is fundamentally important in the formation and maintenance of tissues. Changes in the adhesion of the cell can help characterize certain diseases like arthritis [32], cancer [33], osteoporosis [34] and atherosclerosis [35]. For example, generally, it has been found that the cell adhesiveness is lower in human cancers [36]. Adhesion also plays a vital role in wound healing, immune responses, in the drug delivery process and also has applications in biosensors. The shape of cells and its regulation can be influenced by their adhesion with each other or to a substrate [37]. Thus, it may be biologically relevant to study the adhesion-induced changes in the shapes of the vesicles. Our work in this regard allows us to study the shape changes and the transformations induced by the adhesion of the vesicles to a rigid surface. Experimentally, vesicle adhesion can be studied for, e.g., using the micro-pipette aspiration technique [2, 38]. Theoretically, the adhesion of vesicles can be studied as a competition between the elastic bending energy and the adhesion energy [39].

Here the reader is introduced to the different regimes in which adhesion of membranes can be studied, and some literature review has been presented about the work done on shape transformations under adhesion – for vesicles with the vesicle membrane composed of single and multi-components.

Ana-Sunčana Smith and Udo Seifert in their paper [40] have described the three different length scales to study adhesion. At the macroscopic scale, the adhesion interaction of the vesicle with the substrate can be introduced in the form of an effective adhesion strength W [40]. When the vesicle is adhered to the surface, the membrane segment which is closest to the surface experiences forces like the attractive van der Waals force, the electrostatic force and also the structural forces [39]. The vesicle membrane can be bound to this surface if the effective interaction potential has a minimum at some distance say z. This range, z, of the potential is typically small and of the order of nm while the radius of the vesicle is of the order of few μm. As we are interested in the macroscopic property like the shape of the vesicle, the spatial variations of the vesicle which are at a much smaller scale like that at about z, are ignored and the microscopic interaction potential is thus replaced by an effective contact potential which can be quantified by W [39]. In our work, the adhesion interaction is considered in such a form of an effective adhesion strength.

At the mesoscopic length scale, the attraction potential is considered to be a sum of van der Waals, electrostatic and structural forces. But at this scale, the shape fluctuations also play a significant role in the interaction of the membrane

with the surface. However due to the substrate present, the shape fluctuations are restricted which results in an effective repulsion. This kind of vesicle interaction with the substrate surface is called non-specific adhesion and this is a result of the coupling between the adhesion potential with the membrane fluctuations and the bending properties of the membrane.

At the microscopic scale, the interaction between the vesicle membrane and the surface is defined as a contribution from the ligand-receptor pairs and the repelling molecules which are embedded into the membrane. This kind of interaction is called specific adhesion. However, the mesoscopic fluctuations affect the interaction of the membrane with the substrate surface by affecting the distribution of the ligand-receptor pairs. So at the microscopic level it is an inevitable prerequisite that the non-specific interactions are made very small such that they do not interfere with the binding of the ligand-receptor pairs.

For a macroscopic study of adhesion on flat surfaces, Seifert and Lipowsky in their papers [39] and [41], had introduced adhesion interaction in the form of the effective adhesion strength to study the shapes of the vesicles. In paper [41], they have shown that in the (V, A) ensemble, a vesicle can undergo a nontrivial transition between free and bound states and transition between two bound states, under a non-zero value of this adhesion strength. They have identified a critical value of adhesion strength, $w_a(v)$ value required to adhere the vesicles, and have predicted that for a given $W = W_a = (w_a\kappa/R^2)$, vesicles of size R $> R_a$ will be bound and that of R $< R_a$ will be free. A similar study on the (P, A) ensemble was done in paper [39]. In paper [42], shape transformation sequences between free and bound states and between two different bound states of different families of shapes have been shown by changing the area of the vesicle. Topological changes in the shape like that of vesicle fusion and vesicle rupture have also been studied and several regimes have been identified for the bound vesicles, bound discs and free vesicles and these regimes depend on the relative sizes of the two length scales described in the paper.

There has been an extensive study [43–53] on the interactions between the vesicle membranes and the adhering nano structures. Different wrapping states and shape transformations have been identified. In paper [43], membrane wrapping states of prolate and oblate ellipsoids are investigated and they have found that spherical particle undergo complete wrapping and the ellipsoidal particles have an enhanced stability in the partially wrapped states, thereby resulting in a lower uptake of ellipsoidal particles by cells. In paper [44], shape transformations of oblate shaped vesicles when adhered by a spherical particle to the axisymmetric centre have been investigated. The phase diagram calculated, allows for a better understanding of the shape transforma-

tions in the biological systems like virus-vesicle endocytosis and nanoparticle-vesicle complexes. The process of exocytosis or budding of a particle out of the vesicle is studied theoretically in paper [45] and the relation between spontaneous curvature of the vesicle and the full release of the nanoparticle has been investigated. Stable and metastable states of full release, partial budding and no budding have been identified. In paper [46], interaction of a membrane with parallel tubes has been studied and they have identified three interaction pathways - membrane wrapping, tube-membrane fusion and tube pearling respectively. The results further suggested that tube pearling can be promoted under weak membrane-tube adhesion but a strong membrane-tube adhesion can induce significant wrapping and prevent pearling. Such a study is important for understanding the formation of membrane tubes which originate from one biological cell to connect with another cell.

Here we discuss some studies related to the multi-component vesicles. In [54], adhesion of multi-component vesicles to flat and curved substrates is investigated. The vesicle membranes are already composed of two distinct phases: liquid-ordered and liquid-disordered. Stable shapes on increasing w have been identified and also the difference in their stability has been studied when different phases are in contact with the adhesion surface. Their numerical study suggests that adhesion can promote phase separation with their composition function turning into a tanh like shape.

In [55], the authors suggest that adhesion leads to phase separation but importantly they convey that there are three mechanisms that lead to phase separation. These mechanisms depend on the interactions between sticker molecules, repeller molecules as well as on the entropic contributions from the shape fluctuations. Phase diagrams for bound and unbound states are also studied.

In [56], Seifert has studied the spherical vesicles composed of two components and their shape evolution with increase in temperature that leads to a formation of a bud. The local concentration profile and the shape profile are both obtained on minimization of the bending energy studied under the area difference elasticity model (ADE). Shape change like budding was found to encourage phase segregation.

In [1], vesicles consisting of two components, where each component is characterized by a different spontaneous curvature, are studied. They show that the mixing and segregation of membrane components can be achieved by changing the volume or on elongation of the vesicle – if there is a complex formation of membrane component with a macromolecule. Importantly, they have shown that the tubular protrusions obtained on elongation can be completely occupied by the component with higher spontaneous curvature.

1.3 Formation of nanodomain and the possible mechanism of segregation

In the earlier section, we have already seen that biological membranes are generally made of many different types of lipids and molecules like proteins and other different amphiphiles, which are embedded in the bilayer membrane and can contribute towards the functional properties of the bio-membranes [16]. It has been found that the segregation of such membrane components can be linked to various biological mechanisms like membrane signaling, trafficking, endocytosis, protein sorting, two-dimensional crystallization, etc [57–59]. Aggregation of certain proteins within the cellular compartments can also be linked to certain neurodegenerative diseases like Alzheimer's disease, Parkinson's disease and Huntington's disease [60]. Thus mixing and de-mixing of components is a biologically important mechanism to investigate. This thesis involves the study of the adhesion of two-component vesicles and the effect of adhesion on the shape and the lateral distribution of the components.

Mechanism of nanodomain formation:

In multi-component membranes, it is possible that a nanodomain is formed on the aggregation of one kind of lipid molecules, two different kinds of lipid molecules, lipid molecules with other amphiphiles (for e.g., proteins), different kinds of molecules, etc. Such aggregation of components are possible due to the interactions between the membrane components and due to the intrinsic shape of the membrane components [10]. The nanodomains can be thought of as macromolecules (very large molecules), and the area they occupy is much larger compared to the area occupied by a single lipid molecule. These complexes can therefore be considered as separate membrane components, which may induce some curvature [61] on the bilayer membrane. Thus, each component can be characterized by a different spontaneous curvature associated with it which describes the preferred curvature of the membrane at the point where that component is present. The amount of the local spontaneous curvature induced by the nanodomain may depend on the concentration of the nanodomain component at that point.

Mechanism of segregation:

In a vesicle system, when the like components strongly attract each other as compared to the interaction between the unlike components, then the loss in entropy competes with the gain in energy. However, at lower temperatures, the entropy con-

tribution is less significant, and the components phase separate. When the inter-molecular interactions between the components are comparable or if the temperature is very high, the thermodynamic phase separation is hindered. However, the components might still segregate if there is a large difference in the spontaneous curvatures by which the two components are characterized [1]. When these large and small spontaneous curvature components occupy the regions of the membrane characterized by the large and small membrane curvatures respectively, then considering the Helfrich bending energy [62] (explained in chapter 2), the elastic energy decreases compared to the case of uniformly mixed components. Thus, the gain in bending energy due to the lateral segregation of components competes with the loss of entropy of mixing. This is analogous to the competition between entropy and the inter-molecular energy. Many studies suggest a two-way relationship between the shape and the distribution of components where it is possible that the shape of the membrane can influence the lateral distribution of components, and conversely, the distribution of the components within the plane of the membrane can influence the membrane shape [56, 63–65]. In various biological works, they have hypothesized the segregation of components based on the coupling between the local membrane curvature and the concentration of the components [66–69]. Parthasarathy et al., have developed an experimental platform which shows that for an already phase-separated membrane with L_o and L_d domains existing at a temperature below the transition temperature, these domains get preferentially positioned in the regions of low and high membrane curvatures respectively due to membrane deformations. Thereby they have shown that lipid phases can spatially organize themselves on sensing the gradients of membrane curvature [70, 71].

1.4 Goal of the thesis

We have seen some interesting shapes and shape transitions that occur in nature, and were also experimentally observed using giant phospholipid vesicles in Fig. 1.5. Biologically, the shape of the cells and cell organelles can dictate their functional properties. The broader goal of the thesis is to study the stability of such structures and their shape transitions under adhesion using a simple vesicle system made up of a lipid bilayer membrane. As seen before, the study of adhesion also holds great biological importance for e.g., in the context of adhesion of cells in the tissue and organ formation, but still, the theoretical studies related to the shape transformations of vesicles adhered to a surface are scarce. This thesis is an attempt to further the understanding of the adhesion-induced shape transformations of single and multi-component vesicles.

Our study on the stability of vesicle shapes and their possible shape transitions induced due to adhesion is divided broadly into two parts. The first part of the thesis pertains to the study of a single component vesicle, where it is assumed that the vesicle membrane is only composed of lipid molecules of one kind. This single component study is further sub-divided into two parts depending on how adhesion is introduced in the system. Here, the aim is to identify stable structures and limiting structures on increasing adhesion, and to also possibly identify new vesicle structures that may not be stable in the free state of the vesicle. We plan to predict possible shape transitions between adhered vesicles of different shape classes based on the total energy study of the vesicle system. We want to probe the effect of change in spontaneous curvature and the change in reduced volume on the adhesion of the vesicle to the flat surface. We also want to study the effect of vesicle shape on the susceptibility of vesicles to adhesion. The second part of the thesis involves the study of vesicles where the vesicle membrane is assumed to be composed of two kinds of membrane components which are characterized by their spontaneous curvatures. We attempt to study the effect of shape change under adhesion on the lateral distribution of components inside the membrane, and vice versa – by simultaneously minimizing for the shape and component distribution. This will allow to further enhance our understanding of the curvature-induced sorting of membrane components. Separation of components inside the bio-membrane can help in the activation-deactivation of certain proteins, which may help in the regulation of some cell functions. The goal here is to thus study the effect of adhesion on the promotion or suppression of the segregation of components and to elucidate the relationship between the shapes of the vesicles and the distribution of components.

We hope that the results of this thesis help further our understanding of the stability of the cell structures and their shape evolution under adhesion. We also hope that the results herein help to promote our understanding of the lateral distribution of components within the biological membranes under the effect of adhesion and their relation with the shape of the cell.

1.5 Organization of the thesis

Chapter 2 introduces the reader to theoretical models like the spontaneous curvature model (SC) and the area difference elasticity model (ADE) which are useful for the study of biological and model lipid bilayer membranes.

Chapter 3 presents the mathematical description of the surface of an axisymmetric vesicle membrane and further presents the mathematical framework of our model used

for the single component as well as the multi-component study of vesicles under the chosen parameterization.

Chapter 4 presents the results to the study of the adhesion of vesicles where the vesicle membrane is composed of a single kind of component – by varying the size of the membrane area attached to the flat surface. Stable shapes and complete stability ranges of the different classes of adhered vesicle shapes have been identified for a range of different parameters. New class of shapes has been obtained and described.

Chapter 5 presents the results to the study of the adhesion of vesicles where the vesicle membrane is composed of a single kind of component – by varying the adhesion strength of the flat surface. The influence of the spontaneous curvature, adhesion strength and the reduced volume on the stability of the vesicle shapes under adhesion has been examined. Minimum adhesion strength required for the transition between the free vesicle state and it's adhered state has been identified. Possible shape transitions between adhered shapes of different classes have also been investigated. It has been shown that the budding of an adhered vesicle may be induced by the change of the adhesion strength. The importance of the free vesicle shape for its susceptibility to adhesion has also been discussed.

Chapter 6 presents the results to the study of the adhesion of vesicles where the vesicle membrane is composed of two kinds of components – by varying the size of the membrane area attached to the flat surface. The curvature-induced lateral distribution of components due to the shape transitions brought about by the adhesion change has been studied. The close relationship between the shape of the vesicle under adhesion and it's lateral distribution of components has been investigated. In particular, the effect of adhesion on the mixing/segregation of components for the different classes of vesicle shapes stabilized, has been probed. It has been shown that budded structures like pears can support the mixing of components, whereas relatively simple and non-budded structures like oblates can support segregation of components.

Chapter 7 presents the summary of the main conclusions of the thesis.

Chapter 2

Mathematical modelling of membrane systems

This chapter describes the importance of bending energy cost in the determination of the vesicle shapes and takes the reader through different models developed for calculating the bending energy of a vesicle.

2.1 Theoretical models

Since the discovery of the red blood cells, researchers have tried to answer questions related to the stability of their shape. In 1964, Rand and Burton assumed that there are two kinds of stresses, which they called the "Tension forces" and the "Rigidity" of the membrane. The first kind of force tends to increase the membrane area and the other kind of force tends to change the curvature of the membrane (i.e. to bend it). They did experiments which suggested a relation between the different deformations of the cell and the resistance of the cell to the bending and stretching stresses. [72]. In 1966, Fung pointed out the importance of bending in the stability of the biconcave shape of red blood cells when stressed [73,74]. After that, Canham in 1970 considered that bending energy [75] was enough to explain the shape of discocyte erythrocytes, and he used the following quadratic form of bending energy which is based on the concepts of structural engineering, i.e., bending of a thin plate, and also assumed that the shear stresses reduce to zero [75,76].

$$U = \frac{\kappa}{2} \int_{area} (C_1^2 + C_2^2) dA \tag{2.1.1}$$

where, $\kappa = \frac{Eh^3}{12(1-\nu^2)}$ is the bending rigidity of the membrane [75], and where, E is the Young's modulus of elasticity, h is the thickness of the membrane, ν is the Poisson's ratio, $C_1 = 1/R_1$ and $C_2 = 1/R_2$ are the principal curvatures with R_1 and R_2 being the principal radii of curvatures.

However, in order to describe all shape changes of the erythrocyte, one should take into account also the shear energy of the erythrocyte membrane [77]. The form of bending energy was further derived by Helfrich in 1973. Helfrich assumed that

the biological membranes could be considered homogeneous down to the molecular level, and therefore, their mechanical properties can be described by a continuum-mechanical approach. He further assumed that the membranes are fluid and thus would lead to a zero shear stress. In this model, only a change in the curvature of the membrane contributes to the bending energy. The contribution from the tilt of the membrane molecules [78, 79] to the bending energy is negligible as it is assumed that the average direction of the hydrocarbon chains is normal to the bilayer. For the flaccid vesicles which have a volume less than the maximum volume possible for a given surface area of the vesicle, i.e., $v < 1$, the membrane area changes negligibly as the energy cost on compressing the membrane laterally is much larger compared to the energy cost on bending, and the area can therefore be considered a constant [80]. He, too, assumed a quadratic dependence of the elastic energy on the curvature of the membrane. The bilayer membrane is treated as a two dimensional fluid since the height of the bilayer is very negligible compared to its lateral length dimension. In Helfrich spontaneous curvature model (SC), the elastic energy of the bilayer is given by [62],

$$F = \frac{\kappa}{2} \oint (C_1 + C_2 - C_0)^2 dA + \kappa_G \oint C_1 C_2 dA \tag{2.1.2}$$

where, C_0 is the spontaneous curvature or the preferred curvature of the bilayer membrane [80] that accounts for any possible asymmetry in the bilayer, which may arise due to different chemical compositions of the two monolayers or due to any difference in the environment on either side of the bilayer. $C_1 = 1/R_1$ and $C_2 = 1/R_2$ are the principal curvature values which describe the surface, κ is the bending rigidity of the membrane and κ_G is the Gaussian bending rigidity. According to the Gauss-Bonnet theorem, the second term in the Eq. 2.1.2 is invariant, unless, there are changes in the topology of the closed vesicle shape. Bending energy, thus, arises from the mismatch between the local curvature which dictates the shape of the vesicle (given by C_1 and C_2) and the spontaneous curvature. Deuling and Helfrich in their paper [80] introduced the reduced volume (v) as the model parameter within the spontaneous curvature model, such that, $v = V/V_s$, and where V is the vesicle volume, $V_s = (4\pi/3)R_s^3$ and R_s is defined by $A = 4\pi R_s^2$. A denotes the surface area of the vesicle. When the volume of a vesicle, V, is decreased below V_s, shape transformations take place which then depend on reduced volume, v, and reduced spontaneous curvature, $c_0 = C_0 R_s$ [62]. We know that A and V act as constraints to the system under which equilibrium vesicle shapes are obtained. It was found that the scale of the bending rigidity, κ is larger compared to the scale of thermal energy, thus thermal fluctuations can be neglected and the average equilibrium shape of the

vesicle corresponds to the minimum of the bending energy [2].

A more generalized model was later introduced that allows for a proper description of the bilayer nature of the membrane and describes the shapes of the closed vesicles. It is called the area difference elasticity model (ADE), and was quantitatively described by Miao et al. (1994) [81] based on the previous theoretical considerations of Evans [74], Evans and Skalak [82], Stokke et al. [83] and Helfrich [84]. The timeline to the development of the ADE model (which is just a special case of Helfrich-Evans membrane bending energy including local and non-local bending energy [82,85]) is as follows: The very importance of the bilayer coupling on the shape of the vesicle was recognized early on by Evans (1974) [74], Helfrich (1974) [16,84] and Sheetz and Singer (1974) [86], which was qualitatively expressed as the bilayer couple hypothesis. The hypothesis suggests that the two monolayers of the closed bilayer membrane can react differently to the perturbations, while still being coupled to one another. Evans and Helfrich [74,84], further, have also quantitatively described the bilayer couple hypothesis. To which, Evans (1974) [74] and Evans and Skalak (1980) [82] have shown the relation between the geometry-induced area-difference ΔA of the two monolayers and the average curvature of the bilayer surface, whereas, Helfrich (1974) [84] has shown the relation between the spontaneous curvature and the density difference between the two monolayers of the bilayer. Later, Svetina, Ottova-Leitmannová and Glaser (1982) [87], based on the work of Evans, Helfrich and Sheetz and Singer [86], introduced in the corresponding mathematical model a constraint on the area-difference parameter, ΔA.

If the bilayer is unconnected and there are no edge restrictions, then such a bilayer will not be resistant to bending because the two monolayers will just slide past each other on being bent. However, if there are some edge constraints or if it's a closed vesicle, then the two monolayers will bend simultaneously and are prevented from sliding past each other – which will cause one monolayer to be stretched and the other to be compressed, resulting in a generation of net area difference between the two monolayers when such a bilayer is bent [74, 82]. This suggests the importance of incorporating the bilayer nature of the lipid membrane in the model. An area difference is generated because the lipids cannot always freely jump from one monolayer to the other due to the large timescale of flip-flop, thereby preventing the bilayer from reaching the equilibrium density of lipids after being bent. Lipid molecules are, however, observed to undergo flip-flops also through the "transient" pores or defects formed in the membrane to relieve the differential tension [88, 89].

This model is based on the sum of the local and non-local bending energies [Helfrich (1973) [62];Evans (1974) [74], (1980) [85]; Helfrich (1974) [84]; Evans and Skalak

(1980) [82]; Stokke et al. (1986) [83]]. The total free energy of the bilayer membrane within the Helfrich-Evans model (where the non-local term is the consequence of relative stretching of both lipid layers) can be described as [80–82, 85],

$$F = \frac{\kappa}{2} \oint (C_1 + C_2 - C_0)^2 dA + \frac{\kappa_r}{2Ad^2}(\Delta A - \Delta A_0)^2 \tag{2.1.3}$$

where, κ_r is the non-local bending constant. ΔA_0 represents the difference between the relaxed areas of the two monolayers, which depends on the difference in the number of molecules between the two monolayers and also on the equilibrium areas of the individual molecules of the two leaflets. ΔA is a variable quantity which depends on the integral of membrane curvature (shape) over the whole vesicle surface and d is the distance between the two monoloyers of the bilayer.

$$\Delta A = d \oint (C_1 + C_2) dA \tag{2.1.4}$$

Based on the relation between the average mean curvature,

$$< H >= \frac{1}{A} \int \frac{1}{2}(C_1 + C_2) dA \tag{2.1.5}$$

and ΔA [90], which is: $< H >= \Delta A/2Ad$, we could rewrite the Helfrich-Evans bending energy (Eq. 2.1.3) into the form [89]:

$$F = \frac{\kappa}{2} \int (C_1 + C_2 - C_0)^2 dA + 2\kappa_r A(< H > -H_0)^2 \tag{2.1.6}$$

where, $H_0 = \Delta A_0/2Ad$ is the spontaneous average mean curvature.

The first term in Eqs. 2.1.3 and 2.1.6 is the local and the second term is the non-local contribution to the bending energy [82]. As mentioned above, the scale of the energy associated to bilayer stretching is several orders of magnitude larger than that associated to bilayer bending, thus surface area, A, is effectively a constant. Volume, V, also acts as a constraint to this model. The shapes depend only on the following parameters: v, C_0, ΔA_0 or H_0, κ and κ_r. The reduced volume parameter, v is defined as before while C_0 is the local spontaneous curvature. The non-local bending energy term [82] is important in describing the shapes of the phospholipid vesicles [91, 92].

This non-local bending energy term [82, 83] can be expressed as a function of the effective spontaneous curvature or the effective spontaneous mean curvature [82, 89, 93, 94]. In the Helfrich-Evans energy (Eq. 2.1.3), the non-local bending energy term can be approximately written as [90]: $-\kappa_r \Delta A \Delta A_0/Ad^2$, therefore Eq. 2.1.3 can be

written in the form of:

$$F = \frac{\kappa}{2} \oint (C_1 + C_2 - C_{0,eff})^2 dA \tag{2.1.7}$$

where,

$$C_{0,eff} = C_0 + \frac{\kappa_r \Delta A_0}{\kappa A d} \tag{2.1.8}$$

In our study, we have therefore calculated the shapes of the vesicles using the spontaneous curvature model where the spontaneous curvature is actually the effective spontaneous curvature as described in Eq. 2.1.8 and that we consider this effective spontaneous curvature as a constant. It was shown by Hwang and Waugh [95], that for the unilamellar phospholipid vesicles, the ratio between the non-local and local bending constants i.e., κ_r and κ have been estimated to be of the same order of magnitude.

Further, Urbanija et al. [89], in their paper have shown that the energy contribution from the orientational ordering of the lipid molecules and the direct interaction between them is responsible for explaining the continuous shape transitions of the prolate vesicles to the pears vesicles with a narrow neck. In fact, the pears vesicles are minimized at a lower energy minima when we consider these two contributions. These considerations are also responsible for explaining the discontinuous transition to the limiting pear structure. Both of these transitions are observed experimentally but cannot be explained by the ADE model alone. Thus, individually, both the ADE model and the SC model are insufficient in explaining certain shape transition sequences.

Chapter 3

Mathematical description of the vesicle surface

Here the reader can get familiarized with the mathematical framework used in the description of the vesicle surface and derivation to some of the basic differential geometry concepts that are used in our model. We further describe the total energy functionals used for describing both the single component and the two-component vesicle systems under adhesion.

3.1 Arc-length parameterization of the vesicle surface

In our study, we focus on vesicle shapes that are axisymmetric about the z-axis. The profile of such shapes can be represented using the arc-length parameterization, which allows for a description of overhangs.

Due to the axisymmetry condition, it is sufficient to parameterize just the 1D shape profile (defined in the x-z plane) which revolves around the z-axis (x = 0) to generate a 2D vesicle surface. The angle of revolution is represented by ψ (range is between $0 < \psi < 2\pi$).

Under this parameterization, the shape profile is represented by the function $\theta(s)$, where s is the arc-length and $\theta(s)$ is the angle between the horizontal axis and the tangent at a given point s on the vesicle profile.

The parametric equations which describe the height and the radius of the vesicle are described in Eqs. 3.1.1 and 3.1.2 respectively.

$$z(s) = \int_0^s ds' \sin\left(\theta(s')\right) \tag{3.1.1}$$

$$r(s) = \int_0^s ds' \cos\left(\theta(s')\right) \tag{3.1.2}$$

To ensure that the vesicle shape profile is smooth, we impose the following con-

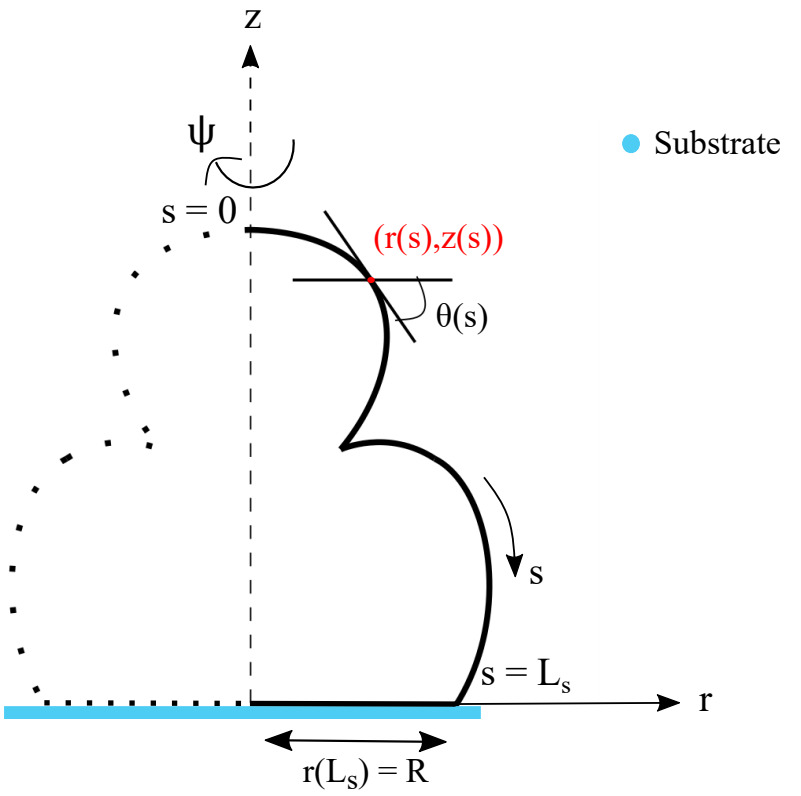

Figure 3.1: The parameterization of the shape profile is shown.

straints [96],

$$\theta(0) = 0 \tag{3.1.3}$$

$$\theta(L_s) = \pi \tag{3.1.4}$$

where, L_s represents the length of the shape profile.

The adhesion of the vesicle is also introduced in the form of a constraint as defined by Eq. 3.1.5 – for the calculations done under the fixed radius of adhesion study. However, when we study the vesicle adhesion under the constraint of fixed adhesion strength, W, the constraint 3.1.5 is replaced with the constraint 3.1.6.

$$r(L_s) = R \tag{3.1.5}$$

$$r(L_s) \geq 0 \tag{3.1.6}$$

Eq. 3.1.5, also allows us to define the contact area between the vesicle surface and the flat substrate, also called the area of adhesion, A_c, given by, $A_c = \pi R^2$. Thus, R can be defined as the radius of adhesion of the vesicle. The contact area is circular due to the axisymmetry assumption of our vesicles.

The unknown function $\theta(s)$ which describes the shape profile of the vesicle is assumed to be periodic and approximated using the Fourier sine series as shown in Eq. 3.1.7,

$$\theta(s) = \theta_0 \frac{s}{L_s} + \sum_{i=1}^{N} a_i \sin[\frac{\pi i s}{L_s}] \tag{3.1.7}$$

where, N is the total number of Fourier modes and a_i are the Fourier amplitudes. θ_0 is the angle made by the profile when it touches the adhesion surface i.e. $\theta_0 = \theta(L_s)$. We call this angle the contact angle and to ensure that the vesicle profile is smooth at all points, we assume that it measures π i.e. $\theta_0 = \pi$.

3.2 Derivation of the expression for principal curvatures under arc-length parameterization

Let us define a vector $\mathbf{R}(x, y, z)$ in the 3D Euclidean space, which can describe all the points on the surface generated by the revolution of the parameterized curve (defined in the x-z plane) about the z-axis. The coordinates of this vector written in terms of ψ and s are given by,

$$\mathbf{R} = \{\cos(\psi)r(s), \sin(\psi)r(s), z(s)\} \tag{3.2.1}$$

where, $r(s)$ is as defined in Eq. 3.1.2; ψ and s are the local coordinates on the surface; x, y and z are the coordinates of the 3D Euclidean space.

Following steps [97, 98] should be taken to derive the equations defining the principal curvatures of the surface under the arc-length parameterization:

First, we construct the metric tensor g_{ij} using the coefficients of the first fundamental form as,

$$g_{ij} = \begin{bmatrix} \frac{\partial \mathbf{R}}{\partial s}.\frac{\partial \mathbf{R}}{\partial s} & \frac{\partial \mathbf{R}}{\partial \psi}.\frac{\partial \mathbf{R}}{\partial s} \\ \frac{\partial \mathbf{R}}{\partial s}.\frac{\partial \mathbf{R}}{\partial \psi} & \frac{\partial \mathbf{R}}{\partial \psi}.\frac{\partial \mathbf{R}}{\partial \psi} \end{bmatrix} = \begin{bmatrix} 1 & 0 \\ 0 & (r(s))^2 \end{bmatrix} \tag{3.2.2}$$

where,

$$\frac{\partial \mathbf{R}}{\partial s} = \{\cos(\psi)\cos(\theta(s)), \cos(\theta(s))\sin(\psi), \sin(\theta(s))\} \tag{3.2.3}$$

$$\frac{\partial \mathbf{R}}{\partial \psi} = \{-\sin(\psi)r(s), \cos(\psi)r(s), 0\} \tag{3.2.4}$$

The unit normal $\mathbf{n}$ is calculated as,

$$\mathbf{n} = (\frac{\partial \mathbf{R}}{\partial \psi} \times \frac{\partial \mathbf{R}}{\partial s})/(det(g_{ij}))^{1/2} = \{-\cos(\psi)\sin(\theta(s)), -\sin(\psi)\sin(\theta(s)), \cos(\theta(s))\} \tag{3.2.5}$$

Next, we define $\mathbf{Y}$ with second order derivatives of $\mathbf{R}$ and use it to generate L_{ij} which gives the coefficients to the second fundamental form.

$$\mathbf{Y} = \begin{bmatrix} \frac{\partial^2 \mathbf{R}}{\partial s \partial s} & \frac{\partial^2 \mathbf{R}}{\partial s \partial \psi} \\ \frac{\partial^2 \mathbf{R}}{\partial \psi \partial s} & \frac{\partial^2 \mathbf{R}}{\partial \psi \partial \psi} \end{bmatrix} \tag{3.2.6}$$

$L_{ij} = \mathbf{Y} \cdot \mathbf{n}$

The H_{ij} tensor which is also called the curvature tensor is given by,

$H_{ij} = {g_{ij}}^{-1} \; L_{ij} =$

$$\begin{bmatrix} \frac{d\theta(s)}{ds} & 0 \\ 0 & \frac{\sin(\theta(s))}{r(s)} \end{bmatrix} \tag{3.2.7}$$

The diagonal elements represent the two principal curvatures C_1 and C_2,

$$C_1 = \frac{d\theta(s)}{ds} \tag{3.2.8}$$

$$C_2 = \frac{\sin(\theta(s))}{r(s)} \tag{3.2.9}$$

Thus, under the arc-length parameterization, the principal curvatures can be defined as shown in Eqs. 3.2.8 and 3.2.9. But these steps can also be followed to define principal curvatures under different parameterizations of the surface as well.

3.3 The energy functional for the adhered vesicle system

The total energy of the adhered vesicle system can be written as follows,

$$F_{tot} = F_b + F_{adh} = \frac{\kappa}{2} \oint (C_1 + C_2 - C_0)^2 dA + \kappa_G \oint (C_1 C_2) dA - W A_c \tag{3.3.1}$$

Where F_b is the bending energy of the Helfrich type and is defined for both the single component and the multi-component vesicle studies in the following sections. Adhesion is accounted for differently in different calculations – for e.g., either in the

form of adhesion strength or adhesion radius, and is shown for different calculations later on.

Under the arc-length parameterization, the total energy functional becomes,

$$F_{tot} = F_b[\theta(s)] + F_{adh} = \frac{\kappa}{2}[\int_0^{2\pi} d\psi \int_0^{L_s+r(L_s)} \mathcal{H}(s)r(s)ds] - W\pi r(L_s)^2 \tag{3.3.2}$$

The bending energy is described by the curvatures expressed in their parameterized form as derived in section 3.2. When we substitute Eq. 3.1.7 into Eqs. 3.1.1 and 3.1.2 and further substitute them in Eq. 3.3.2, we can replace the functional minimization by the minimization of the function of many variables [65,96,98]. The functional 3.3.2 turns into a function of many variables. The numerical minimization is done under the constraints of fixed surface area, A and volume, V, which are implemented using the Lagrange multipliers, where,

$$A = \pi r(L_s)^2 + 2\pi \int_0^{L_s} dsr(s) \tag{3.3.3}$$

$$V = \pi \int_0^{L_s} dsr(s)^2 \sin\theta(s) \tag{3.3.4}$$

Minimization under the constraint of fixed adhesion radius, R, is done where,

$$R = \int_0^{L_s} ds \cos\theta(s) \tag{3.3.5}$$

As briefly explained in the earlier chapter, we consider a sphere having the same surface area, A, as that of the investigated vesicle system and derive the volume, V_s, and the radius, R_s, of the sphere which act as the volume and the length units of our system respectively,

$$R_s = \sqrt{A/4\pi} \tag{3.3.6}$$

$$V_s = \frac{4}{3}\pi {R_s}^3 \tag{3.3.7}$$

The reduced volume, v, can then be defined as V/V_s. For the study of single component vesicles, we do not consider any topological changes, and we have assumed that the Gaussian bending rigidity is same for the adhered and free membrane parts. Therefore the Gaussian energy contribution is constant. In the study of the multi-component vesicles where the vesicle membrane is composed of two kinds of components, the Gaussian bending rigidity of each component, κ_G^A and κ_G^B are assumed to be same, and therefore, there is no contribution from the line integral of

the geodesic curvature at the nanodomain boundary, but the energy contribution now only depends on any topological changes of the closed vesicle [99]. We also assume that the Gaussian bending rigidity of the bound and unbound membrane is same. Thus, under our above assumptions and the fact that we do not consider any topological changes of the vesicles, the Gaussian energy term is a constant in this case as well. For this reason, the Gaussian bending energy can be avoided in Eq. 3.3.2 and in the future.

3.4 Energy functional for a single component vesicle system

In our work, the study of adhesion-induced shape transformation of the vesicles is first undertaken for a simple vesicle system where the vesicle membrane is assumed to be built up of only one kind of membrane component. We study the equilibrium shapes of the adhered vesicles, and the shape transitions are induced by either changing the size of the adhesion area of the vesicle in contact with the flat surface or by changing the adhesion strength of the substrate. The bending energy for the study of single component vesicles is described using the Helfrich's energy functional, where the membrane component that makes up the vesicle is characterized by it's spontaneous curvature value C_0.

We first study the adhesion of single component vesicles by changing the size of the adhesion area of the vesicle, and the total energy of such a vesicle system where the adhesion is incorporated in the form of a constraint on the adhesion radius is given by,

$$F = \frac{\kappa}{2} \oint (C_1 + C_2 - C_0)^2 dA \tag{3.4.1}$$

The reduced (dimensionless) form of this equation is obtained by dividing the energy functional F by the bending energy of a sphere – calculated for zero spontaneous curvature, $F_{sphere} = 8\pi\kappa$,

$$\frac{F}{F_{sphere}} = \frac{1}{4} \int_A (c_1 + c_2 - c_0)^2 da \tag{3.4.2}$$

where, $c_0 = C_0 R_s$, $c_1 = C_1 R_s$ and $c_2 = C_2 R_s$ are the reduced spontaneous curvature and the reduced principal curvatures respectively, and $a = A/4\pi R_s^2$ is the reduced area.

The energy functional of the vesicle when it is described under the arc-length

parameterization is as follows,

$$F[\theta(s)] = \frac{\kappa}{2}[\pi r(L_s)^2 C_0^2 + (2\pi)\int_0^{L_s} dsr(s)(\frac{d\theta(s)}{ds} + \frac{sin(\theta(s))}{r(s)} - C_0)^2] \qquad (3.4.3)$$

The first part of the above equation is the bending energy contribution due to the mismatch between the curvature of the flat adhered membrane surface and the spontaneous curvature associated with the membrane component, while the second part of the equation is the bending contribution from the shape of the free membrane surface part of the vesicle. The energy functional is minimized under the constraints of fixed surface area, A and volume, V, while the effective adhesion is introduced in the form of a radius constraint, R, as described in section 3.1. The shape profile, $\theta(s)$ is obtained on minimization. We have assumed that the bending rigidity of the bound and unbound membrane segments is equal to κ.

In the second part of the study of the single component vesicle system, we characterize this effective adhesion potential per unit area by the adhesion strength W of the flat surface, which is an effective interaction contribution from the different mechanisms towards adhesion. The shape transformations of the vesicles are now carried out by changing the adhesion strength, W. As before, the minimization is done under the constraints of fixed surface area, A and volume, V. The shape profile $\theta(s)$ and the area of adhesion (A_c), which can be calculated from the radius of adhesion, $r(L_s)$, are obtained on minimization.

The total energy of the system when the adhesion is incorporated in the form of an effective adhesion strength, is given by,

$$F = \frac{\kappa}{2}\oint (C_1 + C_2 - C_0)^2 dA - WA_c \qquad (3.4.4)$$

The reduced form of the total energy functional under the constraint of such an effective adhesion potential can be written as,

$$\frac{F}{F_{sphere}} = \frac{1}{4}\int_A (c_1 + c_2 - c_0)^2 da - \frac{w}{2}(\frac{A_c}{A}) \qquad (3.4.5)$$

where, $w = WR_s^2/\kappa$ is the reduced (dimensionless) adhesion strength. The ratio $(\frac{A_c}{A}) = \frac{A_c}{4\pi R_s^2}$ is the reduced contact area. The values of $(\frac{A_c}{A})$ are 0.5 for the pancake-like shaped vesicles of very small reduced volume and 0 for a spherical vesicle ($v = 1$).

The total energy functional in the parameterized form which describes the vesicle

under adhesion can be written as,

$$F[\theta(s)] = \frac{\kappa}{2}[\pi r(L_s)^2 C_0^2 + (2\pi)\int_0^{L_s} dsr(s)(\frac{d\theta(s)}{ds} + \frac{sin(\theta(s))}{r(s)} - C_0)^2] - W\pi r(L_s)^2 \tag{3.4.6}$$

The third term in the functional corresponds to the adhesion energy, where W is the adhesion strength, and it is calculated over the contact area of adhesion, $A_c = \pi r(L_s)^2$. The bound membrane segment experiences different attraction forces because of the adhesion surface as compared to the unbound membrane part, and this may result in the difference in the densities of the lipid molecules in both the membrane parts and a corresponding difference in the bending properties of the membrane parts. However, for simplicity purpose, we have assumed that the bending rigidity of the bound and unbound vesicle membrane is same and equal to κ.

The total energy function of a single component vesicle system for both the first and second part of our work – with contribution from both the bending and the adhesion of the membrane surface is then numerically minimized with respect to the Fourier amplitudes, a_i, and the length of the shape profile, L_s.

3.5 Energy functional for a two-component vesicle system

We further extend our study to the vesicles under adhesion which have a vesicle membrane composed of two kinds of membrane components, and they are studied under the framework of the Helfrich bending energy model. This kind of multi-component system is more closer to the complex systems found in nature. The components A and B in our model [1] are represented by the spontaneous curvatures C_0^A and C_0^B respectively and their corresponding bending rigidities κ^A and κ^B. The lateral redistribution of these components can influence the shape of the membrane and vice versa, the local curvature can induce lateral redistribution of components to the region having a more favourable curvature such that the overall bending energy is minimized [56, 63]. The work done here aims to study such a direct coupling between the local curvature or the shape of the membrane vesicle under adhesion, and the concentration of components. The shape transformations are brought about by changing the size of the adhesion area of the vesicle in contact with the flat surface. The physical significance of such a system can be in a situation where the system consists of two similar kinds of lipid molecules and where one kind of lipid forms a complex with a large molecule like that of a macromolecule.

The macromolecule complexed with the lipid nanodomain of one kind can be considered to be the component A, and the nanodomain of the other kind of lipid molecules can be considered to be the component B of our model system. Such a model can also be useful for a vesicle system with the membrane composed of a single kind of lipid molecules, where the macromolecule complexed with the lipid nanodomain forms the component A and the single lipid molecules form the component B. Based on the discussion in section 1.3, the coupling of the macromolecule to the lipid nanodomain may induce a large curvature to the membrane surface which can be characterized by the local spontaneous curvature. Thus, this direct relationship between the concentration of the complexed lipid nanodomain and the local spontaneous curvature is incorporated in the Helfrich bending energy functional of our model. Such a bending energy functional as shown in Eq. 3.5.1 was first introduced in [65].

The total energy functional which describes our two-component system is given by,

$$F = \frac{\kappa}{2}\int_A (C_1 + C_2 - C_0(\phi))^2 dA \tag{3.5.1}$$

where C_1 and C_2 are the local principal curvatures and the function $C_0(\phi)$ is the local spontaneous curvature of the membrane which depends on the local concentration of both the components, however, it can be expressed in terms of the concentration of component A, $\phi^A(s) = \phi(s)$, alone. This is because we know that the concentration of component B at a given point s is given by, $\phi^B(s) = (1 - \phi(s))$. The functional is integrated throughout the surface area of the vesicle, and dA is the infinitesimal area element. The individual rigidities of component A and component B are assumed to be equal in our calculations i.e., $\kappa^A = \kappa^B = \kappa$.

The reduced form of the energy functional is given by,

$$\frac{F}{F_{sphere}} = \frac{1}{4}\int_A (c_1 + c_2 - c_0(\phi))^2 da \tag{3.5.2}$$

where, $c_0(\phi)$ and c_1, c_2 are the reduced spontaneous curvature and the reduced principal curvatures respectively. $c_0(\phi)$ can be further expressed as a function of reduced spontaneous curvatures $c_0^A = C_0^A R_s$ and $c_0^B = C_0^B R_s$ (refer Eq. 3.5.4).

The parameterized form of the total energy functional can be written as,

$$F[\theta(s), \phi(s)] = \frac{\kappa}{2}[(2\pi)\int_0^{L_s + r(L_s)} ds r(s)[\frac{d\theta(s)}{ds} + \frac{sin(\theta(s))}{r(s)} - C_0(\phi(s))]^2] \tag{3.5.3}$$

The functional F is minimized under the constraints of constant surface area A,

volume V and the constraint on the average concentration of the component A, ϕ_{avg} $= 1/A \int \phi dA$. Note, that the function $\theta(s)$ describing the shape profile is composed of two parts. For the range between $0 < s < L_s$, $\theta(s)$ is approximated using the Fourier sine series as explained in section 3.1 and for the range between $L_s < s < L_s + r(L_s)$, $\theta(s) = \pi$, which means that the shape profile is a straight line extending from $r = 0$ to $r(L_s)$. This allows us to define adhesion which is introduced in the form of a constraint (refer Eq. 3.1.5).

It is assumed that the spontaneous curvature is a linear function of the concentration $\phi(s)$ and can be expressed as,

$$C_0(\phi(s)) = (C_0^A - C_0^B)\phi(s) + C_0^B \tag{3.5.4}$$

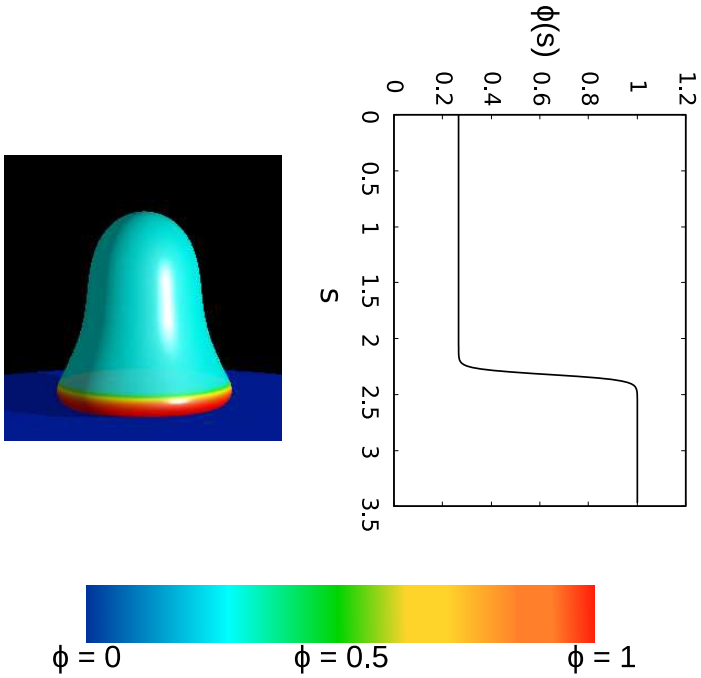

Figure 3.2: The local concentration profile on the right corresponds to the vesicle shape plotted on the left, and the colour code is presented where blue stands for $\phi = 0$ i.e. minimum concentration of component A and red stands for $\phi = 1$ i.e. the maximum concentration of component A.

The concentration profile, $\phi(s)$, is postulated to be described by the tanh function in analogy to it's use in the description of the phase separated mixtures.

$$\phi(s) = (\phi_A - \phi_B)[tanh(\zeta(s - s_0))] + \phi_B \tag{3.5.5}$$

here, ϕ_A and ϕ_B are the upper and lower limits of $\phi(s)$ respectively, i.e., the extremum concentrations of component A on either side of the interface region. When $0 < \phi_A = \phi_B < 1$, then we can say that the component A is uniformly distributed

throughout the surface as $\phi(s)$ becomes a constant function. A special case of this uniformly distributed case is when $\phi_A = \phi_B = 0.5$, this is when the concentration of component A is 50% and the concentration of component B is 50% at each point s on the surface, and we call this the mixed state. The parameters ζ and s_0 represent the width and the position of the interface between the two regions.

In our study, we describe the distribution of the components using a colour code. The region rich in component A is represented by the colour red where $\phi(s) = 1$, and the region which is devoid of component A completely and alternately is therefore rich in component B is described by the colour blue, where $\phi(s) = 0$. The green region represents a mixed state where it is equally occupied by the components A and B i.e. $\phi(s) = 0.5$.

For the two-component bending energy functional, the functional is numerically minimized not just with respect to the shape profile but also with respect to the concentration profile. Hence along with a_i and L_s, the multi-variable function is also minimized with respect to variables ϕ_A, ϕ_B, ζ and s_0 which describe the concentration profile. After minimization, we obtain the shape profile $\theta(s)$ and the concentration profile $\phi(s)$ corresponding to the minimum energy. Again for simplicity purpose, there is no difference between the bending rigidity of the bound and unbound vesicle membrane.

Chapter 4

Study of the single component vesicle system by varying the size of the area of adhesion with the flat surface

Adhesion of cells and vesicles is biologically important for many cell functions and plays an important role in many biotechnological applications like that in biosensors or in the drug delivery systems, among others, as seen in chapter 1. Here we theoretically study the adhesion of the lipid vesicle where the vesicle membrane is composed of a single kind of lipid – by varying the size of the adhesion area of the membrane in contact with the flat surface (substrate). We obtain the equilibrium shapes of the vesicles which are stable or metastable under adhesion by minimizing the Helfrich bending energy of the spontaneous curvature model for a few values of the reduced volume and spontaneous curvature. The complete stability range of different families of equilibrium shapes stabilized under adhesion has been studied, and solutions to a new class of shapes have also been identified. Budding of vesicles was induced by adhesion when the vesicles were pinned to the surface with a certain contact area of adhesion.

4.1 Phase diagram of the spontaneous curvature model for free vesicles

The phase diagram for the spontaneous curvature model of the single component membrane has already been studied in detail by Seifert et al [92]. We have reproduced this phase behavior, and it matches well with their obtained results. The phase diagram was reproduced with 160 Fourier amplitudes for $c_0 = 0$ as shown in Fig. 4.1 and with 80 Fourier amplitudes for non-zero reduced spontaneous curvatures as shown in Fig. 4.2 and Fig. 4.3. The calculation of vesicle shapes for the free state of vesicles for both zero and non-zero reduced spontaneous curvatures is a starting point for our study of equilibrium vesicle shapes under adhesion. For $c_0 = 0$, three families of axisymmetric shapes are found to be stable i.e., the stomatocytes for lower, oblates

for intermediate, and prolates for higher reduced volume. For $c_0 = 2.4$ and $c_0 = 3$, prolates and pear shapes are the most stable for different ranges of reduced volume, v. We investigate the stability of vesicle shapes under adhesion for a few values of reduced volumes depending on their position in the phase diagram of the free-state vesicles. We perform a detailed analysis of the shape transformations of the vesicles due to their adhesion to a flat surface.

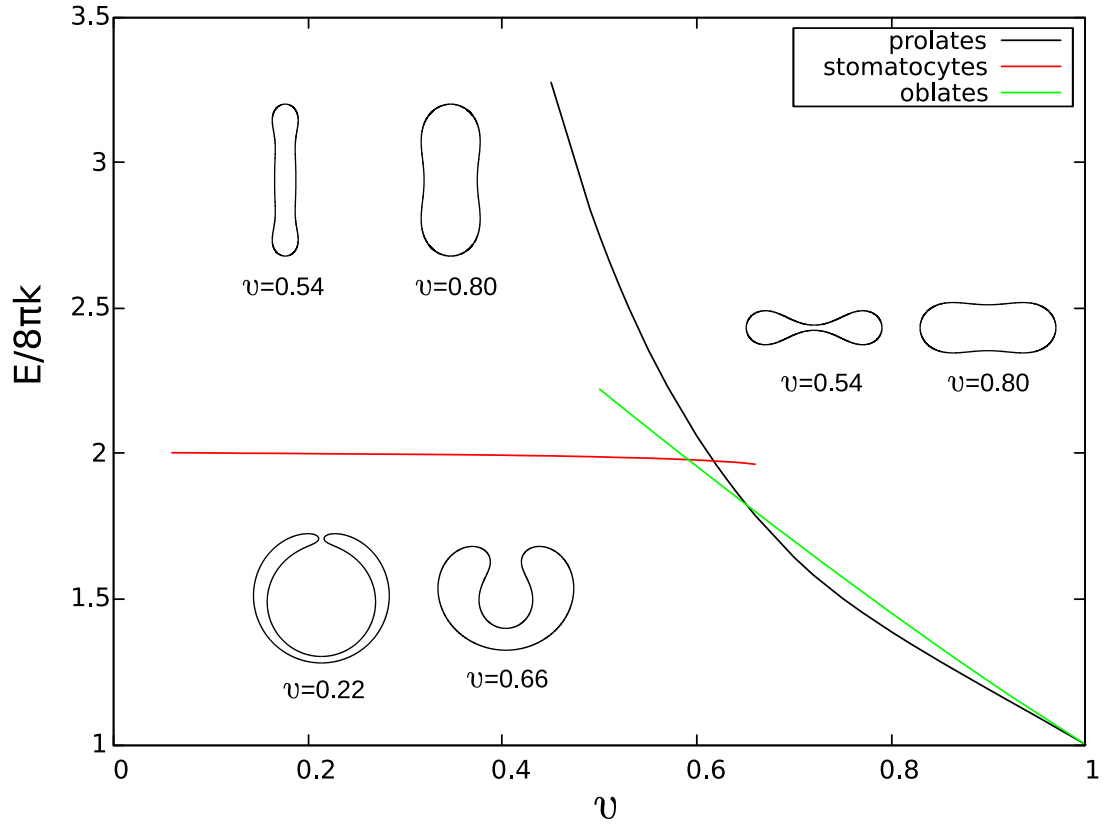

Figure 4.1: Phase diagram for the spontaneous curvature model for $c_0 = 0$.

4.2 Study of vesicle adhesion by varying the size of the area of adhesion

The adhesion of a vesicle to a substrate can be studied in different length scales. To study the effect of adhesion on the shape of the vesicle, we study the system under the macroscopic length scale, where the various mechanisms of adhesion can be described under the umbrella of an effective interaction potential. There are many different mechanisms of adhesion, like the adhesion due to the interaction of the sticker molecules incorporated in the adhering surfaces [100, 101], or the adhesion due to an external force which brings in contact the two adhering vesicles or a vesicle and a solid substrate, etc. Many forces like the attractive van der Waals force, the electrostatic

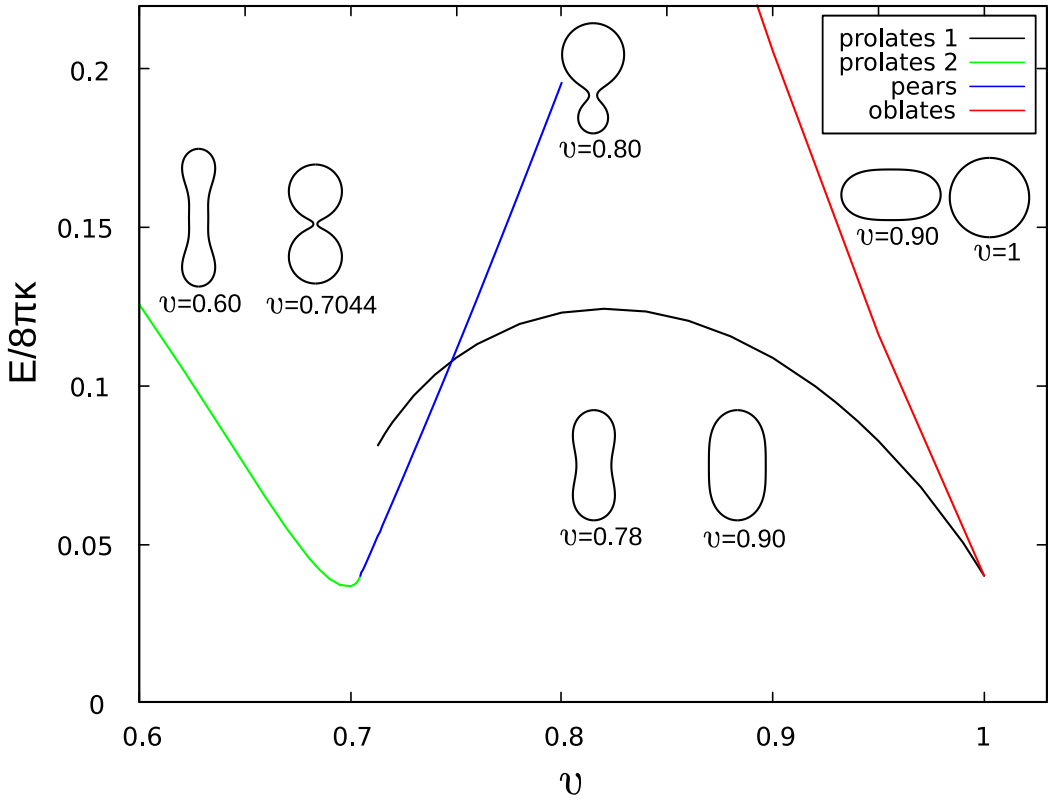

Figure 4.2: Phase diagram for the spontaneous curvature model for $c_0 = 2.4$.

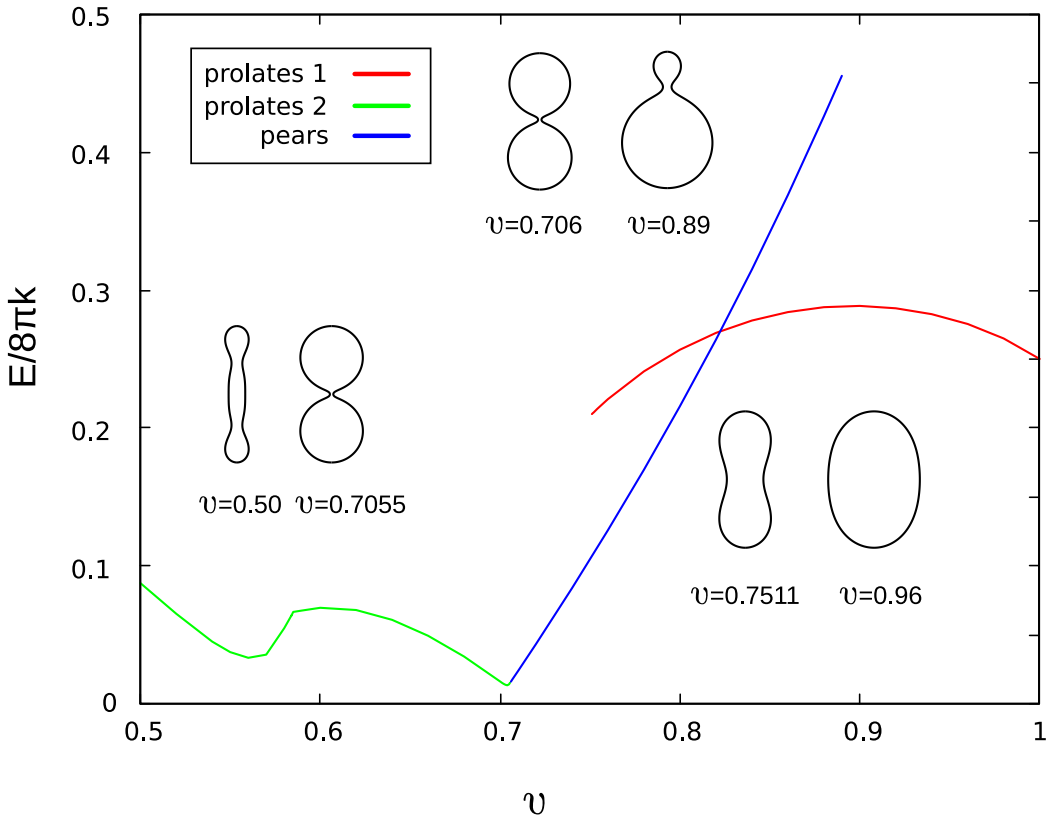

Figure 4.3: Phase diagram for the spontaneous curvature model for $c_0 = 3.0$.

force, and the structural forces can result in such an effective potential [40]. In our study, we do not distinguish the different mechanisms that contribute individually to adhesion but consider the effect of such an effective interaction potential on the size of the membrane area adhered to the flat surface.

In our study, we are therefore interested in the shapes of the vesicles with different sizes of the vesicle surface in contact with the flat surface (substrate). We assume that the vesicle is already attached, and that part of the vesicle, which is attached to the adhesive surface – is fixed. In experiments, this can be achieved for example, by the sticker molecules. We can also imagine that the vesicle is kept in place by laser tweezers. We are not investigating the situation where the vesicle can freely move over the adsorbing surface and change its orientation. The ensemble that mimics the experimental situations is the one with the constant surface area, A and volume, V. We numerically minimize the bending energy functional 3.4.3 to obtain equilibrium shapes. The integral of the energy functional is taken over the complete surface area, A, of the closed vesicle. No topology changes are assumed, therefore the integral over the Gaussian curvature contributes a constant value. We parameterize the shape of the rotationally symmetric vesicle as shown in Eq. 3.1.7 and introduce adhesion in the form of a constraint as shown in Eq. 3.1.5. The region of the adhered vesicle membrane is circular because of our assumption of axial symmetry of the vesicle shape. The size of the adhered membrane can be indicated by the radius, R, of this circular patch attached to the adhesion surface. We change the radius R from 0 to R_{max} where $R = 0$ corresponds to a free vesicle and R_{max} corresponds to the maximum possible adhesion. Beyond R_{max}, a vesicle is ruptured.

Under the assumptions that we have made, all the shapes studied are stable or metastable. We are convinced that within the assumed parameterization of the vesicle membrane, we have found all the solutions. We study the stability range and the shape transformations of the adhered vesicles.

In our calculations, $E/8\pi\kappa$ is the reduced bending energy, $c_0 = C_0 R_s$ is the reduced spontaneous curvature, $R/R_s = r$ is the reduced adhesion radius.

In Fig. 4.4, we show four families of shapes obtained for the reduced spontaneous curvature $c_0 = 0$ and the reduced volume $v = 0.545$, calculated for different values of the reduced adhesion radius, r. The reduced volume was chosen as $v = 0.545$ because for this value, solutions for three different types of vesicle shapes exist in their free state. Thus, three of these families originate from the solutions obtained for free vesicles. They are shown in the second, third, and fourth rows of Fig. 4.4. The first shape profile in each row represents the stable solution for the smallest and the last

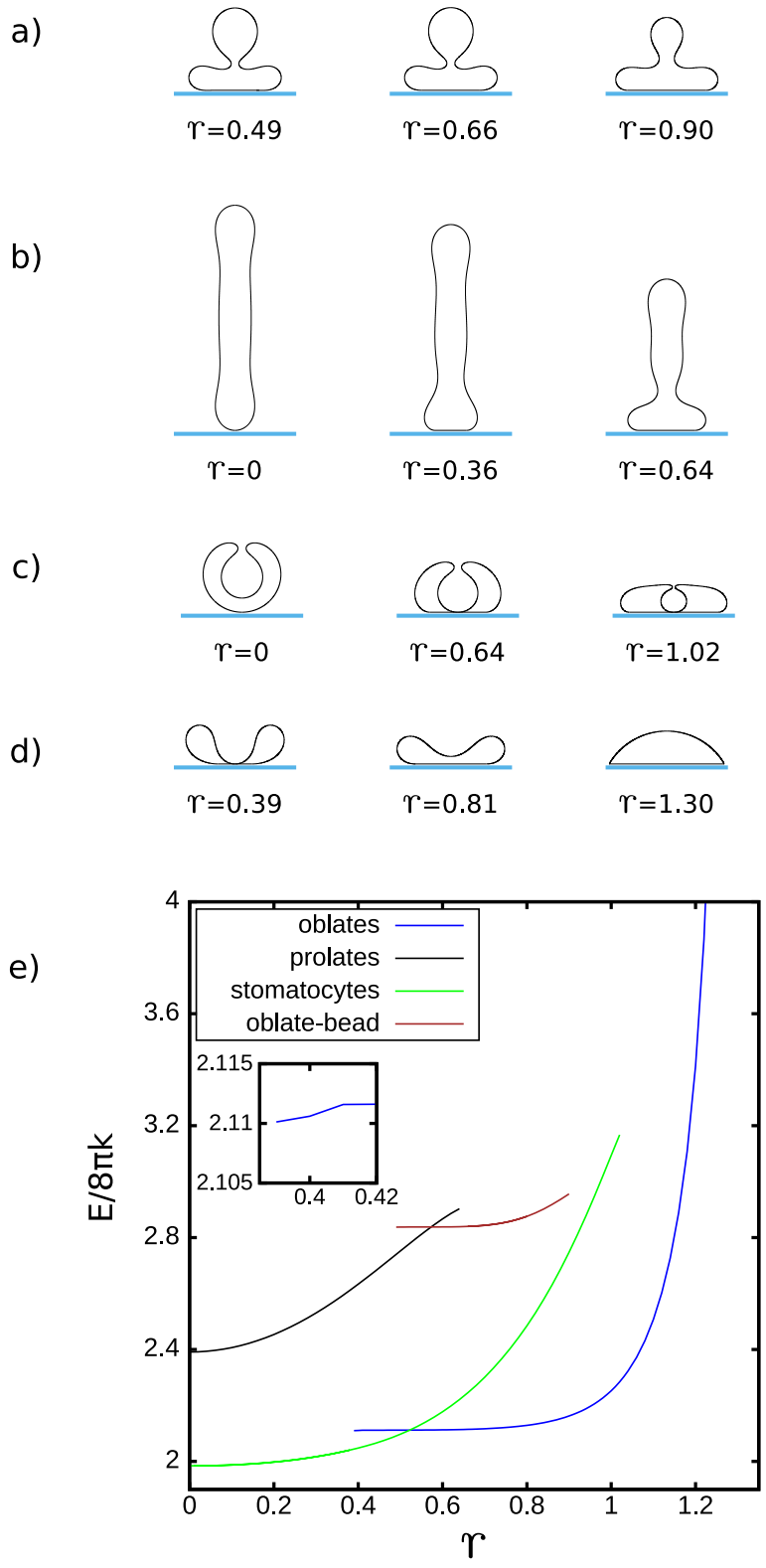

Figure 4.4: Shape profiles for the reduced volume, $v = 0.545$ and reduced spontaneous curvature, $c_0 = 0.0$ and different values of the reduced adhesion radius, r. (a) new branch of the solutions: oblate-bead, (b) prolate, (c) stomatocyte, (d) oblate branch. (e) Elastic energy, $E/(8\pi\kappa)$, as a function of the reduced adhesion radius, r, for different families of solutions for the reduced volume, $v = 0.545$ and the reduced spontaneous curvature, $c_0 = 0.0$. The inset shows that the bending energy does not change smoothly when the membrane at the north pole of the vesicle touches the membrane at the south pole.

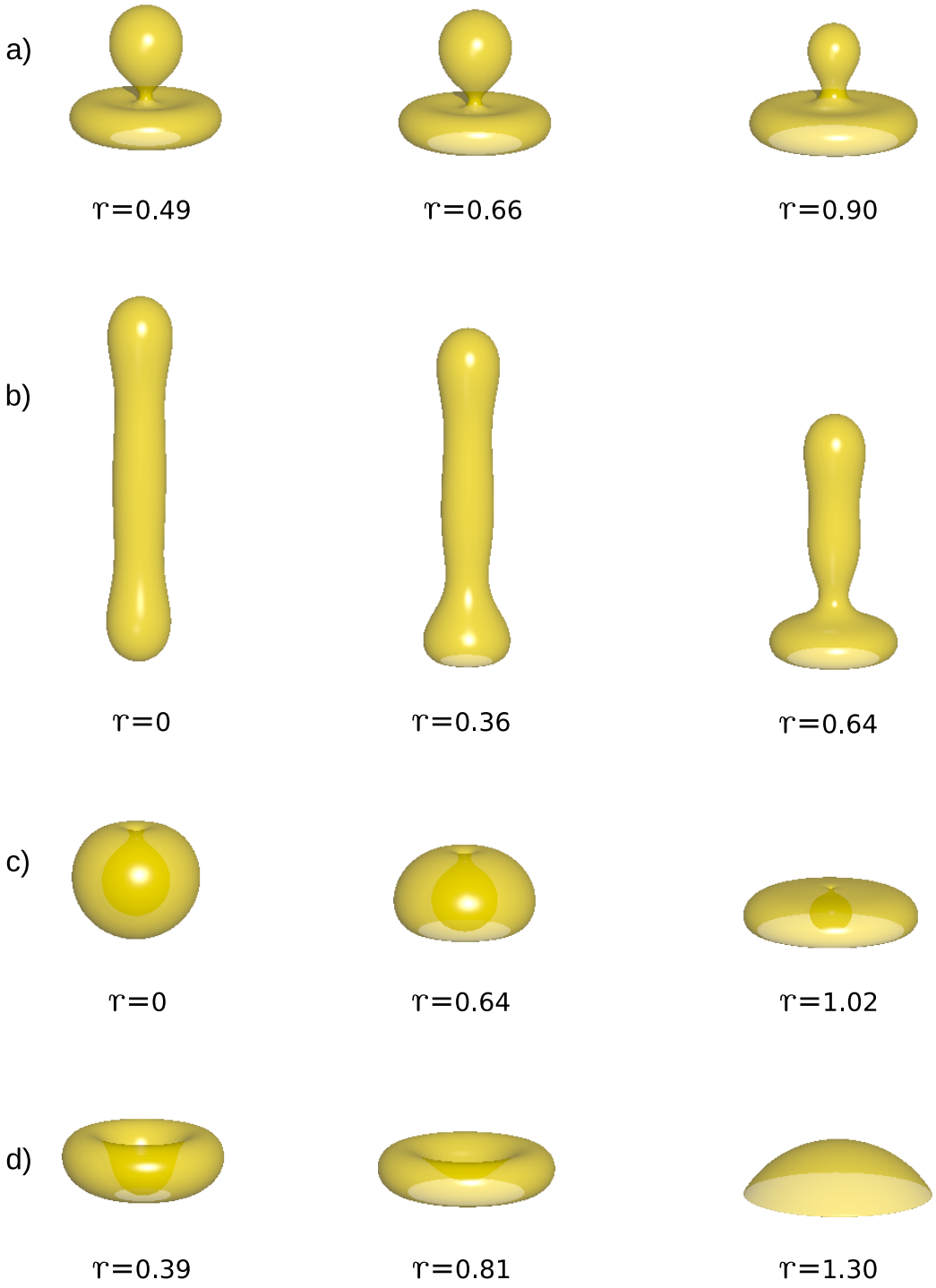

Figure 4.5: 3D shapes for the reduced volume, $v = 0.545$ and reduced spontaneous curvature, $c_0 = 0.0$ and different values of the reduced adhesion radius, r. (a) new branch of solutions: oblate-bead, (b) prolate, (c) stomatocyte, (d) oblate branch. The area with a lighter shade shows the region of the membrane attached to the flat surface.

one for the largest value of the reduced adhesion radius, r. In the middle, the solutions for the intermediate values are presented. For the prolate and stomatocyte branches, the first profiles are plotted for $r = 0$. Thus, they are identical to the free vesicle. For the oblate branch, the first profile is plotted for $r = 0.39$. It has to be recalled that the solution for free vesicles of the oblate branch for the small values of the reduced volume self-intersect or have concave shapes, which makes it impossible to maintain this shape when the vesicle adheres to a flat surface – at least when the adhesion radius is small. When the adhesion radius for oblate and stomatocyte vesicles is sufficiently large, we obtain the solutions where the membrane at the south pole and the north pole of the vesicle touches each other. This is reflected in the values of the elastic energy where we observe a cusp in the curve plotted for the elastic energy as a function of the reduced adhesion radius, as shown in the inset of Fig. 4.4e for oblates. However, for stomatocytes, this transition is smooth. The new family of shapes shown in Fig. 4.4a is stable only in the case of adhered vesicles. Thus, the first stable solution is obtained for the reduced adhesion radius greater than zero. It is worth stressing that adhesion may induce such a new transformation of a vesicle which leads to the shape not observed in the case of free vesicles and is shown in Fig. 4.4a.

The plot of the values of the elastic energies as a function of the reduced adhesion radius for all four branches and for the full range of stability is shown in Fig. 4.4e. Considering the values of the elastic energy, we can conclude that the most probable configurations for the adhered vesicles with the reduced spontaneous curvature $c_0 = 0$ and the reduced volume $v = 0.545$ are the configurations which originated from the stomatocyte branch for low adhesion radius and oblate vesicle for large adhesion radius. Since the adhesion radius depends on the strength of the adhesion, we can expect that for the small adhesion strength, we should observe stomatocyte-like configurations (Fig. 4.4c), and for large adhesion strength we should observe oblate-like configurations (Fig. 4.4d). It is also worth noting that prolate-like (Fig. 4.4b) vesicles are not likely to survive in an adhered state. We have performed a series of calculations for oblate vesicles with a few values of the reduced volume and zero reduced spontaneous curvature to check how much of the vesicle membrane can adhere to the flat surface. We have found that despite large values of the reduced volume, the vesicles can be deformed in such a way that a relatively large part of the membrane can adhere to a flat surface. We have calculated that the maximal adhesion radius can be as large as $r = 0.70$ in the case of the reduced volume $v = 0.98$, and for $v = 0.90$, it is as large as $r = 0.96$. The shape of the non adhered part of the vesicles is approximately spherical near the end of their stability range. It is interesting to note that the height of the vesicle increases when larger and larger part of the vesicle

membrane is attached to the flat surface. The relation between the height of the vesicle and the adhesion process may be useful in the analysis of experimental results. The changes in the height of a vesicle may indicate potential changes in the strength of the adhesion.

The solutions for oblate and prolate shapes with the reduced spontaneous curvature $c_0 = 0$ always have up-down symmetry. When the spontaneous curvature is sufficiently different from zero, this up-down symmetry is broken, and the solutions with pear-like shape are obtained. In such a case, the adhered vesicle may behave in a different way depending on whether the smaller or, the larger spherical part of the membrane adheres to the flat surface. In Fig. 4.6, we present the calculations performed for the reduced spontaneous curvature $c_0 = 2.4$ and the reduced volume $v = 0.80$.

In the first row (Fig. 4.6a), we present the shape transformations caused by the attachment of the smaller spherical part of the vesicle to the flat surface. It can be noticed that the neck which connects the two spherical parts of the vesicle gets smaller when the adhered surface area of the vesicle membrane gets larger and larger, i.e., the adhesion radius is increasing. It has been estimated that $r = 0.51$ is the limiting reduced adhesion radius for the stability of the vesicle. The limiting shape of the vesicle at $r = 0.51$ is shown in the last column of Fig. 4.6a. We can speculate that such behavior may lead to the budding of the vesicle due to its adhesion. The vesicle behaves in quite the opposite way when it is attached to the surface from the other end, the larger spherical part. When the adhesion radius is increased, the neck widens until the limiting configuration is obtained for $r = 0.61$, as shown in Fig.4.6b. Thus, the vesicles which have a pear shape may behave in a different way when adhered, depending on which part of the vesicle is attached to the adhesion surface. In Fig. 4.6c, we present the shape transformation of a prolate vesicle when the adhesion radius is increased. It is worth noting that the attached prolate vesicles are stable for a wide range of the reduced adhesion radius $0 < r < 0.82$. The second interesting feature of the adhered prolate vesicle is it's unique shape which is different from any free vesicle shape obtained in the spontaneous curvature model (see the rightmost configuration in Fig. 4.6c). It can be expected that it will be more probable to change the shape from prolate to oblate for adhered vesicles with such a large reduced volume when the radius of adhesion is high, and indeed this is what we can deduce from the plot of the elastic energy (see Fig. 4.6e). However, it is still surprising that metastable adhered prolate vesicles exist for $0.6 < r < 0.82$.

In Fig. 4.8, the possible shape transformation of vesicles for the reduced volume $v = 0.7277$ and the reduced spontaneous curvature $c_0 = 2.4$ are presented. They

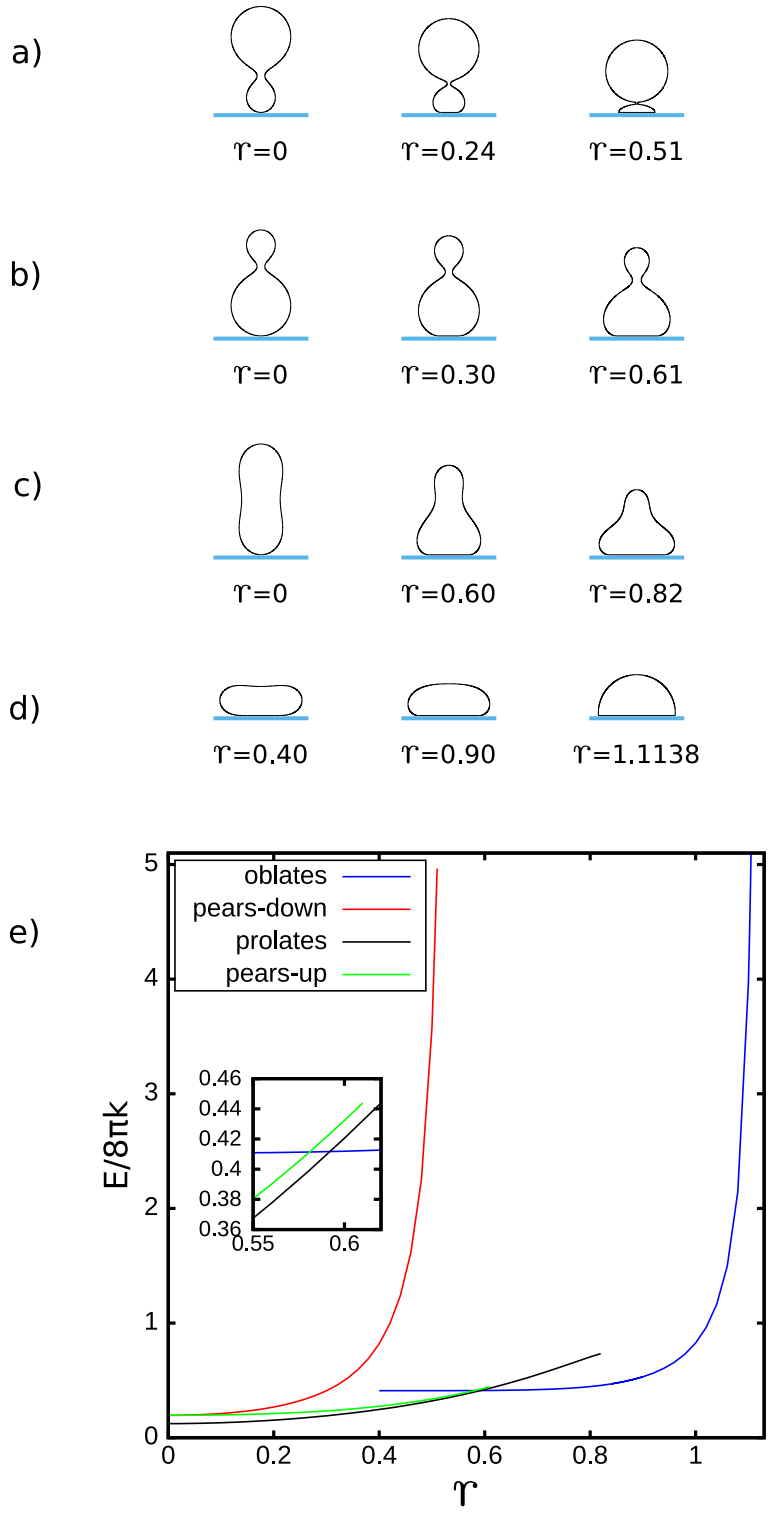

Figure 4.6: Shape profiles for the reduced volume, $v = 0.80$ and reduced spontaneous curvature, $c_0 = 2.4$ and different values of the reduced adhesion radius, r. The pear branch with the vesicle attached to the surface with smaller (a) and larger (b) bead, the prolate (c) and oblate (d) branch. (e) Elastic energy, $E/(8\pi\kappa)$, as a function of the reduced adhesion radius, r, for different families of solutions for the reduced volume, $v = 0.80$ and the reduced spontaneous curvature, $c_0 = 2.4$. The inset shows the values of the bending energy for different configurations at the intersection.

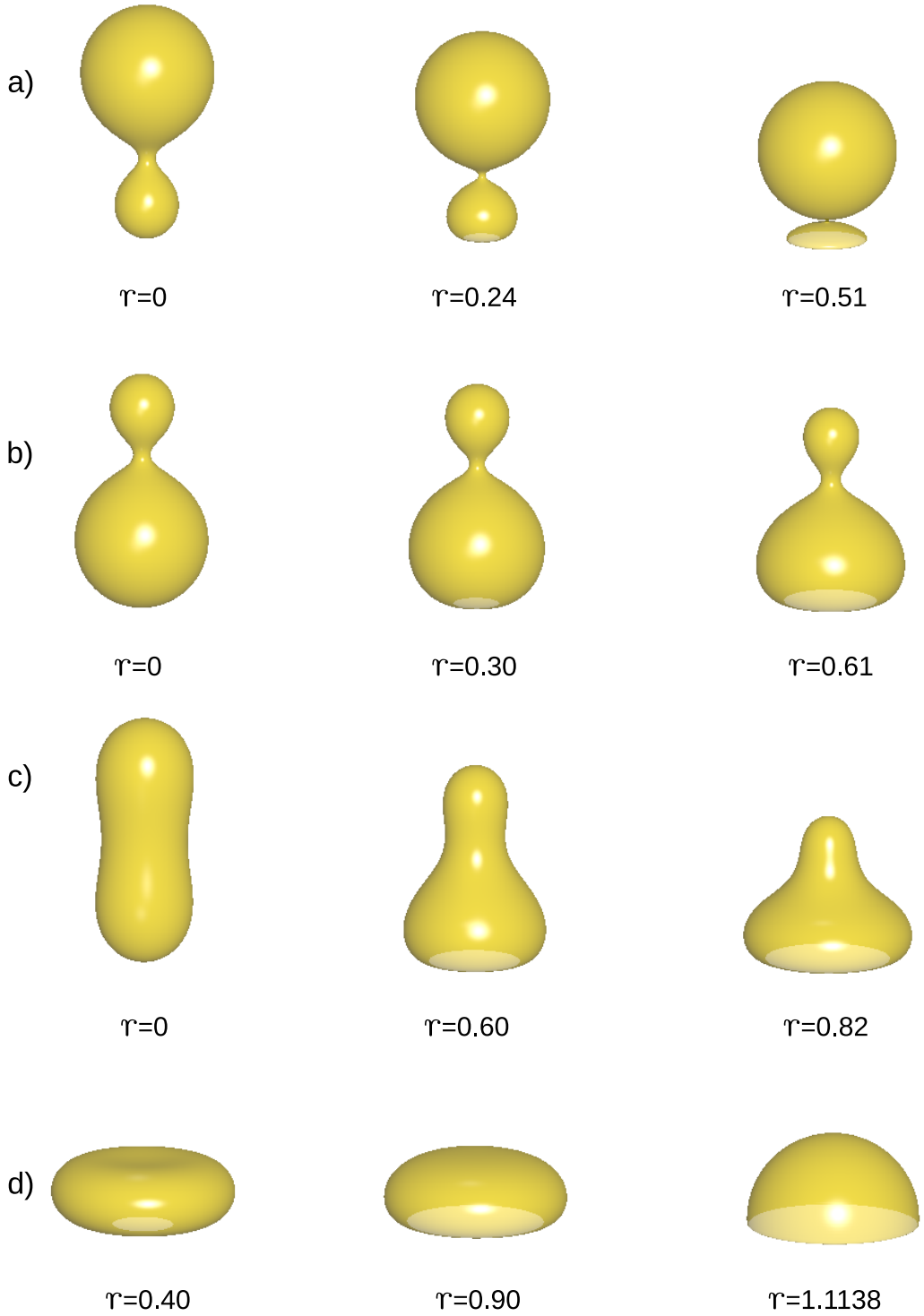

Figure 4.7: 3D shapes for the reduced volume, $v = 0.80$ and reduced spontaneous curvature, $c_0 = 2.4$ and different values of the reduced adhesion radius, r. The pear branch with the vesicle attached to the surface with smaller (a) and larger (b) bead, the prolate (c) and oblate (d) branch. The area with a lighter shade shows the region of the membrane attached to the flat surface.

look similar to the transformations presented in Fig. 4.6, which are performed for the same reduced spontaneous curvature and larger reduced volume. However, there is a significant difference. For the smaller reduced volume, the stability range of adhered pear vesicles is increased to as large a reduced adhesion radius as $r = 0.9$. Surprisingly, the stability range of the prolate vesicle is substantially decreased. We have obtained adhered prolate vesicles only for the reduced adhesion radius in the range $0 < r < 0.14$. For this range of the reduced adhesion radius, the shape of the vesicle does not change significantly. There are no longer even metastable configurations obtained which are significantly different from the shapes of free vesicles as it was in the case of larger reduced volume. For $v = 0.8$, the stability range of pear-like shape was smaller than the stability range of prolate-like vesicles, but for $v = 0.7277$ it is reversed. We may speculate that budding of the vesicles due to adhesion is more probable for the vesicles with lower reduced volume, v. The adhered oblate vesicles are stabilized for larger reduced adhesion radii as shown in the elastic energy plot in Fig. 4.8e.

The prolate vesicles are stabilized by larger spontaneous curvature. Here, we would like to examine how such prolate vesicles behave when attached to a flat surface. The shape profiles calculated for the reduced volume $v = 0.545$ and the reduced spontaneous curvature $c_0 = 3.0$ are shown in Fig. 4.10. We can see that the range of the reduced adhesion radius for attached stable prolate vesicle is quite wide $0 < r < 0.8$. For sufficiently large r, the vesicle is composed of two parts connected by a small neck. One part attached to the surface has an oblate shape, and the second part forms a prolate-shape bud. It is interesting to note that for the same values of the reduced adhesion radius, two different configurations of vesicles composed of two parts connected by a small neck can exist. In the first configuration, this bud has a spherical shape (Fig. 4.10a), and in the second configuration, this bud has a prolate shape (Fig. 4.10b). The configuration with the spherical bud is more stable for larger values of the reduced adhesion radius, and the configuration with the prolate bud is stable for smaller values of the reduced adhesion radius as shown in the plot of the elastic energy in Fig. 4.10d. There is a value of the reduced adhesion radius, r, at which these two configurations with buds have the same elastic energy. It might indicate the possibility of an easy transformation from one configuration to the other. Similarly, at a larger value of the reduced adhesion radius, the oblate vesicle (Fig. 4.10c) and the oblate vesicles with a bud (Fig. 4.10a), have the same energy. We can also notice that the spherical bud changes its shape with the increasing reduced adhesion radius, r. The bud gets smaller and smaller until it disappears approximately at $r = 1.12$. It is also interesting to note that the neck radius increases with the increase in adhesion of the oblate vesicles with a spherical bud, but the opposite happens for the oblate vesicles

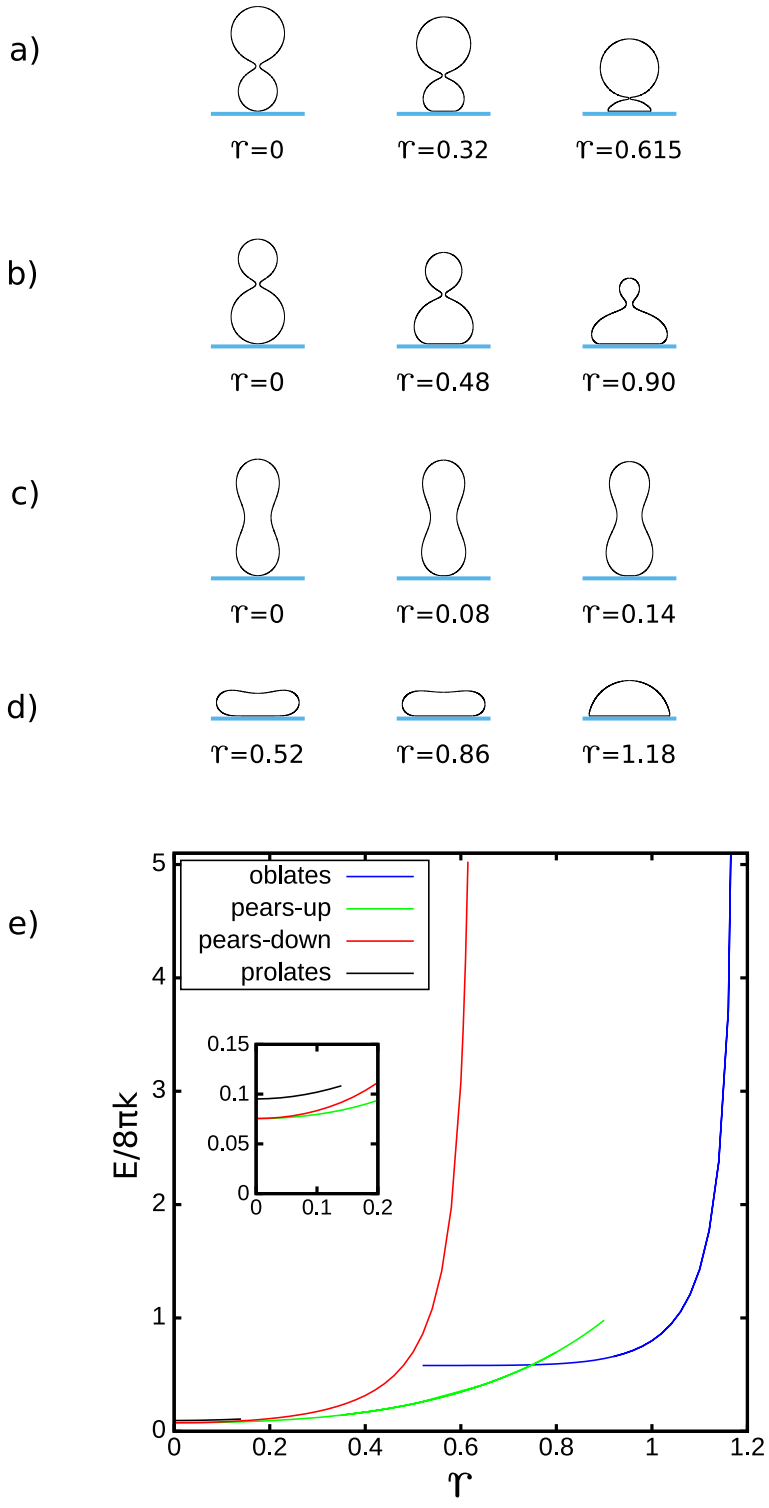

Figure 4.8: Shape profiles for the reduced volume, $v = 0.7277$ and reduced spontaneous curvature, $c_0 = 2.4$ and different values of the reduced adhesion radius, r. The pear branch with the vesicle attached to the surface with smaller (a) and larger (b) bead, the prolate (c) and the oblate (d) branch. (e) Elastic energy, $E/(8\pi\kappa)$, as a function of the reduced adhesion radius, r, for different families of solutions for the reduced volume, $v = 0.7277$ and the reduced spontaneous curvature, $c_0 = 2.4$. The inset shows the values of the bending energy for small reduced adhesion radii.

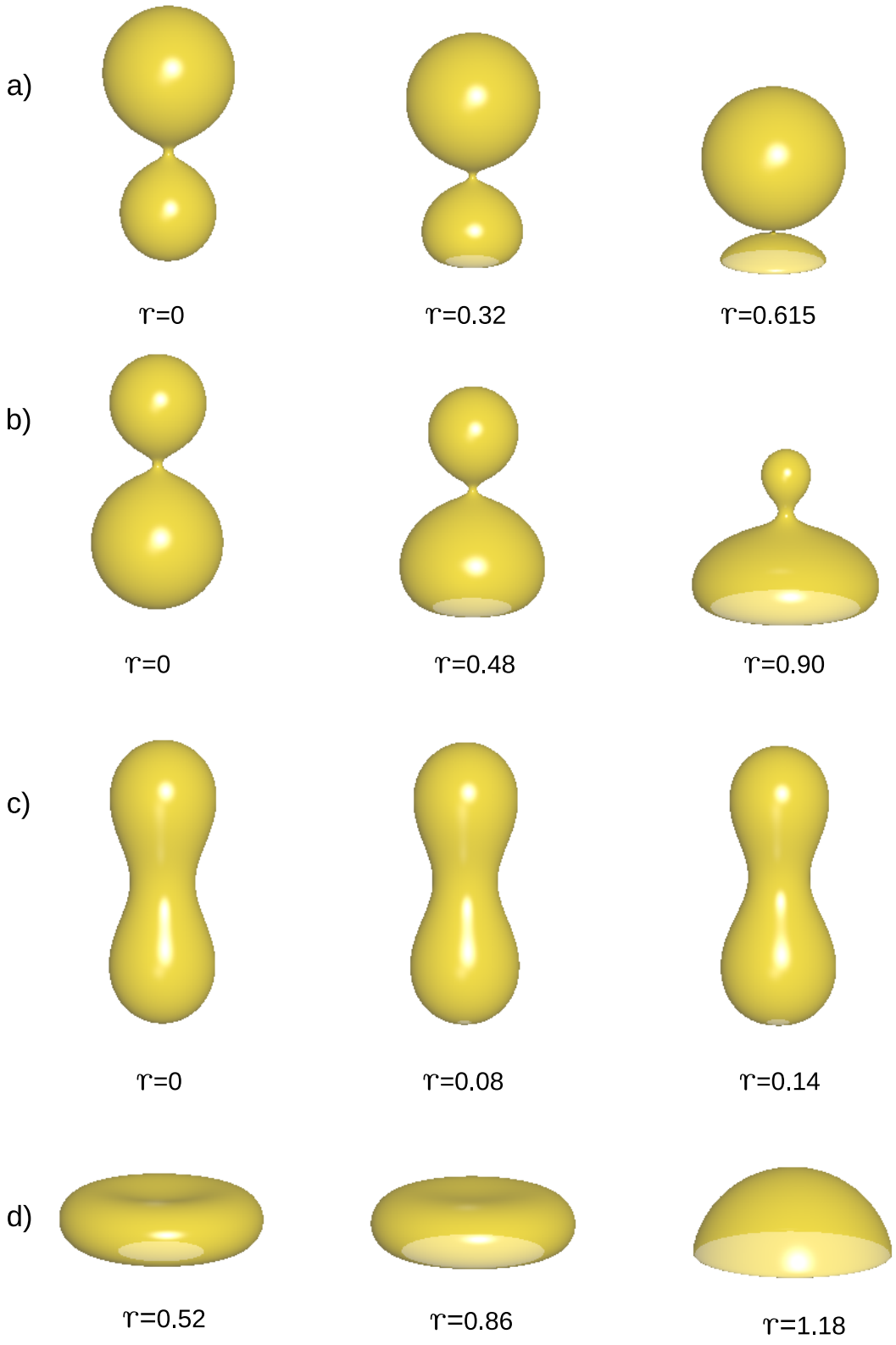

Figure 4.9: 3D shapes for the reduced volume, $v = 0.7277$ and reduced spontaneous curvature, $c_0 = 2.4$ and different values of the reduced adhesion radius, r. The pear branch with the vesicle attached to the surface with smaller (a) and larger (b) bead, the prolate (c) and the oblate (d) branch. The area with a lighter shade shows the region of the membrane attached to the flat surface.

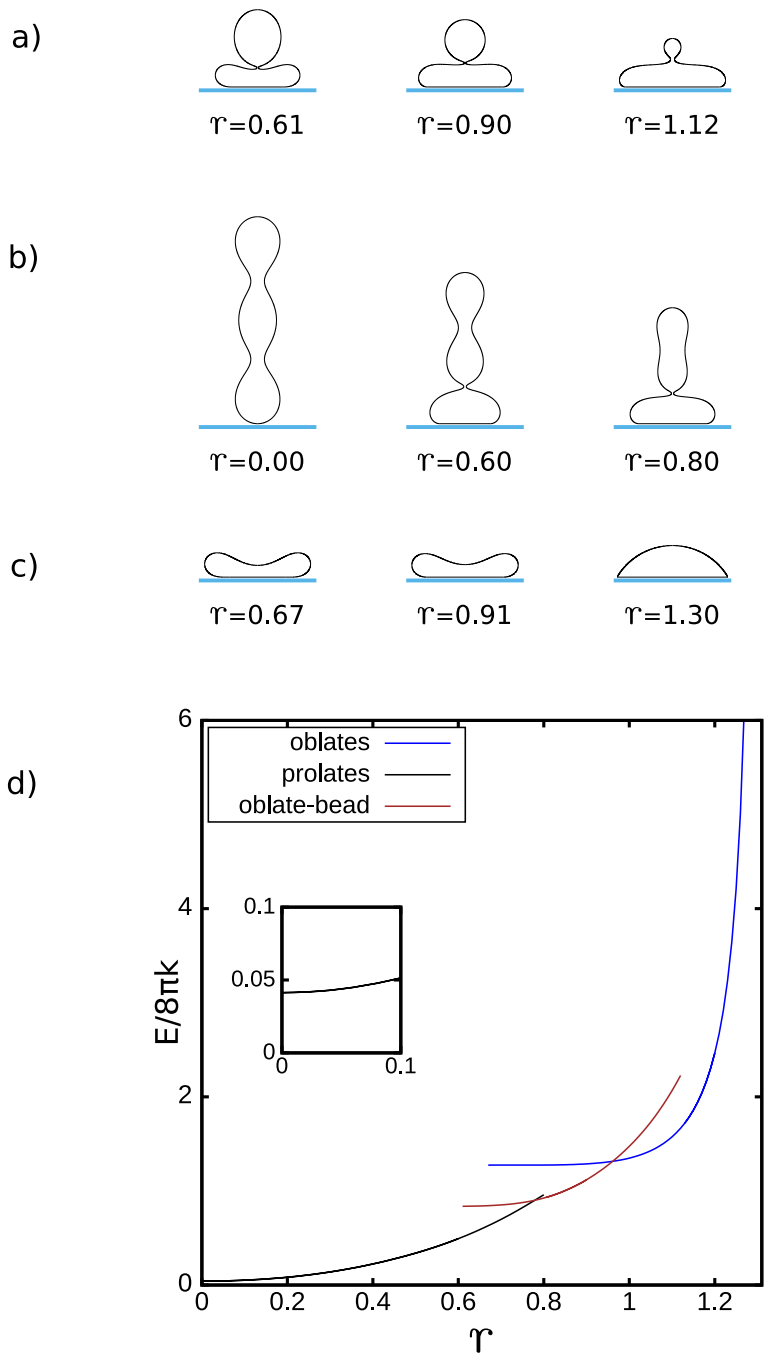

Figure 4.10: Shape profiles for the reduced volume, $v = 0.545$ and reduced spontaneous curvature, $c_0 = 3.0$ and different values of the reduced adhesion radius, r. (a) the oblate with a bead branch, (b) the prolate branch, (c) the oblate branch. (d) Elastic energy, $E/(8\pi\kappa)$, as a function of the reduced adhesion radius, r, for different families of solutions for the reduced volume, $v = 0.545$ and the reduced spontaneous curvature, $c_0 = 3.0$. The inset shows the values of the bending energy for small reduced adhesion radii.

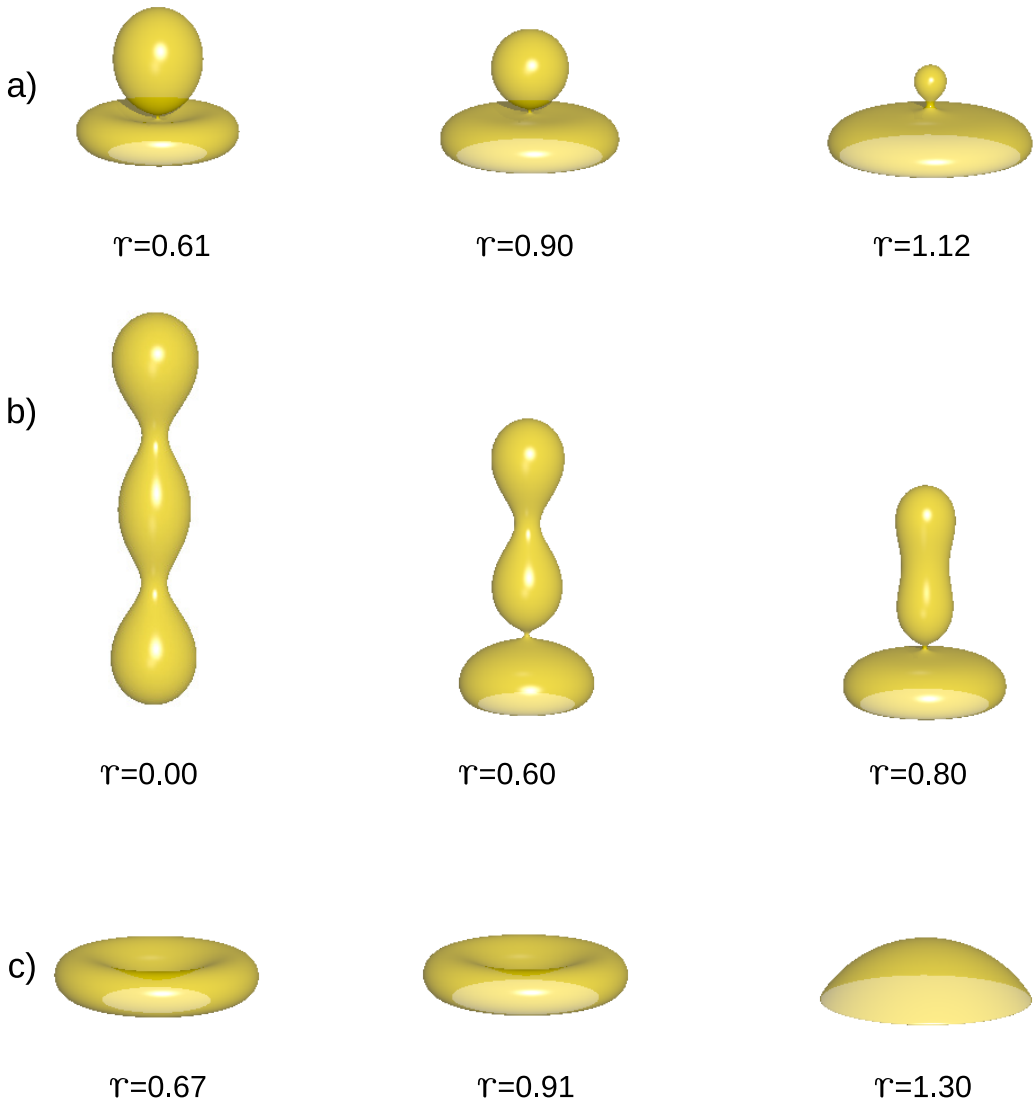

Figure 4.11: 3D shapes for the reduced volume, $v = 0.545$ and reduced spontaneous curvature, $c_0 = 3.0$ and different values of the reduced adhesion radius, r. (a) the oblate with a bead branch, (b) the prolate branch, (c) the oblate branch. The area with a lighter shade shows the region of the membrane attached to the flat surface.

with a prolate-like bud. The prolate bud also gets smaller in length on increasing adhesion. For the largest values of r, the only stable configurations are adhered vesicles with oblate shape (Fig. 4.10c). There is a range of values of the reduced adhesion radius where the stable solutions for all three configurations of adhered vesicles are obtained as shown in Fig. 4.10d.

In the calculations for $v = 0.545$, we have shown that the increasing reduced adhesion radius, r causes the decrease in the size of the spherical bead for the vesicles composed of two parts connected by a small neck. Here, we would like to examine the shape transformations when we start with the free vesicle composed of two equal spherical beads separated by a small neck. Such free vesicles are obtained for the reduced volume $v = 0.705$ and the reduced spontaneous curvature $c_0 = 3.0$. In Fig. 4.12, we present possible transformations of a symmetric prolate and oblate vesicle for $v = 0.705$ and $c_0 = 3.0$. We can see that also in this case when the reduced adhesion radius r is increasing, the bead which is not attached to the surface stays spherical and gets smaller. The bead which is attached to the surface becomes oblate and gets larger. For sufficiently large r, the spherical bead disappears and the only stable solutions are the adhered oblate vesicles. We can see from the plot of the elastic energy (Fig. 4.12c) that the adhered prolate vesicles are stable for quite a wide range of the reduced adhesion radius $0 < r < 1.0$. The adhered oblate vesicles are obtained only for larger values of the reduced adhesion radius $0.55 < r < 1.2$.

In the case of pear-shaped adhered vesicles, we have observed so far that the configurations with a larger spherical part attached to the flat surface have a wider range of stability. In Fig. 4.14, we present the vesicle shapes for the reduced volume $v = 0.89$ and the reduced spontaneous curvature $c_0 = 3.0$. It is quite surprising that for such choice of parameters, the pear-shaped configurations with the smaller sphere attached to the surface (Fig. 4.14a) have a wider range of stability than the pear-shaped configurations with the larger bead attached to the surface (Fig. 4.14b). The latter solutions are stable only up to $r = 0.02$. For larger r, adhered prolate vesicles become stable up to $r = 0.68$ (Fig. 4.14c). The adhered oblate vesicles are stable for the full range of the reduced adhesion radius, r as shown in the plot of the elastic energy in Fig. 4.14e.

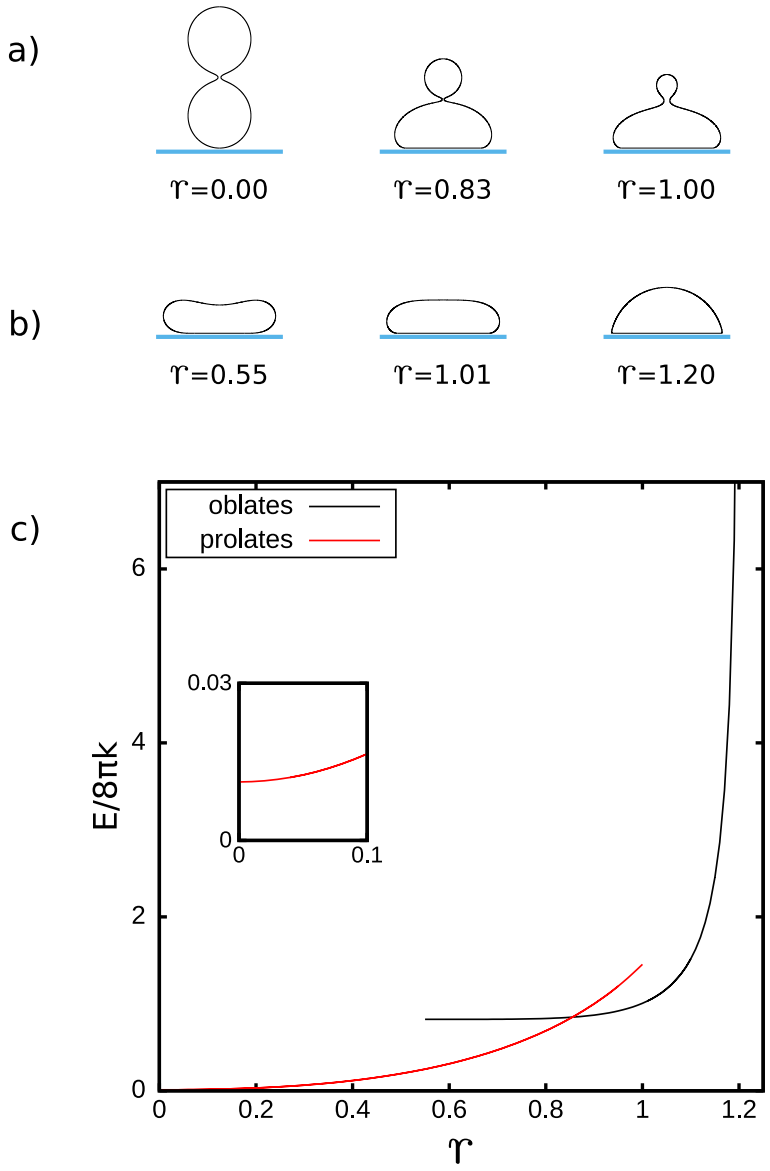

Figure 4.12: Shape profiles for the reduced volume, $v = 0.705$ and the reduced spontaneous curvature, $c_0 = 3.0$ and different values of the reduced adhesion radius, r. (a) prolate and (b) oblate branch. (c) Elastic energy, $E/(8\pi\kappa)$, as a function of the reduced adhesion radius, r, for different families of solutions for the reduced volume, $v = 0.705$ and the reduced spontaneous curvature, $c_0 = 3.0$. The inset shows the values of the bending energy for small reduced adhesion radii.

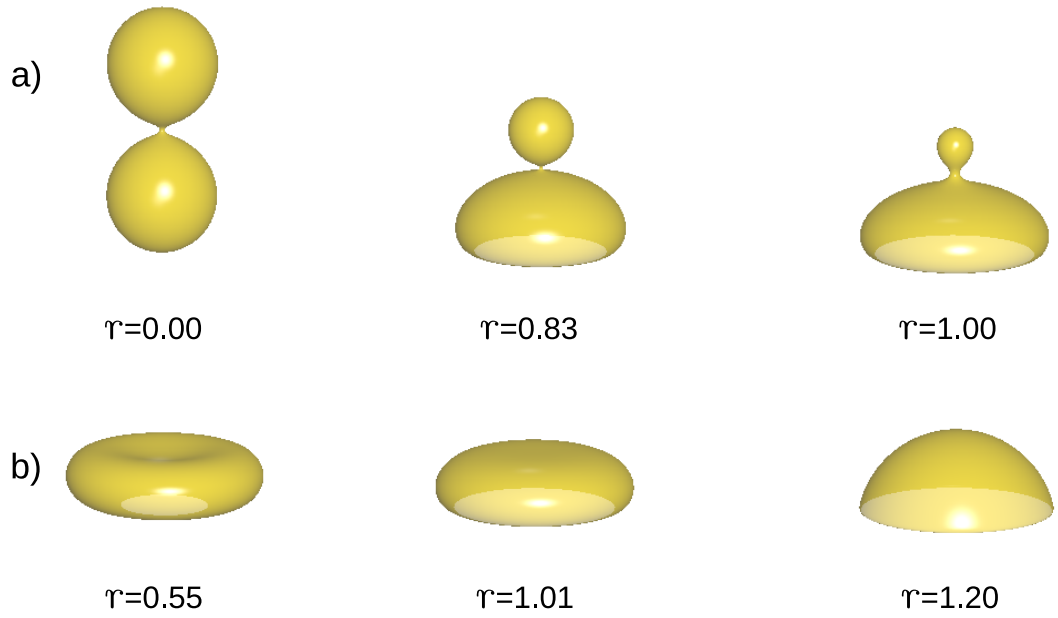

Figure 4.13: 3D shapes for the reduced volume, $v = 0.705$ and the reduced spontaneous curvature, $c_0 = 3.0$ and different values of the reduced adhesion radius, r. (a) prolate and (b) oblate branch. The area with a lighter shade shows the region of the membrane attached to the flat surface.

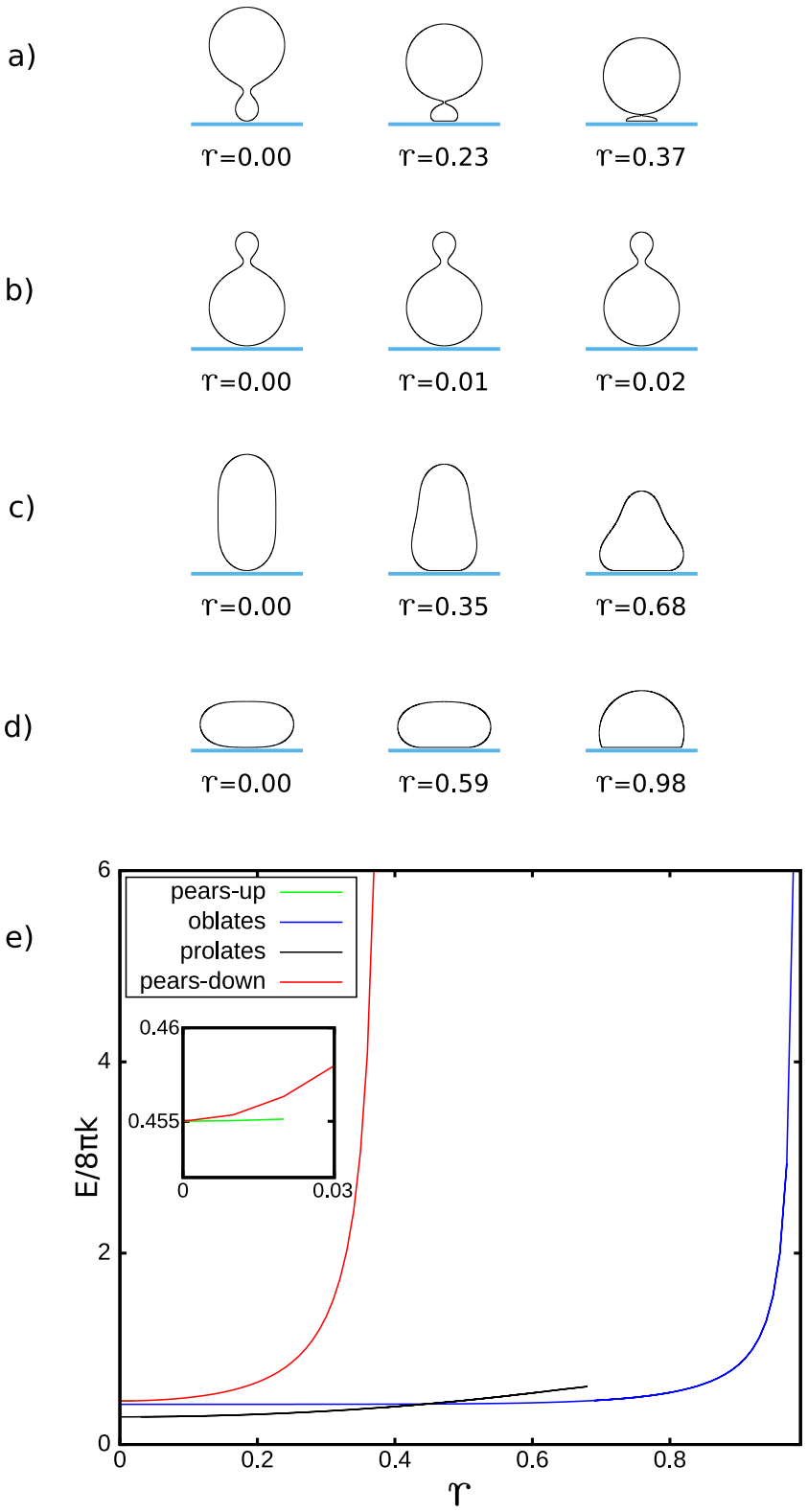

Figure 4.14: Shape profiles for the reduced volume, $v = 0.89$ and the reduced spontaneous curvature, $c_0 = 3.0$ and different values of the reduced adhesion radius, r. The pear branch with the vesicle attached to the surface with smaller (a) and larger (b) bead, the prolate (c) and oblate (d) branch. (e) Elastic energy, $E/(8\pi\kappa)$, as a function of the reduced adhesion radius, r, for different families of solutions for the reduced volume, $v = 0.89$ and the reduced spontaneous curvature, $c_0 = 3.0$. The inset shows the values of the bending energy for small reduced adhesion radii.

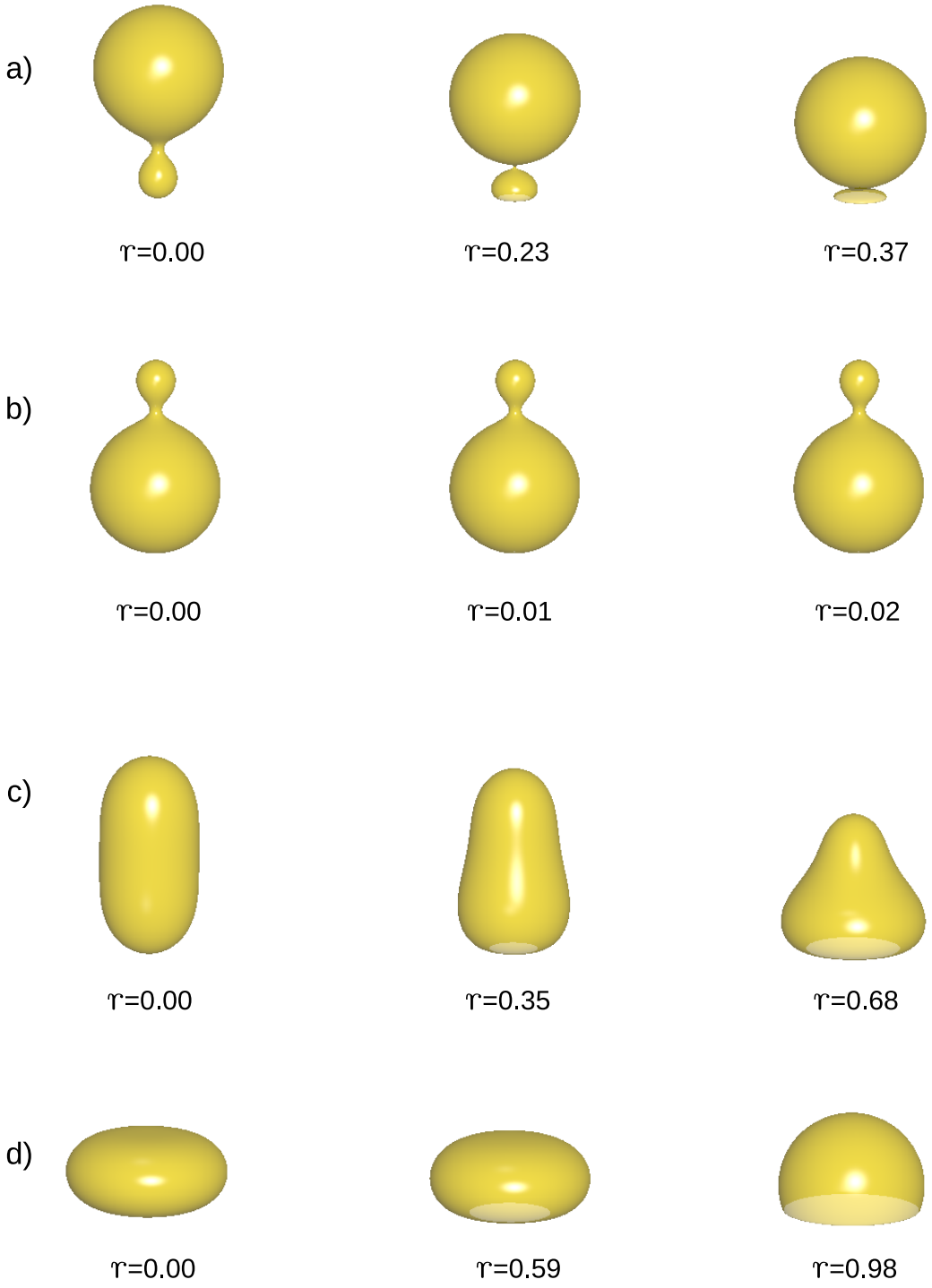

Figure 4.15: 3D shapes for the reduced volume, $v = 0.89$ and the reduced spontaneous curvature, $c_0 = 3.0$ and different values of the reduced adhesion radius, r. The pear branch with the vesicle attached to the surface with smaller (a) and larger (b) bead, the prolate (c) and oblate (d) branch. The area with a lighter shade shows the region of the membrane attached to the flat surface.

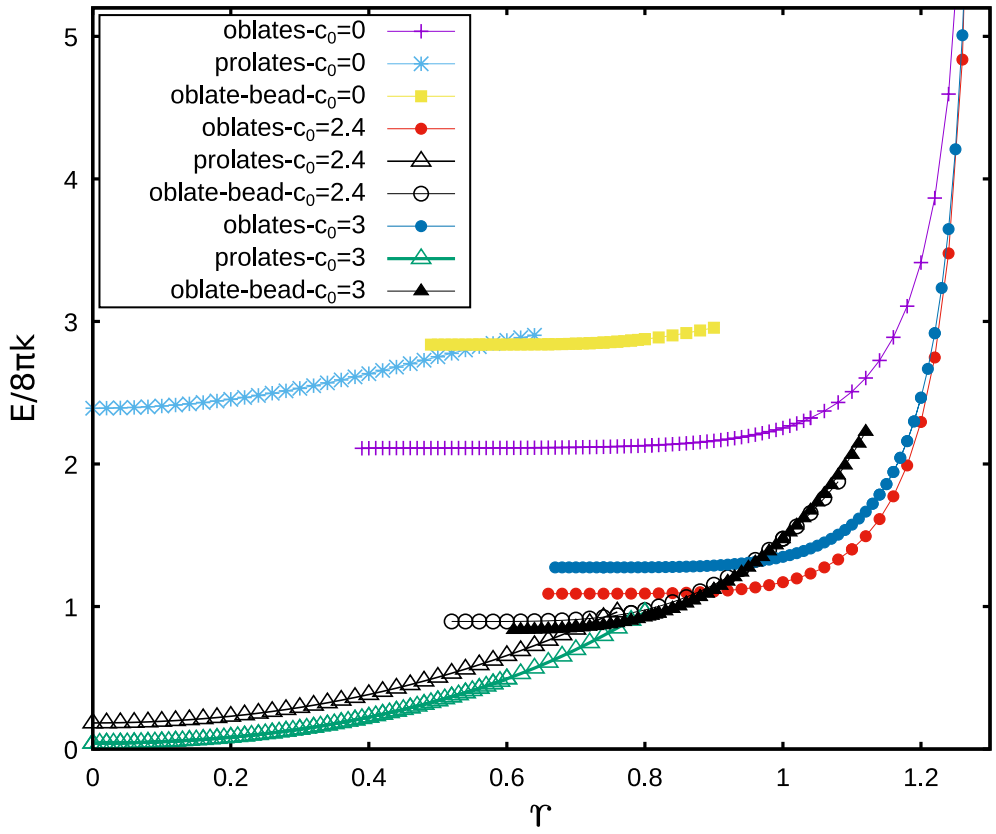

Figure 4.16: Comparison of elastic energy, $E/(8\pi\kappa)$, as a function of the reduced adhesion radius, r, for different families of solutions and across few reduced spontaneous curvatures $c_0 = 0, 2.4, 3$. The reduced volume $v = 0.545$.

In Fig. 4.16, we compare the stability range of different families of solutions like oblates, prolates, and oblate-bead for different values of c_0. We can see that as the c_0 increases, the stability range of the oblate reduces with the largest range obtained for $c_0 = 0$ and the lowest for $c_0 = 3$. The range of the prolate branch however increases with the increase in c_0, suggesting an increase in the probability of obtaining prolate shapes with the increase of c_0 under adhesion. For the oblate-bead branch, the increase in c_0 causes the oblate-bead shapes to be stable for larger reduced adhesion radii.

In Fig. 4.17, we have shown the shape profiles of vesicles obtained on changing the c_0 for a given value of reduced adhesion radius, r. On comparing the shape transitions observed by increasing the spontaneous curvature with that obtained by increasing the area of adhesion for a given branch of vesicle shape, we notice that both these kinds of shape transitions are qualitatively similar in the case of prolate and oblate vesicles but are different for the oblate-bead shapes. An increase in c_0 leads to the closing of the neck at the lower part of the prolate vesicle. Closing of the neck is also induced on an increase in c_0 for the oblate-bead vesicles. This is unlike what is observed for the oblate-bead branch on increasing the reduced adhesion radius r, for a given v and c_0. An increase of c_0 therefore promotes budding in prolate-like

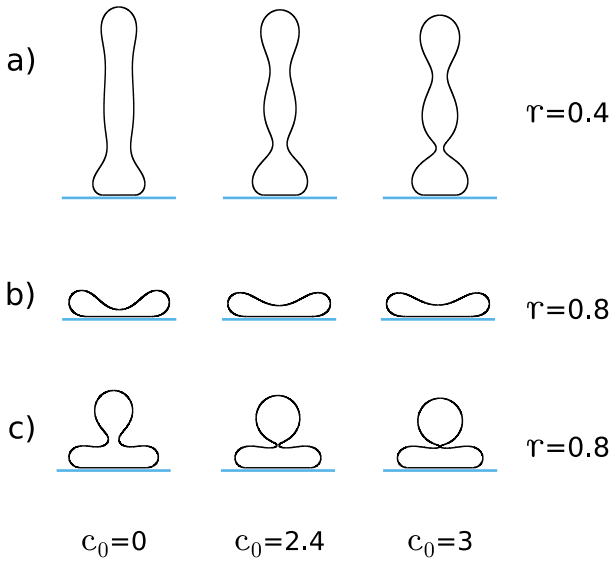

Figure 4.17: Effect of change in c_0 from $c_0 = 0$ to $c_0 = 3$ on the shape profiles of (a) prolate vesicles for $r = 0.4$ (b) oblate vesicles for $r = 0.8$ and (c) oblate-bead vesicles for $r = 0.8$. The reduced volume $v = 0.545$.

and oblate-bead-like vesicles. The trend of the bending energy within the range of c_0 values studied in Fig. 4.16 shows that an increase in c_0 for a constant adhesion area lowers the bending energy of the prolate shapes – thereby suggesting an increase in stability and an increased probability of obtaining prolates for larger c_0 under fixed adhesion potential. $c_0 = 2.4$ and $c_0 = 3$, however, are the preferred reduced spontaneous curvature values for the adhered oblate and adhered oblate-bead (small r region) vesicles respectively – for which they have the lowest bending energy in the range of the investigated spontaneous curvatures.

4.3 Summary and Conclusions

We have studied the behavior of lipid vesicles adhered to a flat surface within the framework of the spontaneous curvature model. The calculations were performed for a few values of the reduced spontaneous curvature and reduced volume. We have identified the stability range of different branches of solutions as a function of the reduced adhesion radius. We have observed the formation of new structures caused by the adhesion of a vesicle to a flat surface. We have discovered that the adhesion of a vesicle may cause the formation of a spherical or a prolate bud connected by a small neck to the vesicle adhered to the flat surface. Such a shape transformation may lead to budding, which may be important in biological processes. It is important to note that we were able to observe budding for $c_0 = 0$ under adhesion, which has not been observed for this spontaneous curvature for the free state of vesicles. We have

observed that the width of the neck connecting the bud depends on the size of the vesicle patch attached to the surface. Thus, it may be possible to induce or arrest the budding of the vesicles or biological cells with the change of the adhesion potential. We have also observed that the tendency of neck widening or neck closure with the increase in adhesion depends on the shape of the vesicle. Thus, adhesion can either induce fusion or fission, depending on the shape. The shape of the vesicle and the adhesion potential strength can thus influence the budding process. In many cases, we have obtained multiple solutions with the same energy for the same set of parameters. Such degeneracy may result in an interesting phenomenon where the adhered vesicle can be transformed from one state to another state of the same energy. We have also identified that the behavior of oblate-bead shapes is different under the change of c_0 for a given r than under the change of r for a given c_0. In the former case, it leads to the narrowing, and in the latter, it leads to the widening of the neck.

The adhesion of a membrane surrounding biological cells is a phenomenon that may be important in many biological processes. Thus, it will be valuable to understand such processes based on the studies performed within relatively simple theoretical models of membranes. We have demonstrated that adhesion may lead to many qualitatively different shape transformations depending on the reduced volume and the reduced spontaneous curvature. We may speculate that such versatile behavior may be exploited in many biological processes. We hope that the results presented here will help understand the behavior of the biological systems observed in experiments and will help design new experiments.

Chapter 5

Study of the single component vesicle system by varying the adhesion strength of the flat surface

This chapter explores the study of the vesicle system under adhesion where the adhesion is introduced in the form of adhesion strength, W of the flat surface by which it attracts the vesicle membrane touching the surface. The calculations have been carried out under the Helfrich spontaneous curvature model. Here, we have examined the influence of the spontaneous curvature, adhesion strength and the reduced volume on the stability of the vesicle shapes under adhesion. We have identified the minimum adhesion strength required to obtain a transition between a free vesicle state and it's adhered state for vesicles belonging to the different shape classes. We have also investigated possible shape transitions between different classes of adhered vesicles which is a step forward in our investigation of the single component systems under adhesion – from our previous calculations in chapter 4. It has been shown that the budding of an adhered vesicle may be induced by the change of the adhesion strength. Interestingly, an increase in spontaneous curvature of the vesicle membrane has been found to encourage adhesion. The importance of the free vesicle shape for it's susceptibility to adhesion has been discussed.

5.1 Study of vesicle adhesion by changing the adhesion strength of the substrate

In this second part of our study, the vesicles are not constrained to be adhered to the surface with some enforced value of the contact area, but instead, the system can choose to be either in a free state (non-adhered state) or an adhered state depending on the adhesion strength value associated to the flat substrate. Here, we therefore quantify the effective adhesion potential by the adhesion strength of the substrate. Different values of the adhesion strength may be related to different materials used to build the substrate or different compositions of the vesicle membrane. The change of

the adhesion strength may also result from the change of thermodynamic parameters [102]. The size of the surface area of a vesicle which is in contact with the surface due to adhesion may depend on the strength of the interactions or on the concentration of the sticker molecules [103, 104]. We investigate the stability of vesicles adhered to a flat and rigid substrate with different values of reduced adhesion strength, w of this underlying substrate. We have examined the shapes of adhered vesicles characterized by different values of reduced spontaneous curvature, c_0 for a few values of the reduced volume, v. We have determined the minimal reduced adhesion strength, w for which adhered vesicles become more stable than a free vesicle. The range of stability of different classes of vesicle shapes for different reduced adhesion strength, w was also examined. Possible shape transitions between adhered vesicles were also studied.

The ensemble which mimics the experimental conditions that we investigate is the one with a fixed topology, constant surface area, A and constant volume, V. Such a physical situation is described by the energy functional 3.4.6 which we numerically minimize to obtain the equilibrium shapes of the vesicles. Again, as no topology changes are considered, the integral of the Gaussian curvature contribution to the total energy is a constant value and is therefore neglected. The shapes are parameterized as shown in Eq. 3.1.7 and the adhesion is introduced in the form of adhesion strength as explained in the earlier sections.

The reduced free energy is denoted by $f = F/8\pi\kappa$, the reduced adhesion radius is denoted as $r_{adh} = R/R_s$, the reduced spontaneous curvature is $c_0 = C_0 R_s$ and the reduced adhesion strength is denoted as $w = WR_s^2/\kappa$.

The vesicles with zero membrane spontaneous curvature are investigated first. Compared to former studies [39] of adhesion of vesicles with the reduced spontaneous curvature $c_0 = 0$, we keep the reduced volume of the vesicle fixed. Without adhesion, for low reduced volume and $c_0 = 0$, the stable vesicles are stomatocytes. Free stomatocytes, however become unstable for larger values of reduced spontaneous curvature and reduced volume. For the reduced volume $v = 0.545$, it is possible to obtain three different solutions for free vesicles: stomatocyte, oblate, and prolate. Multiple solutions can be obtained not only for $v = 0.545$, but also for a wide range of the reduced volume. We have investigated how the stability of stomatocyte and oblate vesicles changes with the change of the adhesion strength. We have not been able to obtain stable adhered prolate vesicles when the calculations were performed for fixed reduced adhesion strength, w, and the radius of adhesion was free to change. Instead, the solution obtained from the numerical calculations was that of a free vesicle for the range of the reduced adhesion strength, w studied by us. In Fig. 5.1a, we show the change of the reduced free energy, f as a function of the reduced adhesion strength,

w. In Fig. 5.1b, the change of the reduced adhesion radius, r_{adh} as a function of the reduced adhesion strength, w is shown. From the dependence of the reduced free energy, f on the reduced adhesion strength, w, we can determine when the adhered vesicle becomes more stable than the free vesicle as shown in insets of Fig. 5.1a. In Fig. 5.1c and Fig. 5.1d, we show the evolution of the shapes for adhered oblate and stomatocyte vesicles with the change of the reduced adhesion strength, w. In the first column, the vesicles in a free state are shown as a reference point to the vesicles in adhered states. In the second column, the stable adhered vesicle shapes for the oblate and stomatocyte branch are presented (stable for the lowest reduced adhesion strength w). If we consider the states with the lowest energy, we can infer from Fig. 5.1a that initially for low adhesion strength, the stable vesicles are stomatocytes that are not adhered. However, the first stable adhered vesicles are oblate ones. The energy of the free stomatocytes is marked by the black dashed horizontal line, which is below the solid red line which denotes the energy of adhered oblate vesicles. These two lines intersect before the adhered stomatocytes (denoted by the solid black curve) become stable. Thus, we may speculate that adhesion may be accompanied by a change of vesicle shape from stomatocyte to oblate. This change of the shape takes place between the vesicles pictured in the last column of Fig. 5.1c and Fig. 5.1d – where the configurations with the same free energy are shown. The arrow indicates the direction of a possible energetically favorable shape transition where the stomatocyte vesicle would be flattened and transformed into an adhered oblate vesicle. In the fourth column of Fig. 5.1c and Fig. 5.1d, we show the limiting configurations which result from very large reduced adhesion strength, w. In the third column, the intermediate configurations are shown. As expected, we also notice that in the range of small w, smaller changes of the adhesion strength induce large changes of the adhesion radius for the oblate adhered vesicles as compared to that in the case of stomatocyte vesicles shown in Fig. 5.1b.

The transition from a free state to an adhered state depends on the reduced volume of a vesicle [39]. In order to examine this dependence, we have studied oblate vesicles for several values of the reduced volume, v. We have investigated the range of the reduced volume close to the limiting spherical shape. In Fig. 5.2, we present the plots which illustrate the dependence of the reduced adhesion radius, r_{adh}, the reduced free energy, f, and the smallest value of the reduced adhesion strength for which the adhered vesicles become more stable than the free vesicles, w_{min}, as a function of the reduced volume, v. The reduced adhesion radius corresponding to the reduced adhesion strength, w_{min} is denoted as r_{min}. It can be noted that the radius of adhesion does not change monotonically with v in the range $0.80 \leq v \leq 0.99$. For the smaller

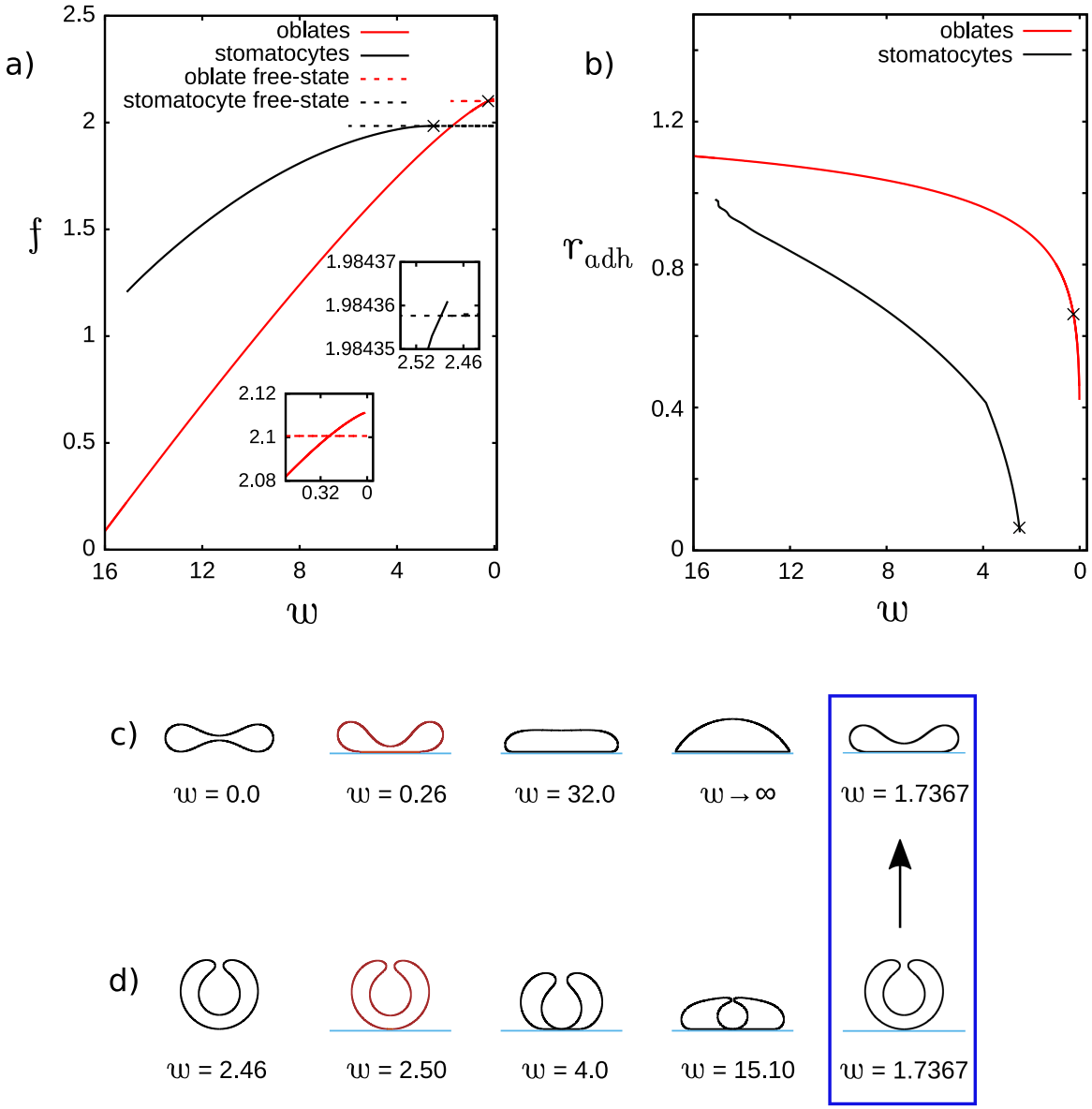

Figure 5.1: The dependence of (a) the reduced free energy, f, and (b) the reduced adhesion radius, r_{adh}, on the reduced adhesion strength, w, for the reduced volume, $v = 0.545$ and reduced spontaneous curvature, $c_0 = 0.0$. The crosses denote the points where the stable adhered vesicles for the smallest value of the adhesion strength w are formed. These points are obtained from the intersection of the reduced free energy curves visualized at larger scale in the insets. Shape profiles for oblate and stomatocyte vesicles are shown for the following sets of the parameters: (c) adhesion strength, $w = 0.0,\ 0.26,\ 32.0,\ w \to \infty,\ 1.7367$, adhesion radius, $r_{adh} = 0.0,\ 0.6611,\ 1.1596,\ 1.2999,\ 0.8656$. (d) adhesion strength, $w = 2.46,\ 2.50,\ 4.0,\ 15.10$ (limiting shape), 1.7367, adhesion radius, $r_{adh} = 0.0,\ 0.0636,\ 0.4229,\ 0.9827,\ 0.0$. The shapes at the intersection of dashed black (free stomatocyte) and solid red (adhered oblate) curves are shown in the blue frame. The profiles pictured in red are the stable adhered configurations obtained for the lowest adhesion strength w.

values of v in this range, r_{min} decreases with increasing v and for the larger values of v, r_{min} increases with v. These two tendencies can be explained when we look at the shape profiles of the adhered vesicles shown in Fig. 5.2. In the range of smaller v, the adhered vesicle has a concave shape, while in the range of larger v, it's shape is convex. In the intermediate range at about $v = 0.90$, both free and adhered vesicles are almost flat at the top and the bottom. We can see in the plot of the reduced adhesion strength, w_{min}, that in this region with almost flat vesicles, the adhered vesicles can be stabilized with the smallest values of w_{min}. This can be attributed to the fact that in this middle region, only small deformations of the vesicle are needed to stabilize vesicles adhered to a flat surface. We may also notice that for the smaller reduced volume, v, smaller value of the reduced adhesion strength, w_{min} is needed to stabilize adhered vesicles than for the larger values of v. The smaller values of the reduced adhesion strength, w_{min}, can be related to the larger values of the adhesion radius. It implies that the adhesion surface is larger, and thus the adhesion energy is significant even for small values of the reduced adhesion strength, w_{min}. Such behavior is possible for lower reduced volume, v since in this case the vesicles have more freedom to be deformed and the increase of the elastic energy of the vesicles due to adhesion can be compensated by the gain of the adhesion energy which depends on the square of adhesion radius. This mechanism does not apply to the vesicles with larger reduced volume, v because they have less freedom to be deformed. If $v \approx 1.0$, the loss of elastic energy is compensated by the adhesion energy in such a way that the radius of adhesion remains small and the adhesion strength is continuously increased as shown in Fig. 5.2a,c. The shape at $v = 1.0$ (sphere) cannot be deformed at all.

With increasing spontaneous curvature of vesicles, their shapes are more and more complex [96]. We have investigated how the complexity of a vesicle shape influences the process of adhesion. We have performed the calculations for the reduced volume, $v = 0.545$, and the reduced spontaneous curvature, $c_0 = 2.4$. For these parameters, we have not obtained adhered stomatocyte vesicles, but rather, we have obtained adhered oblate vesicles and two additional types of vesicles as compared to the case with the same reduced volume and the reduced spontaneous curvature, $c_0 = 0$. These two additional solutions are oblate vesicles with a bead and prolate vesicles. The solutions with the lowest energy are either free prolate or adhered oblate vesicles. In the second column in Fig. 5.3c and Fig. 5.3e, the first stable (with respect to the free state of the same kind) adhered oblate and prolate vesicles are shown respectively. In the insets in Fig. 5.3a, we show the energy at the transition point between stable adhered and free states of oblate and prolate vesicles. The oblate vesicles with a bead shown in Fig. 5.3d exist only in an adhered state. If we consider only the stability of

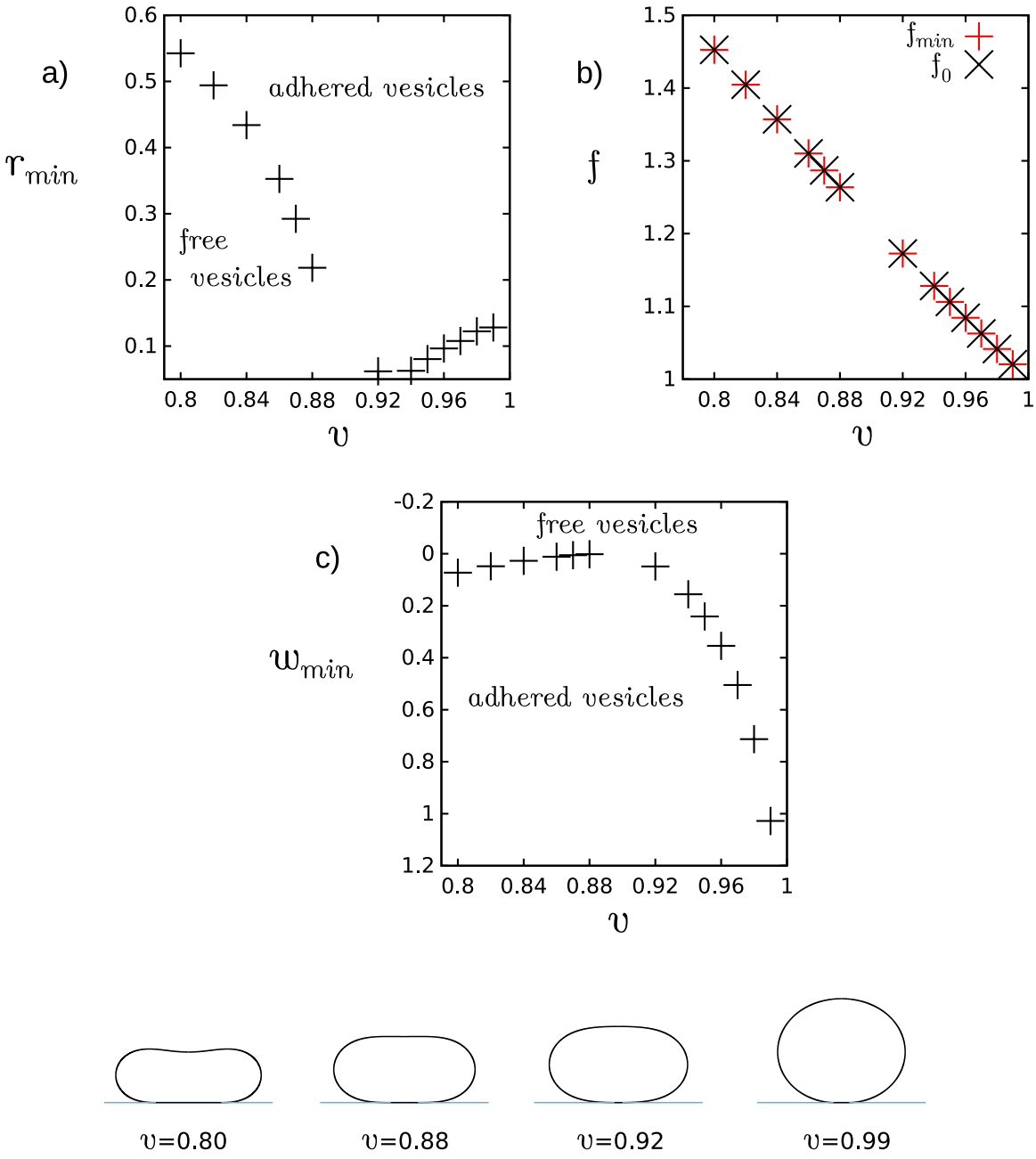

Figure 5.2: The dependence of (a) reduced adhesion radius, r_{min}, (b) reduced free energy, f, and (c) the minimal reduced adhesion strength, w_{min}, on the reduced volume, v. f_{min} denotes the reduced free energy calculated for w_{min} obtained through linear regression and f_0 is the reduced free energy calculated for free vesicle. The reduced spontaneous curvature is $c_0 = 0.0$. The shape profiles represent the stable adhered vesicles for the smallest reduced adhesion strength, w_{min}, for different values of the reduced volume, v.

adhered states, we notice that for low adhesion strength, the oblate vesicles with a bead are stable and for larger adhesion strength, oblates without a bead are stable. Sufficiently large non-zero spontaneous curvature favors free prolate shapes. Oblate shapes are favored when a vesicle adheres to a flat substrate. The adhered oblate vesicles with a bead are the result of a compromise between these two classes of shapes.

We have also investigated the vesicles with the same non-zero reduced spontaneous curvature as in the previous case, $c_0 = 2.4$, but larger reduced volume, $v = 0.8$. For this set of parameters, we obtain three different solutions for the shapes of free vesicles: prolate, pear, and oblate. Prolate and oblate vesicles have up-down symmetry. In the case of pear vesicles, we have two different states of adhered vesicles due to the lack of up-down symmetry. The first one when the smaller bead is attached to the substrate, and the second one when the larger bead is attached to the surface as shown in Fig. 5.4e and Fig. 5.4d respectively. The first stable adhered vesicles for oblate, pear, and prolate branches are shown in the second column of Fig. 5.4c-f. In the first column, the solutions for the vesicles in a free state are presented. In the third and fourth columns, the intermediate and limiting solutions for a large value of the adhesion strength, w are shown. When we consider the solutions with the lowest energy, the free prolate vesicles are stable for lower adhesion strength, w and adhered oblate vesicles are stable for larger w. In the fifth column, we present the configurations with the same free energy for free prolate and adhered oblate vesicles at the possible transformation from free to adhered vesicles for this set of parameters. This is similar to the previous case with smaller reduced volume, $v = 0.545$ and positive spontaneous curvature c_0, where the shape of the stable free state is prolate and the shape of the adhered state is oblate. When we consider only adhered states with the lowest energy, we have a very interesting situation. The adhered oblate vesicles have lower energy except for a small range of the adhesion strength $2.69 < w < 3.11$ where the solution with the lower energy are adhered pear-like vesicles attached with a larger bead to the flat surface. Based on the free energy calculations as shown in Fig. 5.4a, we may expect the existence of two transitions. At $w = 3.11$, the energy of adhered oblate and pear-like vesicles is equal. Thus, by increasing or decreasing the adhesion strength w, the transition between adhered pear-like and adhered oblate vesicles can be induced. The adhered oblate vesicles are already metastable at $w = 0.05$, but adhered pear-like vesicles are metastable only for $w > 2.69$. However, the energy of the adhered pear-like vesicles is significantly smaller at $w = 2.69$ than the energy of adhered oblate vesicles. Thus, we may expect that by increasing the adhesion strength, the adhered oblate vesicles could be transformed to adhered pear-like vesicles. Based on this

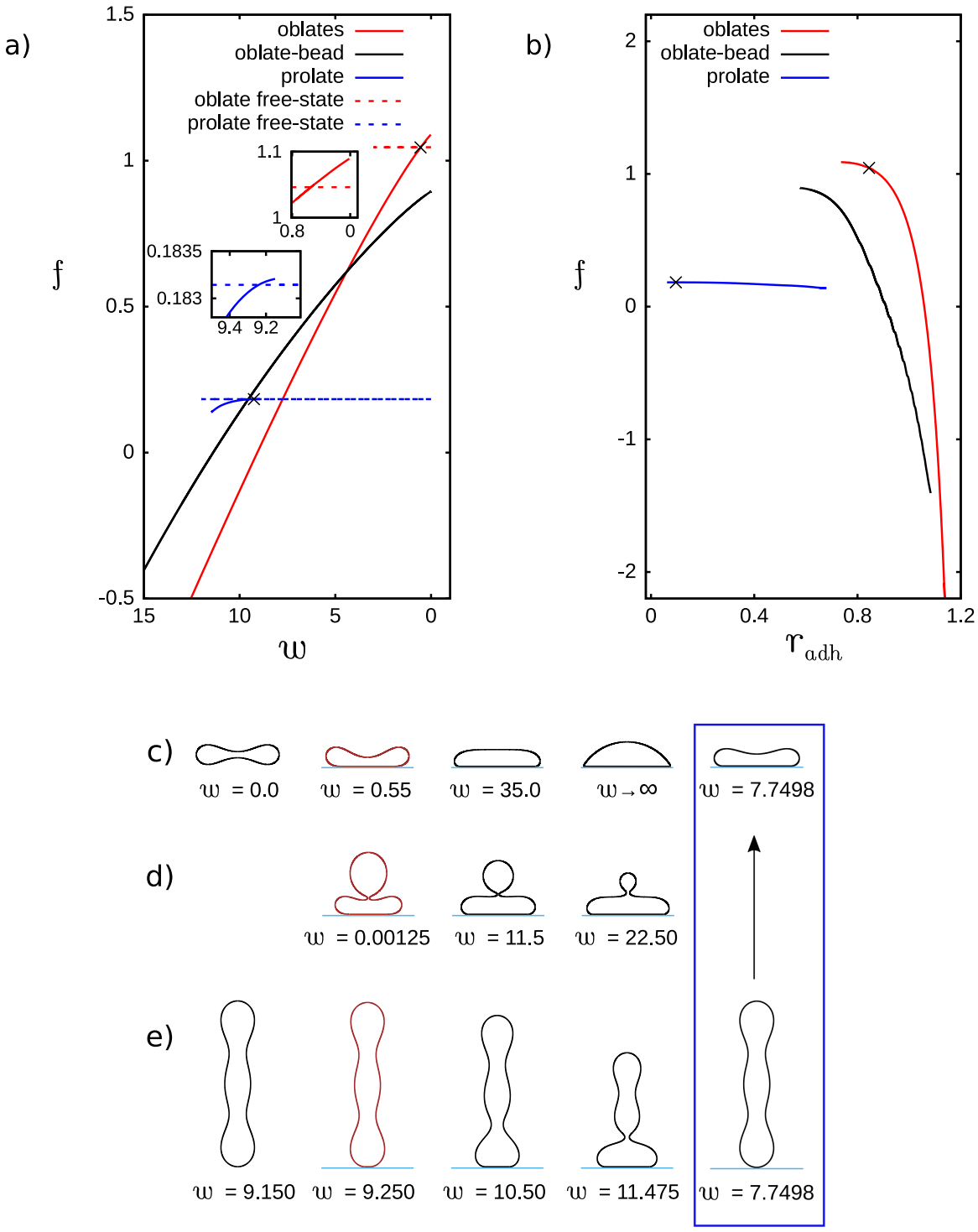

Figure 5.3: The dependence of the reduced free energy, f, on (a) the reduced adhesion strength, w, and (b) reduced adhesion radius, r_{adh}, for the reduced volume, $v = 0.545$ and reduced spontaneous curvature, $c_0 = 2.4$. The crosses denote the points where the stable adhered vesicles for the smallest value of the adhesion strength w are formed. These points are obtained from intersection of the reduced free energy curves visualized at larger scale in the insets.

Figure 5.3: Shape profiles for oblate, oblate-bead and prolate vesicles are shown for the following sets of parameters: (c) adhesion strength, w = 0.0, 0.55, 35.0, $w \to \infty$ (limiting shape), 7.7498, adhesion radius, r_{adh} = 0.0, 0.8447, 1.1666, 1.2940, 1.0446. (d) adhesion strength, $w = 0.00125$, 11.5, 22.50, adhesion radius, r_{adh} = 0.5769, 0.9121, 1.0832. (e) adhesion strength, w = 9.150, 9.250, 10.50, 11.475, 7.7498, adhesion radius, r_{adh} = 0.0, 0.0967, 0.3796, 0.6791, 0.0. The shapes at the intersection of dashed blue (free prolate) and solid red (adhered oblate) curves are shown in the blue frame. The profiles pictured in red are the stable adhered configurations obtained for the lowest adhesion strength w.

result, we can speculate that in biological systems, budding may be induced by a very small variation in the adhesion strength, and it can be easily reversed. It should be stressed here that no change in the distribution of the components or the spontaneous curvature is needed to induce budding. It is enough to increase the surface area of adhesion of the vesicle, for example, by the change of the adhesion strength as shown in Fig. 5.5. We can observe a different behavior depending on whether the pear-like vesicle is attached to the substrate with its smaller spherical part or the larger spherical part. When the smaller bead is attached to the surface, the neck in the middle becomes smaller and smaller on increasing the adhesion strength. Such a process may lead to budding in the end. When the larger part is attached to the surface, the neck widens and the vesicle is transformed to an adhered oblate. Thus, depending on which part of the vesicle is attached to the substrate, it is possible to open or close the gate which is formed by the neck in the central part of the vesicle. This way, by changing the radius of the neck, it is possible for example to prohibit or enhance the mixing of the fluids which are contained in these two parts of the vesicles.

Finally, we have examined how the increase of the spontaneous curvature would influence the adhesion of oblate vesicles with relatively large reduced volumes. We have studied the vesicles with relatively small spontaneous curvatures to ensure the stability of oblate vesicles. We have examined the vesicles with a concave, $v = 0.80$, and a convex, $v = 0.99$ shape and also with the shape which is approximately flat at the poles of the vesicle, $v = 0.85$. For this range of the reduced volume $0.80 \leq v \leq 0.99$, we were able to examine simple vesicle shapes which did not undergo significant shape transformations with the change of the reduced spontaneous curvature, c_0. We have calculated the adhesion strength w_{min} for which the adhered vesicle has the same energy as the free vesicle, for different values of the reduced spontaneous curvature. The value of w_{min} was determined by calculating the reduced free energy, f for several values of the reduced adhesion strength, w and reading off w_{min} for the value of the reduced free energy equal to that of the free vesicle. It follows from the

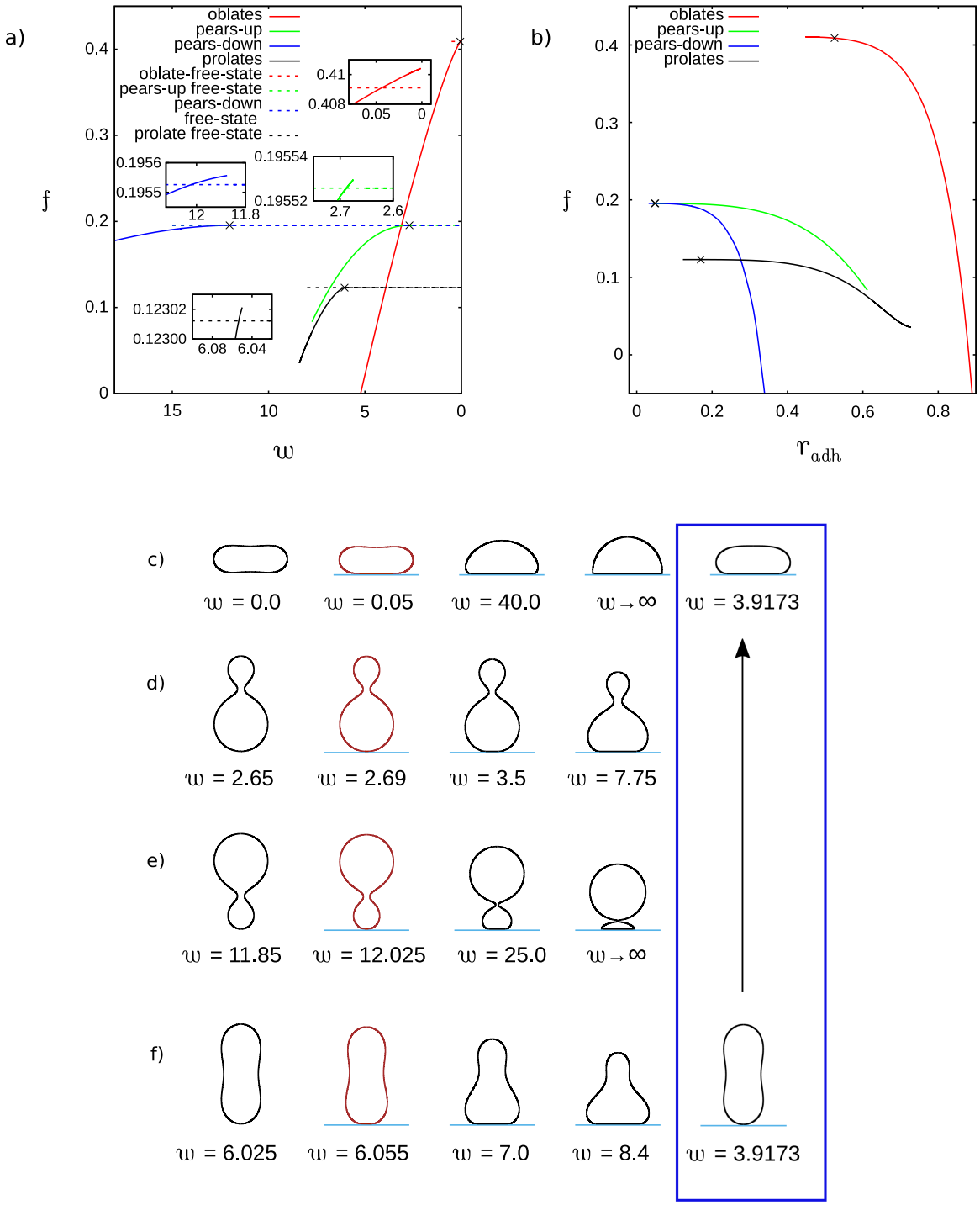

Figure 5.4: The dependence of the reduced free energy, f, on (a) the reduced adhesion strength, w, and (b) reduced adhesion radius, r_{adh}, for the reduced volume, $v = 0.80$, and the reduced spontaneous curvature, $c_0 = 2.4$. The crosses denote the points where the stable adhered vesicles for the smallest value of the adhesion strength w are formed. These points are obtained from the intersection of the reduced free energy curves visualized at larger scale in the insets.

Figure 5.4: The shape profiles for oblate, pears (up/down), prolate vesicles are plotted in each row for the following parameters: (c) adhesion strength, $w = 0.0,\ 0.05,\ 40.0,\ w \to \infty$ (limiting shape), 3.9173, adhesion radius, $r_{adh} = 0.0,\ 0.5248,\ 1.0313,\ 1.1097,\ 0.8531$. (d) adhesion strength, $w = 2.65,\ 2.69,\ 3.5,\ 7.75$, adhesion radius, $r_{adh} = 0.0,\ 0.0492,\ 0.2182,\ 0.6121$. (e) adhesion strength, $w = 11.85,\ 12.025,\ 25.0,\ w \to \infty$ (limiting shape), adhesion radius, $r_{adh} = 0.0,\ 0.0478,\ 0.2747,\ 0.5122$. (f) adhesion strength, $w = 6.025,\ 6.055,\ 7.0,\ 8.4,\ 3.9173$, adhesion radius, $r_{adh} = 0.0,\ 0.1699,\ 0.5187,\ 0.7276,\ 0.0$. The shapes at the intersection of dashed black (free prolate) and solid red (adhered oblate) curves are shown in the blue frame. The profiles pictured in red are the stable adhered configurations obtained for the lowest adhesion strength w.

plots in the first row of Fig. 5.6 that the concave vesicles are stabilized for smaller and smaller values of the adhesion strength with increasing values of the reduced spontaneous curvature, c_0. Contrary to the concave ($v = 0.80$) vesicles, for the convex

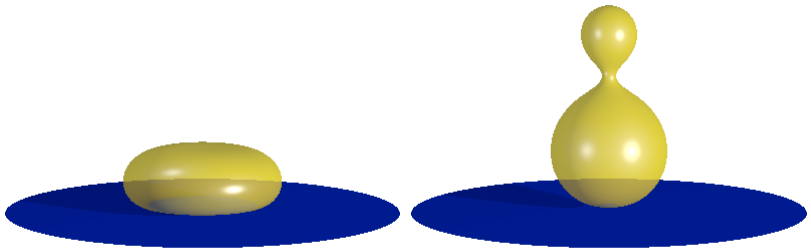

Figure 5.5: Budding of adhered vesicles induced by decreasing the adhesion strength, w. The adhered oblate and adhered pear-like vesicles have equal energy at $w = 3.11$ for the reduced volume, $v = 0.80$, and the reduced spontaneous curvature, $c_0 = 2.4$.

vesicles ($v = 0.99$), the adhesion strength w_{min} increases with the increasing reduced spontaneous curvature c_0. We should stress that the convex vesicle is almost spherical close to the limiting shape with the reduced volume $v = 1.0$. These features may play a significant role in the process of adhesion. In all the cases, the radius of adhesion r_{min} decreases with the increase in reduced spontaneous curvature within the studied range of c_0. The changes are very small and can hardly be noticed in the shape profiles of the vesicles. However, the tendencies in the changes induced by the increase of the reduced spontaneous curvature are clearly illustrated. It is interesting to note that the increase of the spontaneous curvature promotes the adhesion of oblate vesicles to a flat substrate. Smaller adhesion strength w_{min} is needed to obtain stable adhered vesicles. It should be noted that at the same time, the radius of adhesion r_{min} is decreasing with the increasing spontaneous curvature. This suggests that an increase in c_0 encourages an increase in the stability range of adhered oblates towards the

lower adhesion radius. An increase in c_0 ensures the ease of adhesion of the concave and almost flat oblates by reducing the w_{min} values compared to the convex oblates. Intuitively, one would expect an opposite behavior since it should be favorable for the vesicles with the spontaneous curvature close to zero to adhere to a flat surface with zero mean curvature. But, when we consider the local mean curvature on a surface of an adhered vesicle, we find out that the surface of the membrane attached to a flat substrate is small compared to the remaining surface area of the vesicle which is characterized by a non-zero mean curvature.

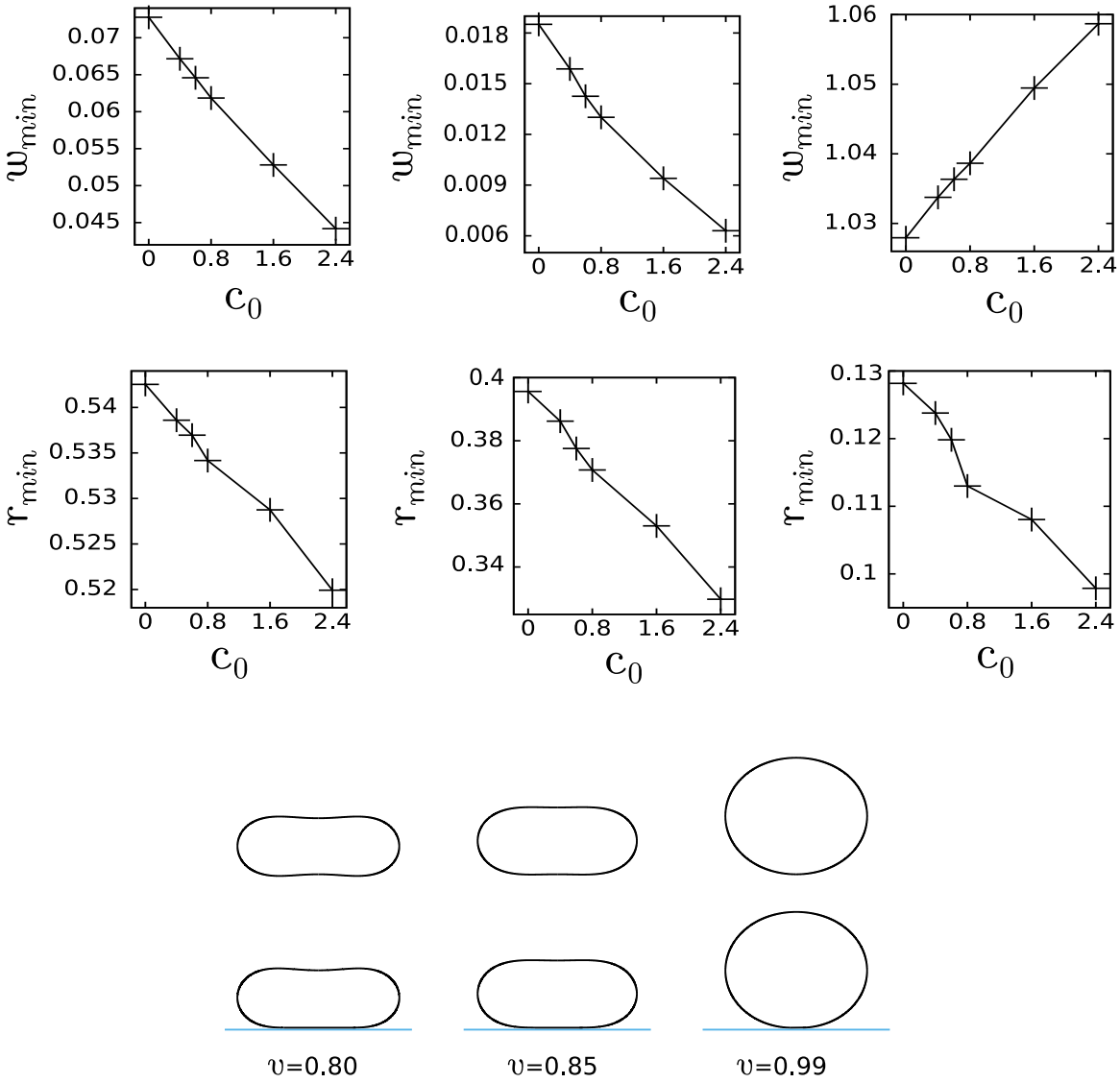

Figure 5.6: The change of the reduced adhesion radius, r_{min}, and the minimal reduced adhesion strength, w_{min}, induced by the change of the reduced spontaneous curvature, c_0, for oblate vesicles with relatively large reduced volume, $v = 0.8,\ 0.85,\ 0.99$. The shape profiles represent free vesicles in the first row and adhered vesicles in the second row with the reduced spontaneous curvature, $c_0 = 2.4$, for the reduced volume, $v = 0.8,\ 0.85,\ 0.99$ in each column respectively.

We have also investigated the susceptibility of vesicles to adhesion for different shapes of the vesicles. The susceptibility to adhesion may be quantified by the size of the surface area of the vesicle membrane attached to the substrate. In our case where we have rotational symmetry, the amount of the vesicle membrane attached to the rigid planar surface can be measured by the adhesion radius, r_{adh}. In Fig. 5.7, we show the rate of change dr_{adh}/dw of the adhesion radius r_{adh} as a function of the adhesion strength w for oblate vesicles with different reduced volume $v = 0.80,\ 0.7277,\ 0.545$ and the same spontaneous curvature $c_0 = 2.4$. As expected, for these values of the reduced volume, the rate dr_{adh}/dw decreases monotonically when the adhesion strength is increased for all three values of the reduced volume, v. We can say that it is more and more difficult to attach larger and larger pieces of the vesicle membrane on increasing the adhesion strength by the same value Δw. It should be noted that a linear increase of the radius is equivalent to the increase of the adhered surface area proportional to the radius squared. We can infer from Fig. 5.7b that for the same adhesion strength, the largest surface area of adhesion is obtained for the vesicles with smaller reduced volume. The vesicles with smaller reduced volume, v, have more freedom to be deformed since they have smaller inner volume surrounded by the same surface area of a membrane. However, larger adhesion strength is required to obtain stable adhered vesicles with larger reduced volume.

It is interesting to note that for smaller values of the adhesion strength, the rate of change of the adhesion radius, dr_{adh}/dw is higher for the vesicles with larger reduced volume as shown in Fig. 5.7a. For larger adhesion strength, this tendency is reversed at about $w = 9$. Such behavior might be related to the value of the limiting adhesion radius, which is larger for the vesicles with smaller reduced volume. Thus, we might expect that the rate of change of the adhesion radius could slow down more for the vesicles with larger reduced volume when the radius is closer and closer to the limiting value.

In Fig. 5.8, we show how the increase of the adhesion strength, w influences the rate of change of the adhesion radius, r_{adh} for prolate vesicles with the spontaneous curvature $c_0 = 2.4$ and the reduced volumes $v = 0.80$ and $v = 0.545$. We would like to investigate how the shape of an adhered vesicle influences its susceptibility to adhesion. We have chosen two vesicles with relatively simple ($v = 0.80$) and complex ($v = 0.545$) shapes. It has to be noted that in the case of adhesion to a flat substrate, the vesicles can assume horizontal configurations as the most stable. However, to investigate the role of the shape on the adhesion process, we can safely study metastable configurations. Moreover, when a sticker molecule is attached to a pole of a vesicle, it is possible to realize the scenario presented by our calculations.

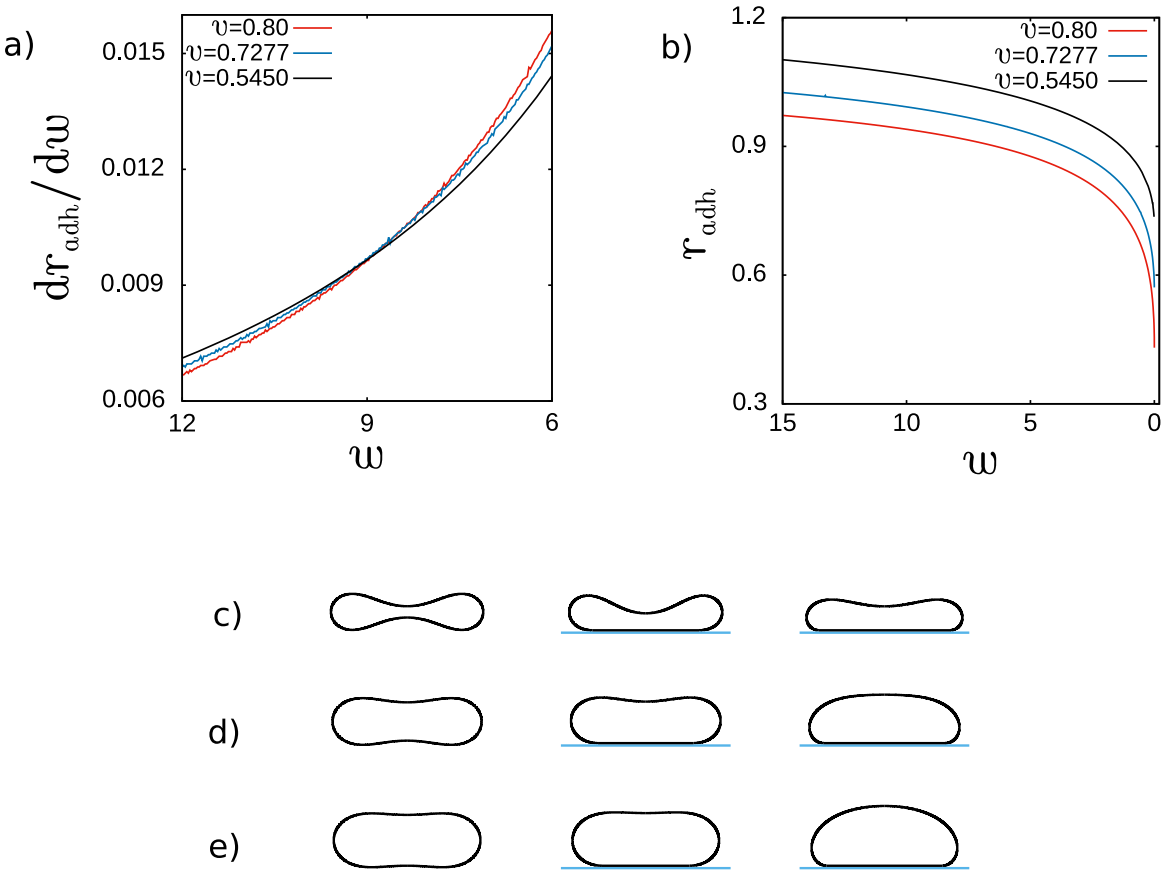

Figure 5.7: (a) The rate of change of the reduced adhesion radius, dr_{adh}/dw, and (b) the reduced adhesion radius, r_{adh}, as a function of the reduced adhesion strength, w, for the oblate vesicles with three reduced volumes, $v = 0.80,\ 0.7277$ and 0.545 and reduced spontaneous curvature, $c_0 = 2.4$. The shape profile of oblate vesicles are plotted for $w = 0.0,\ 1.0,\ 12.0$ in subsequent columns for different values of the reduced volume: (c) $v = 0.545$ (d) $v = 0.7277$ and (e) $v = 0.80$.

The stable adhered prolate vesicles with different reduced volumes exist for different ranges of the adhesion strength. Moreover, smaller adhesion strength is sufficient to stabilize adhered prolate vesicles with larger reduced volume. When prolate vesicles adhere to a flat substrate, the rate of change of the adhesion radius is not monotonous, as shown in Fig. 5.8a. For the prolate vesicles with large reduced volume, the rate decreases for smaller values of w and increases for larger values of w. In Fig. 5.8c, we present the shapes of the vesicles at small and large w, and at the minimum of the rate of change of the adhesion radius r_{adh}. For larger values of w, the adhesion leads to the transformation of an adhered prolate vesicle to an adhered oblate vesicle. Initially, the vesicle has almost up-down symmetry, but with the increase of the adhesion strength, it's shape resembles a pear. Finally, the vesicle with a pear-like shape is no longer stable and it is transformed into an adhered oblate vesicle. The rate of change of the adhesion radius increases when the prolate vesicle resembles more and more

the oblate vesicle. Thus, before the transformation of the adhered prolate vesicle into the adhered oblate vesicle due to the increase of the adhesion strength, we may expect higher susceptibility to adhesion for the vesicle which is being transformed. Small changes in the adhesion strength may induce large changes in the adhesion radius. Such behavior may be encountered in the vicinity of the shape transformations between different classes of shapes. In such cases, we can expect that the adhesion may trigger the transformation of vesicles between two different classes of shapes.

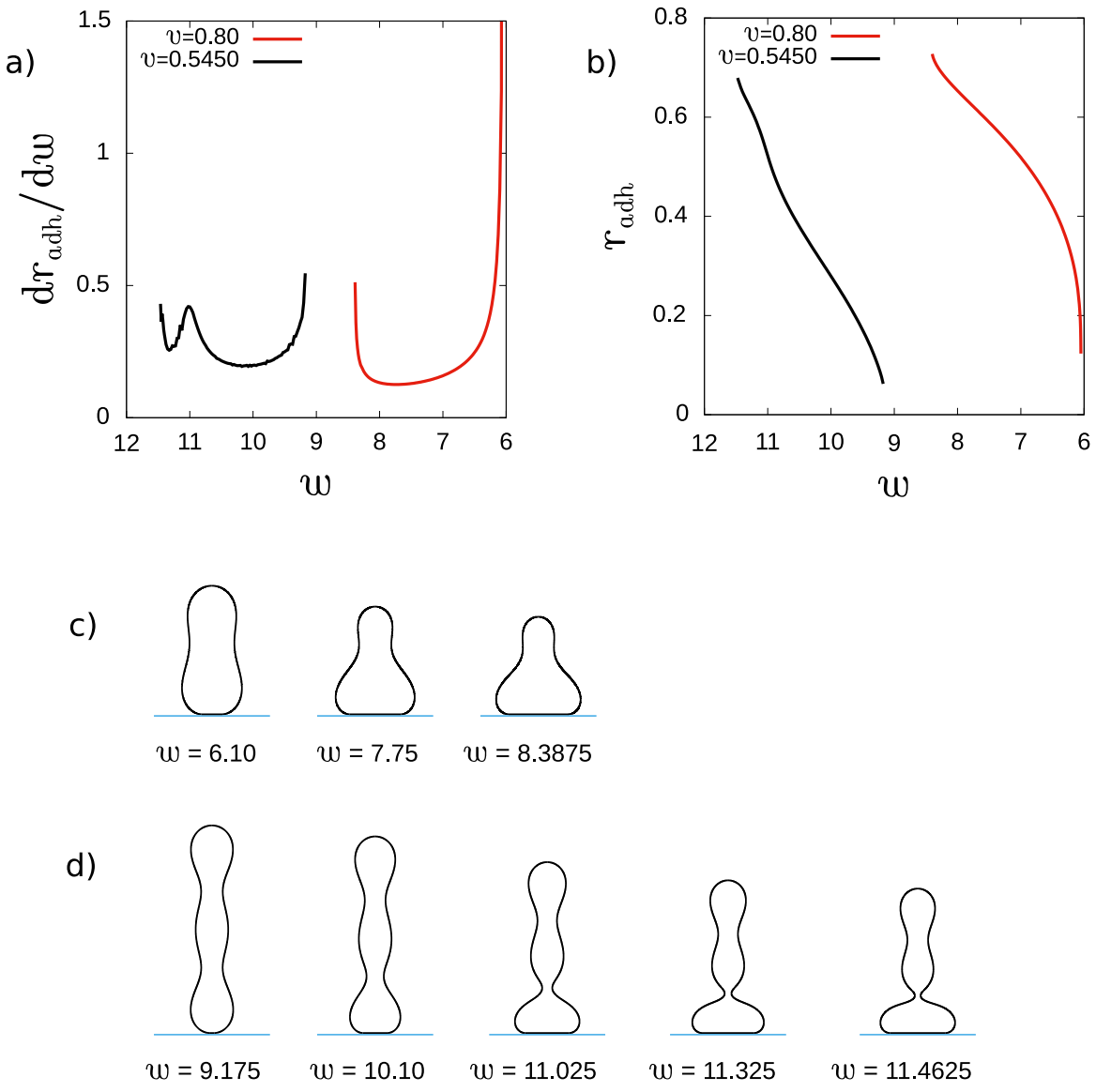

Figure 5.8: (a) The rate of change of the reduced adhesion radius, dr_{adh}/dw, and (b) the reduced adhesion radius, r_{adh}, as a function of the reduced adhesion strength, w, for the prolate vesicles with the reduced volume, $v = 0.80$ and 0.545 and the reduced spontaneous curvature, $c_0 = 2.4$. The shape profiles are plotted in each row for following parameters: (c) $v = 0.80$, $w = 6.10,\ 7.75,\ 8.3875$ (d) $v = 0.5450$, $w = 9.175,\ 10.10,\ 11.025,\ 11.325,\ 11.4625$.

The shape transformations due to the adhesion of prolate vesicles with a smaller

reduced volume are more complex. The adhesion induces the formation of a narrow neck which separates the oblate part of the vesicle at the bottom from the upper prolate part, as shown in Fig. 5.8d. The existence of the narrow neck influences the rate of change of the adhesion radius caused by the increase of the adhesion strength, as shown in Fig. 5.8a. With the increasing adhesion strength, the volume of the prolate part becomes smaller, and the volume of the oblate part becomes larger. The process ends in a discontinuous transformation of the prolate part into a spherical one. Similarly, as in the previous case, the rate of change of the adhesion radius increases just before the transformation, as shown in Fig. 5.8a. However, unlike in the previous case, this increase is not monotonous. We may attribute this behavior to the existence of the small neck which may stabilize the shape before the transformation. The sequence of shapes which illustrate that process is shown in Fig. 5.8d.

5.2 Summary and Conclusions

We have studied the lipid vesicles which adhere to a flat and rigid substrate. We have investigated the influence of the adhesion strength on the stability and shape transformations of several types of vesicles. They were characterized by different reduced volume and reduced spontaneous curvature. The minimal strength of adhesion required to stabilize different classes of vesicle shapes has been determined. The minimal strength of adhesion determines the transition from a free vesicle to an adhered vesicle. The knowledge of the minimal adhesion strength should be helpful in Atomic Force Microscopy studies where the cantilever touching a cell or a vesicle may cause its detachment. We may suspect that our calculations can have biotechnological applications in the drug-delivery process where it is important for the drug-carrying vesicle to get attached to the target site and therefore the knowledge about w_{min} becomes important to ensure it's safe adhesion.

We propose a mechanism to segregate vesicles based on their shape by creating the adhesion materials with the shape compatible with the vesicle's geometry. The vesicles which are locally flat can adhere to flat surfaces even with very small adhesion energy. We may expect that when the surface is locally curved in such a way that it fits to the shape of a vesicle, it will be easy to obtain structures with adhered vesicles. With being able to engineer surfaces with regions of well-defined shapes, it will be possible to segregate the collections of different vesicles according to a preferred shape code in the structure of the adhesive material. We can speculate that such segregation governed by adhesion can be used in biotechnological applications to collect nanoparticles like scavengers (leukocytes) do in the human body.

Our results also suggest that an increase in spontaneous curvature of the vesicle membrane can encourage adhesion and allow us to access adhered vesicle states of lower adhesion radii. It also allows for an easy adhesion due to the decrease in w_{min} values with the increase in c_0. Such a phenomenon may suggest that biologically cells may show aggregation or de-aggregation of high curvature components on the surface to induce or arrest adhesion, or it may suggest that biological cells constituting of high spontaneous curvature components may undergo easy adhesion as compared to cells made of low spontaneous curvature components and in this way cells that are required to undergo stronger adhesion are likely to have a different composition than the cells that are not required to undergo adhesion.

The susceptibility to adhesion for different classes of vesicles (oblate, prolate) has also been studied. Even in such a simple model where the vesicles of simple topology adhere to a flat substrate, it is possible to discover many interesting phenomena. We have also shown that changing the adhesion strength leads to the formation of a spherical bud or it's disappearance.

The adhesion of cells may induce novel and very interesting phenomena in large collection of cells in biological tissue or in artificial cell cultures. The results of our calculations may be useful in the explanation of the behavior of cell cultures confined and grown on a flat substrate [105], as well as in biomedical applications such as protection from the adhesion of platelets to vascular stents [106,107]. In real biological systems such as animal tissues, cells' membrane can adhere to surfaces that are not flat and not rigid, for example, to the neighboring cells. Considering the relative simplicity of our system, we may anticipate to discover many new phenomena related to the adhesion of biological cells to themselves or to rigid objects.

Chapter 6

Study of the multi-component vesicle system by varying the size of the area of adhesion with the flat surface

This chapter talks about the study of vesicles adhered to a flat surface where the vesicle membrane is made up of two kinds of membrane components. Biological cell membranes are a complex architecture and comprise of many different kinds of lipids, proteins and other non-lipid molecules which contribute to the functionality of the cell. The distribution of these membrane components within the membrane can greatly affect the working of the cell. In this chapter, we theoretically study the curvature-induced lateral distribution of components brought about by the shape transitions due to the change in adhesion. The calculations are performed under the Helfrich spontaneous curvature model. We investigate the close relationship between the shape of the vesicle under adhesion and the lateral distribution of it's components. In particular, we probe the effect of adhesion on the segregation/mixing of components for the different classes of vesicle shapes stabilized for the studied parameters. Our calculations show that budded structures like pears can support the mixing of components, whereas relatively simple and non-budded structures like oblates can support the segregation of components.

6.1 Results

Mixing and de-mixing of components are important for the cell to carry out it's normal functions. Segregation of components based on curvature-induced sorting is the guiding hypothesis behind our work, and this hypothesis has been hypothesized to be at play in many experimental studies as discussed in section 1.3. Studies have shown that the vesicle shape can influence the lateral distribution of components, and conversely, the lateral distribution of components can influence the shape. In our work, we study such a two-way relationship between the shape of the vesicles adhered to the flat surface and the lateral distribution of components. We identify the effect of adhesion on the shape-transition of the two-component vesicles and calculate the

equilibrium shapes of these vesicles. Further, we elucidate the effect of adhesion on the promotion and suppression of component segregation. We investigate the stability of the vesicles and the lateral distribution of the components, $\phi(s)$, by changing the adhesion radius, R.

Such a multi-component vesicle system can be modeled by the Eq. 3.5.3 which is numerically minimized to simultaneously obtain the shape and the corresponding concentration profile of the components on the vesicle surface. The role of the entropy of mixing is neglected. The experimental conditions can be replicated by ensuring the constraints of constant surface area A, constant volume V, and a fixed topology. The Gaussian bending rigidity of the two components is assumed to be the same, $\kappa_G^A = \kappa_G^B$. This leads to a constant contribution from the Gaussian bending energy and is thus not taken into account in the calculations. The bending rigidity of components A and B is also assumed to be the same, i.e., $\kappa^A = \kappa^B = \kappa$. Adhesion is introduced in the form of a radius constraint as explained in Eq. 3.1.5.

$f = F/8\pi\kappa$ is the reduced bending energy, $r = R/R_s$ is the reduced adhesion radius, and $c_0^A = C_0^A R_s$ and $c_0^B = C_0^B R_s$ are the reduced spontaneous curvature values corresponding to each kind of membrane component. The area of adhesion for our rotationally symmetric vesicles – is a circle.

The calculations are done for the average concentration, $\phi_{avg} = 0.5$ of the component A over the surface. The reduced spontaneous curvatures associated with the membrane components A and B respectively are, $c_0^A = 8$ and $c_0^B = 0$. Such a large difference in the spontaneous curvature facilitates the curvature-induced segregation of components. We present the results for the reduced volume $v = 0.95$. We have decided to investigate vesicles with relatively large reduced volume because for such vesicles, the number of different classes of shapes is relatively small, yet the system is still interesting to investigate.

6.1.1 Free vesicles for $c_0^A = 8$, $c_0^B = 0$, $\phi_{avg} = 0.5$ and $v = 0.95$

For this set of parameters, we obtain a few different classes of free vesicle as shown in Fig. 6.1. In the solutions corresponding to Fig. 6.1a and Fig. 6.1b, the component with the larger spontaneous curvature is accumulated at the north pole of the vesicle, forming a spherical bud or a circular caplet respectively. The lowest energy shape for the free vesicles at the reduced volume $v = 0.95$ is the one with a spherical bud (Fig. 6.2). We have also obtained a shape with completely mixed components and a very interesting solution with the region at the north pole occupied mainly by the component having lower spontaneous curvature as shown in Fig. 6.1c. The distribution of components of the latter kind is accommodated in the concave shape

at the north pole of the vesicle.

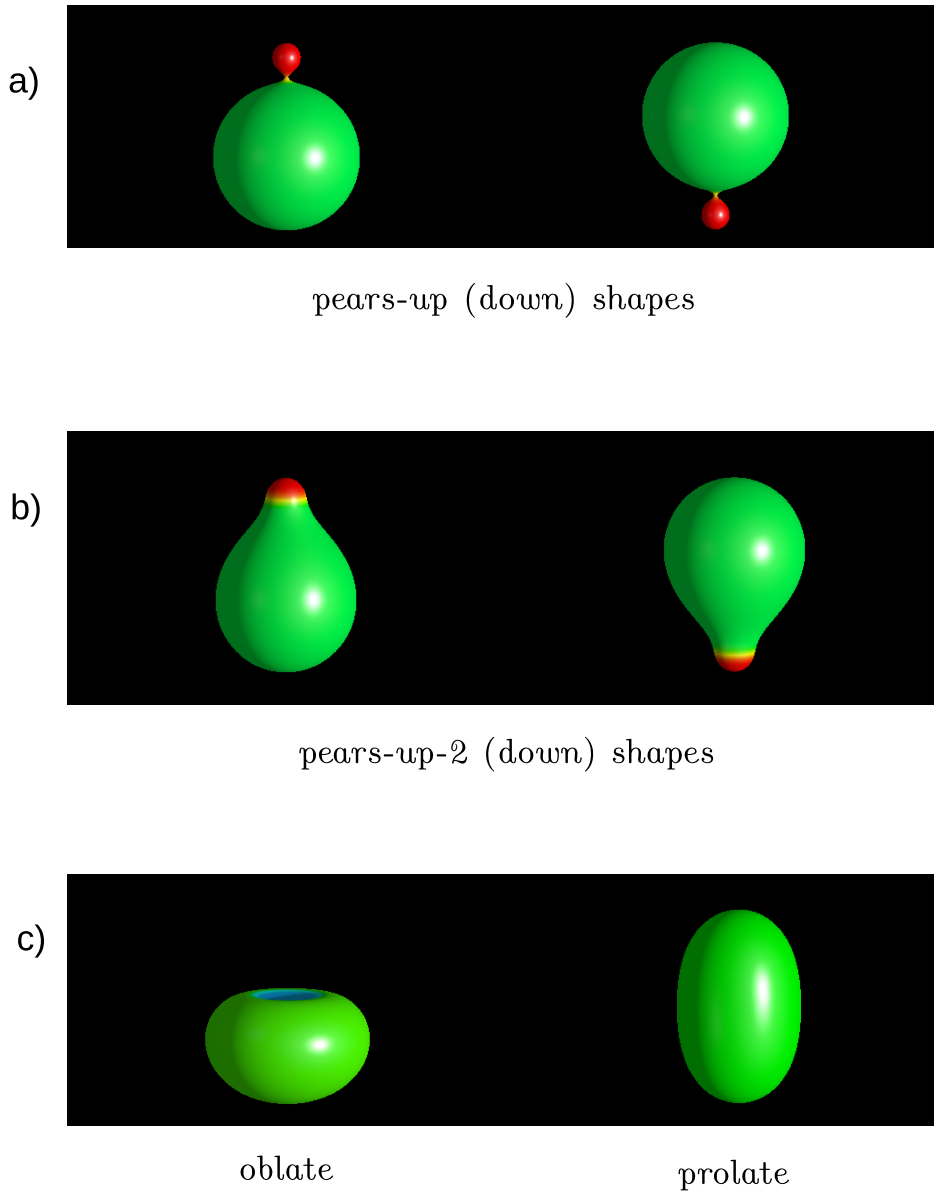

Figure 6.1: Shapes of the vesicles obtained at $r = 0$ and for the parameters $v = 0.95$, $c_0^A = 8$, $c_0^B = 0$ and $\phi_{avg} = 0.5$.

The membrane components are segregated because the equilibrium vesicle shapes have regions of different mean curvature. Thus, this allows the components with larger and smaller spontaneous curvatures to be accumulated in the high and low mean curvature regions, respectively. It should be noted that in the case of free vesicles, the regions with high and low mean curvatures are formed spontaneously in the process where the shape of the vesicle and the lateral distribution of the components are driven by the minimization of the bending energy. However, during the adhesion to a flat substrate, the shape of the vesicle changes in such a way that near the substrate, both low and high mean curvature regions are formed. The membrane part that is

attached to a flat substrate has zero mean curvature, whereas the bilayer at the rim of the adhered region has a non-zero mean curvature. The value of the mean curvature at the rim is related to the size of the adhered region. In general, the larger is the size of the adhered membrane, the higher is the mean curvature generated at the rim. Thus, by varying the size of the adhered membrane region, the proportion of the regions with low and high mean curvatures is varied.

6.1.2 Study of vesicle adhesion by varying the size of the area of adhesion

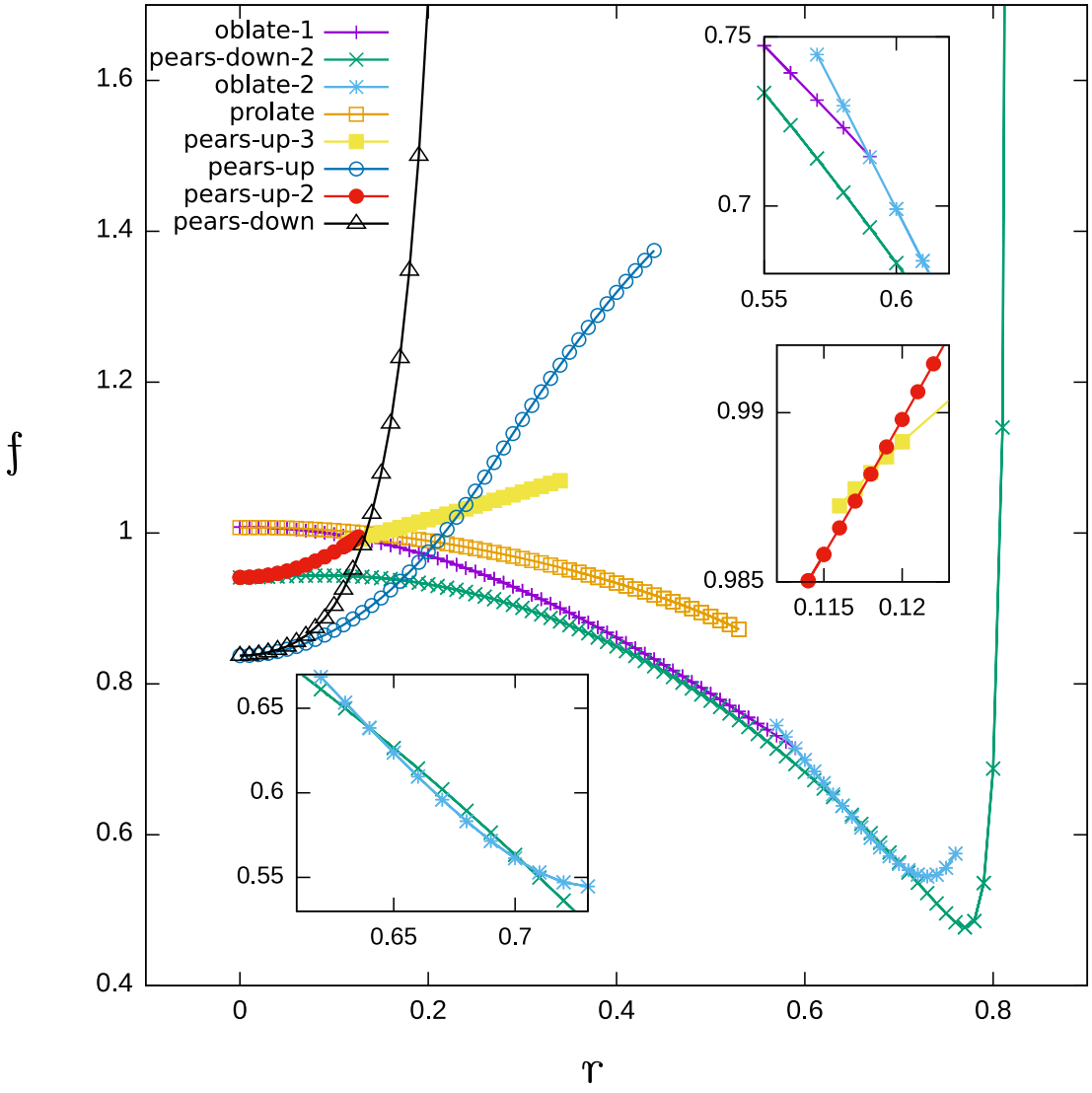

Figure 6.2: Reduced bending energy, $f = F/8\pi\kappa$, as a function of reduced adhesion radius, r is shown for all the solutions obtained at $v = 0.95$, and for the parameters $c_0^A = 8$, $c_0^B = 0$ and $\phi_{avg} = 0.5$.

The bending energy of the solutions obtained for the two-component vesicles is

shown in Fig. 6.2. There are eight classes of solutions obtained under adhesion which can be uniquely described by their shape and the distribution of components over the vesicle surface. These solutions correspond to the different branches of the bending energy diagram (Fig. 6.2). Six out of these eight solutions originate from the solutions of the free state vesicles. The energies corresponding to the limiting structures of the pears-down (Fig. 6.20) and pears-down-2 (Fig. 6.7) branches are not presented in the bending energy diagram as they are large and therefore can be avoided for the clarity of presentation.

From the bending energy trends of Fig. 6.2, we may conclude that the adhesion induced shape change and the corresponding lateral distribution of components is causing the oblate-1 (Fig. 6.3), oblate-2 (Fig. 6.5), pears-down-2 (Fig. 6.7) and prolate (Fig. 6.14a) shapes to be benefited more from the redistribution of components with the increase in adhesion radius, r. This is because, for these branches in the bending energy diagram, the bending energy decreases with the increase in r, and since the adhesion energy is always a negative quantity, the adhered shapes of these vesicles become more stable than the free state solutions. This emphasizes that the lateral distribution of components in these shapes under adhesion is helpful for stabilizing these vesicles over their free state solutions. The lateral distribution of components indicates segregation or mixing, and we can conclude that the mechanism of adhesion induced component segregation is favorable to the stability of, for e.g., oblate-2 (Fig. 6.5) and pears-down-2 (Fig. 6.7) vesicles. Interestingly, adhesion induced, both mixing and segregation of components can stabilize oblate-1 vesicles (Fig. 6.3) for different ranges of adhesion radii. Whereas, adhesion induced mixing of components can stabilize for e.g., pears-up (Fig. 6.18) and pears-up-3 vesicles (Fig. 6.12).

The pears-down-2 vesicle (Fig. 6.7) has the longest stability range which may suggest that the shapes which show strong segregation of components, such that there is a component A rich domain on one side and the other side depleted in component A, are favored most by adhesion, and interestingly those shapes have the component with a larger spontaneous curvature towards the base of the vesicle. The pears-up vesicle (Fig. 6.18) also has a relatively long range of stability under adhesion, thereby suggesting that adhesion also promotes shapes that can transition towards a mixed component state for this reduced volume, v. For small adhesion radius, r, pears-up vesicles have the lowest bending energy and for higher r, pears-down-2 vesicles have the lowest bending energy except for a small range. This means that these two configurations with their corresponding concentration profiles are most stable for this set of parameters.

Oblate-1 and oblate-2 vesicles

Free oblate vesicles are not expected to be stable when the concentration of the component with a large spontaneous curvature is more in the membrane, usually prolate vesicles are the stable ones. However, oblate vesicles are expected to be stable when the surface area of adsorption is large. We have found two types of adsorbed oblate-shaped vesicles which can be characterized by the oblate-1 and oblate-2 branches of the bending energy diagram. The oblate-1 branch originates from a free vesicle and is stable for low adhesion radii between $r = 0$ to $r = 0.59$, whereas the oblate-2 branch has shapes stable only for large adhesion radii between $r = 0.57$ to $r = 0.76$. These two kinds of oblate shapes have different distributions of components. The oblate-1 vesicles have domains that are well defined and have a sharper boundary between them, whereas the oblate-2 vesicles do not have very pronounced domains due to the gradual change in the concentration of components across the surface.

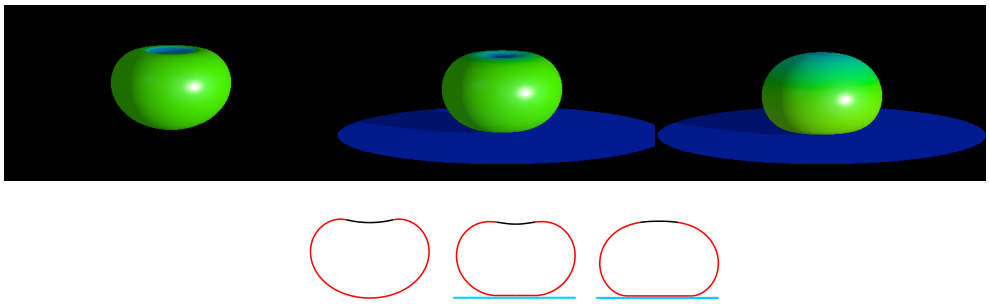

Figure 6.3: Shapes and 2D shape profiles of the oblate-1 vesicles are shown for $r = 0, r = 0.36, r = 0.59$. The regions in the 2D profile marked by different colours correspond to the two domains separated by an interface.

In Fig. 6.3, we show the shapes corresponding to the stability range of oblate-1 vesicles in 3D and the corresponding 2D shape profiles. In Fig. 6.4, we show the concentration profiles corresponding to the distribution of component A obtained on minimization. We see that at $r = 0$, the oblate shape is already slightly segregated with the lack of highly curved component A at the north pole of the vesicle forming a circular domain and the rest of the vesicle is in an almost mixed state with $\phi(s) \approx 0.5$. The components are distributed uniformly in each domains. We see that as the adhesion radius r increases, the difference in the concentration of the high curvature components between the two domains, increases for small r. The high spontaneous curvature components get more and more depleted in the domain at the north pole of the vesicle as compared to the free state of the vesicle, with the increase in r - for small r. Thus, segregation is encouraged for smaller values of r. However, with the further increase in r, this concentration difference between the domains becomes smaller and at the limiting shape, the domains of constant concentration

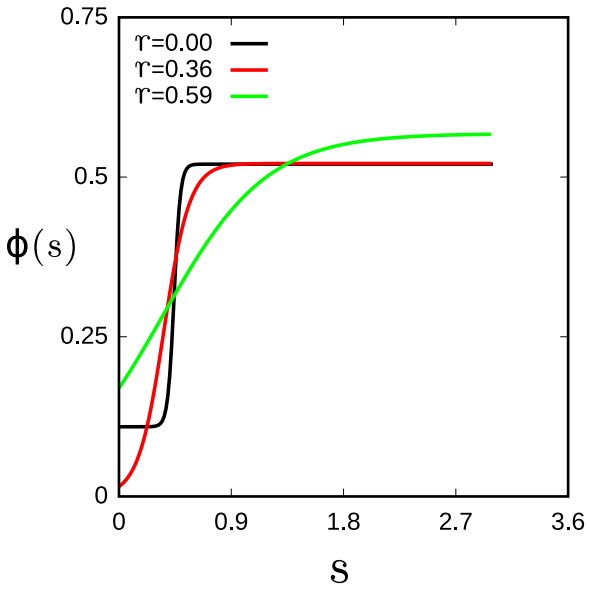

Figure 6.4: Local concentration profiles of the component A, $\phi(s)$ over the total vesicle length are shown for the oblate-1 vesicles for different values of reduced adhesion radii.

are no more well defined. The shapes transition from a concave shape to a convex shape as the adhesion radius increases. From Fig. 6.4, we can see that for small adhesion radii, the local concentration, $\phi(s)$ changes quickly within a short distance between the domain with high concentration and the domain with low concentration of the high curvature components. At larger adhesion radii, the change of the local concentration is gradual. The width of the boundary region between the domains becomes wider with the increase in r. The interplay between the vesicle's shape and the concentration of components is clearly illustrated in this case. The change of the concentration at the north pole of the vesicle is correlated with the variation of the vesicle's shape induced by adhesion. Thus, we can conclude that the increase in the interface region (characterized by a gradual change in the concentration of high curvature components on the vesicle surface) along the branch for larger values of adhesion radius, r, encourages mixing of components towards the north pole and an accumulation of high curvature components at the south pole.

The oblate-2 vesicle shapes are stable only at large adhesion radii. The shapes for the stability range of the oblate-2 vesicles in 3D are shown in Fig. 6.5 along with their corresponding 2D shape profiles. The changes in the local concentration profile of component A over the surface with the increasing adhesion radius r have been shown in Fig. 6.6. From Fig. 6.5, we can conclude that the shapes of this branch have a wide region along which the concentration changes and therefore a gradual gradient of the distribution of component A on the vesicle surface. However, as the adhesion radius increases along the branch, we see that the adhesion actually promotes

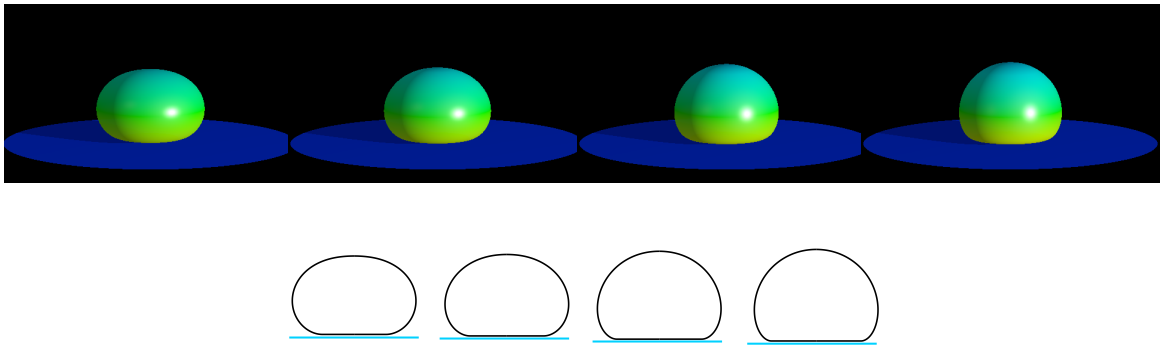

Figure 6.5: Shapes and 2D shape profiles of the oblate-2 vesicles are shown for $r = 0.57, r = 0.65, r = 0.73, r = 0.76$.

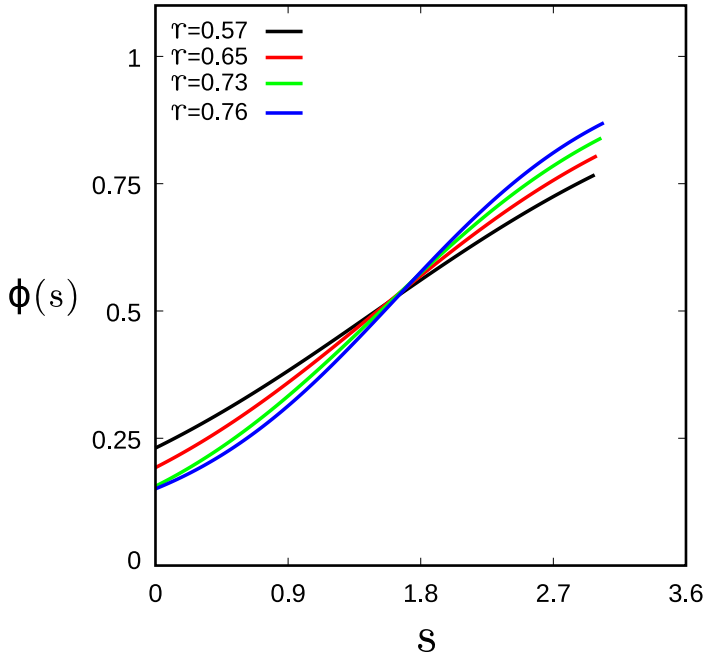

Figure 6.6: Local concentration profiles of component A, $\phi(s)$ over the total vesicle length are shown for the oblate-2 vesicles for different values of reduced adhesion radii.

segregation. This can be concluded from the increase in the slope of the $\phi(s)$ profile from $r = 0.57$ to $r = 0.76$ in Fig. 6.6. Along the oblate-2 branch, the segregation is a result of the migration of the high curvature components from the north to the south pole which causes an increase in the concentration of high spontaneous curvature components towards the base of the vesicle with the increase in adhesion, as seen from the concentration curve, $\phi(s)$.

It should be noted that there is a range of adhesion radius, r, where the solutions of both kinds of oblate vesicles can be obtained and there is one value of the adhesion radius, where the oblate vesicles of both these kinds have the same energy. This implies a possibility of a very interesting phenomenon where there is an easy transition between these two branches. In our model, the distribution of components influences

the shape of the vesicle and vice versa. Thus, we can speculate that small changes in the shape of the vesicle may result in the change of the distribution of the components that is equivalent to the transition from one type of adhered oblate vesicle to another.

Pears-down-2 vesicles

It can be expected that for sufficiently large values of adhesion radius, the adhered vesicles have oblate shapes. However, it is not obvious what the evolution of the vesicle shape will look like with the increase in adhesion radius if we begin from a non-oblate vesicle. For the case of the pear-like configuration attached to the substrate at the narrower end, where the component with high spontaneous curvature forms a circular domain, the transformation is smooth and is shown in Fig. 6.7 along with their 2D shape profiles. The vesicle smoothly transforms from a pear-like to a prolate and

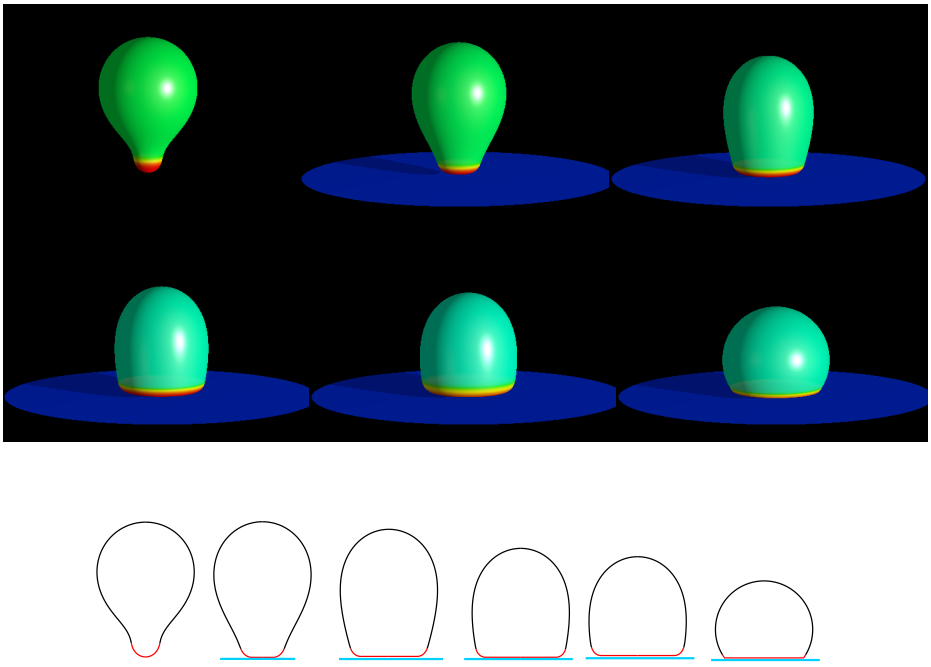

Figure 6.7: Shapes and 2D shape profiles of the pears-down-2 vesicles are shown for $r = 0, r = 0.2, r = 0.5, r = 0.65, r = 0.70, r = 0.82$. The regions in the 2D profile marked by different colours correspond to the two domains separated by an interface.

finally to an oblate shape. We see that an initially segregated pears-down-2 vesicle shape at $r = 0$ undergoes stronger and stronger segregation of components with the increase in adhesion. This leads to the formation of one of the domains comprising of high curvature components and the other domain comparatively depleted of them at the limiting structure. From Fig. 6.8, we can see that the value of $\phi(s)$ decreases for the northern region of the vesicle with the increase in adhesion. This suggests that the high spontaneous curvature component A migrates towards the base of the vesicle and accumulates at the rim of the adhered region and at the substrate to minimize

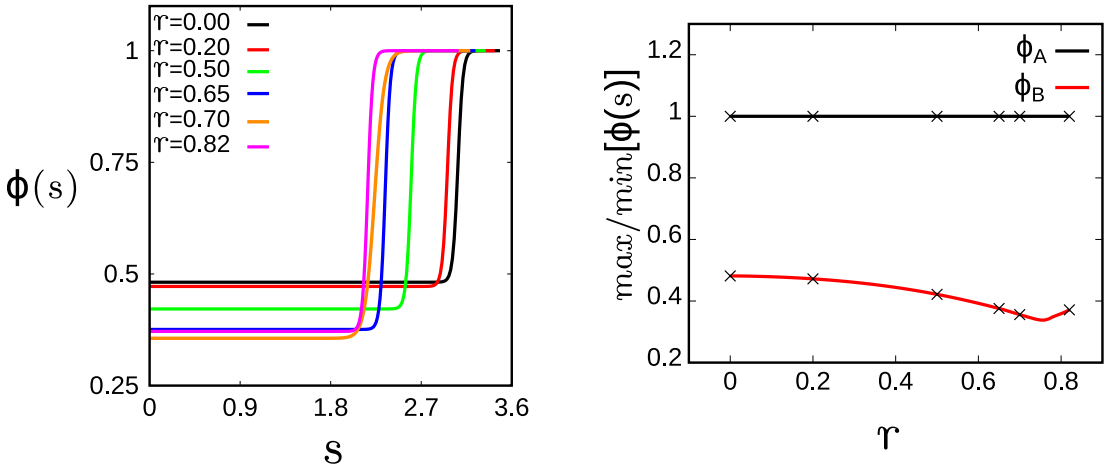

Figure 6.8: Local concentration profiles of component A, $\phi(s)$ over the total vesicle length for different values of reduced adhesion radii are shown on the left and the change in the upper and lower limits of $\phi(s)$, as a function of r is shown on the right for the pears-down-2 vesicles. The crosses correspond to the values of radii for which the vesicle shapes are shown.

the overall bending energy with the increase in adhesion. It is interesting to note that the concentration of the high spontaneous curvature components always remains larger in the region of the vesicle attached to the substrate than the rest of the vesicle, even for very large adhesion radii. In fact, this domain of high spontaneous curvature component keeps on increasing for significantly large adhesion radius as seen from the $\phi(s)$ curves in the Fig. 6.8. The mean curvature at the rim becomes larger for a larger adhesion radius and also the area of the vesicle with larger mean curvature increases. Thus, it becomes natural for the high spontaneous curvature components to be accumulated more and more near the substrate.

The depletion of the high curvature components from the domain at the north pole is also reflected in the decrease of the ϕ_B value with the increase of adhesion radius, r, as seen in the curves of $max/min[\phi(s)]$ vs. r in the Fig. 6.8. However, at high enough adhesion radius, i.e., near the limiting structure, we see that the ϕ_B value increases weakly. This suggests that the high curvature components slightly migrate towards the north pole of the vesicle as it approaches it's limiting shape. The limiting structure is almost a section of a sphere and a similar configuration was obtained for one component vesicles which have a uniform distribution of spontaneous curvature throughout the surface. Red blood cells also show such a structure under strong adhesion [108–110]. It should be noted that the increase of the spontaneous curvature enhances adhesion of one component vesicles to the flat substrate [111]. Thus along the branch, the segregation of components is favored with an increase in adhesion, and the domains are separated by a well-defined narrow boundary. It is interesting to see

that such a non-budded structure can support such a strongly segregated distribution of components. Such shapes can be therefore biologically important for activating various biological functions.

For a very small range between about $0.65 \leq r \leq 0.70$, it is interesting to note that the oblate-2 shapes (gradual change in the concentration of components) have lower energy than the pears-down-2 shapes which have a sudden and a sharp change in concentration of components. Comparison of their energies within this range is shown in the inset of Fig. 6.2 and a corresponding comparison of their shapes is shown in Fig. 6.9. The branches corresponding to these two shapes intersect each other at two points in the bending energy diagram where it is possible to obtain shapes of the same energies but significantly different component distributions. Thus, cells can use adhesion to alternate between two different component distributions by increasing or decreasing adhesion. In such a case, we may suspect that the increase of adhesion above $r \approx 0.65$ may allow the cell to achieve a gradual distribution of protein components and deactivate cell activities that are only sustained through the aggregation of certain proteins.

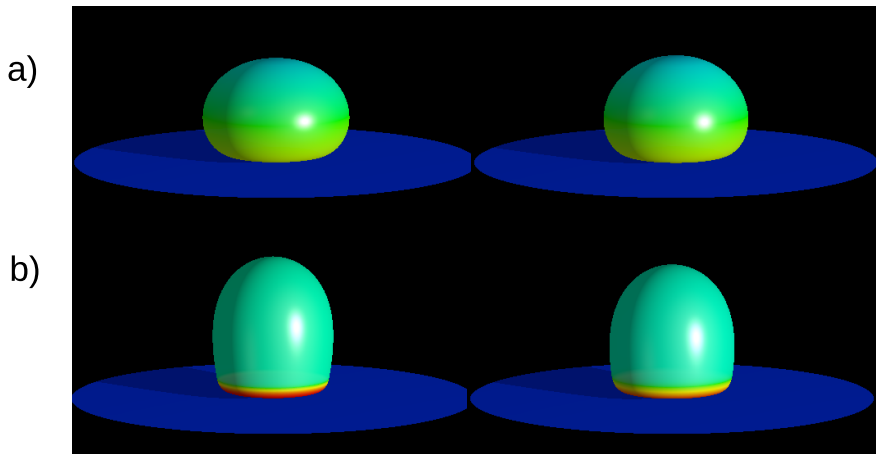

Figure 6.9: Shapes for the oblate-2 (row a) and pears-down-2 (row b) vesicles are shown for $r = 0.65$ and $r = 0.70$.

Pears-up-2 and pears-up-3 vesicles

The pears-up-2 branch has the same origin as that of the pears-down-2 branch at $r = 0$ in the energy diagram, and it is attached to the surface from the wider end. From the Fig. 6.10 and the concentration profiles of Fig. 6.11, we see that there is a negligible change in the distribution of components with the increase in adhesion along the branch and it remains almost similar to that at $r = 0$. The distribution of components in the domains is uniform and the boundary region between the domains

is narrow. The stability range of this branch is very small and the limiting shape is reached at $r = 0.126$.

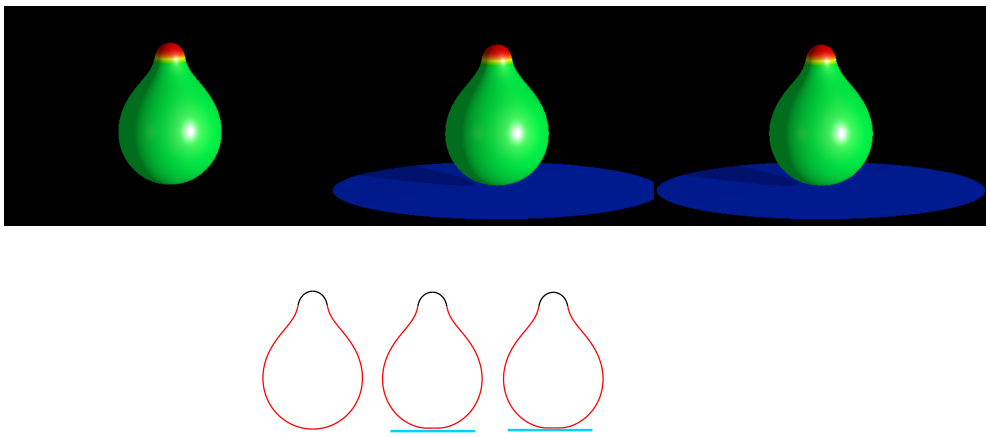

Figure 6.10: Shapes and 2D shape profiles of the pears-up-2 vesicles are shown for $r = 0, r = 0.116, r = 0.126$. The regions in the 2D profile marked by different colours correspond to the two domains separated by an interface.

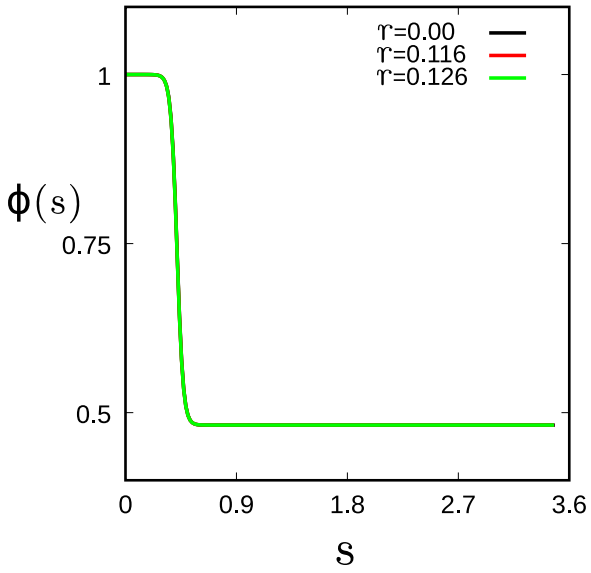

Figure 6.11: Local concentration profiles of component A, $\phi(s)$ over the total vesicle length are shown for the pears-up-2 vesicles for different values of reduced adhesion radii.

This branch has shapes similar to the pears-up-3 vesicles shown in Fig. 6.12, but the configuration profiles supported by the shapes of these two branches vary significantly. For example, let's consider the shapes at $r = 0.116$ for these two branches. The pears-up-2 vesicle can support a stronger accumulation of high curvature components at the north pole and a narrow neck in contrast to the pears-up-3 vesicle which supports a slightly wider upper end and a weaker accumulation of high curvature components in the circular domain at it's north pole. The boundary between the domains

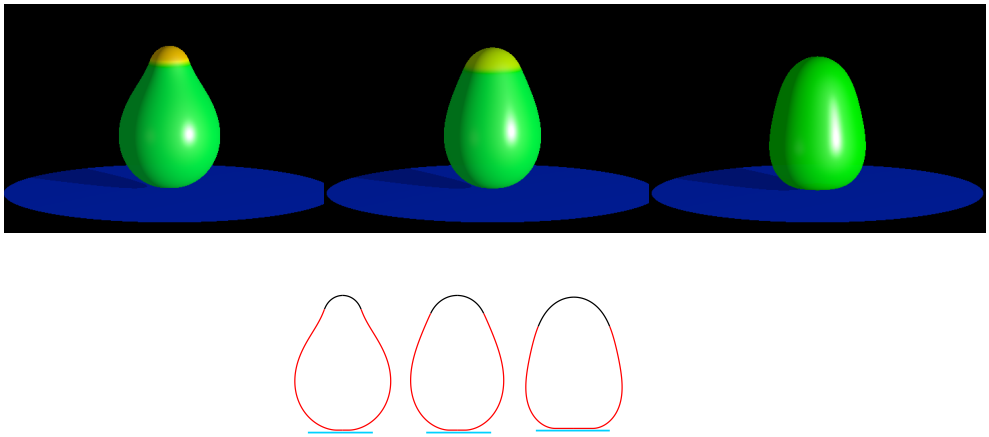

Figure 6.12: Shapes and 2D shape profiles of the pears-up-3 vesicles are shown for $r = 0.116, r = 0.15, r = 0.34$. The regions in the 2D profile marked by different colours correspond to the two domains separated by an interface.

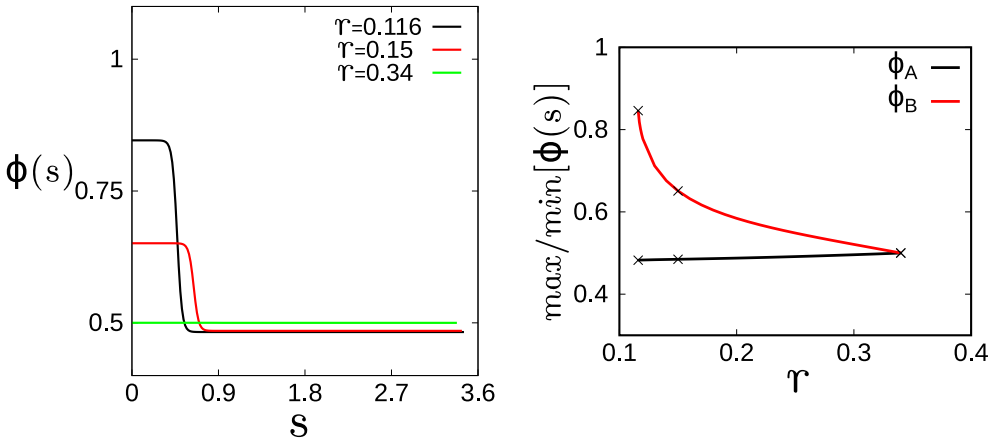

Figure 6.13: Local concentration profiles of component A, $\phi(s)$ over the total vesicle length for different values of reduced adhesion radii are shown on the left and the change in the upper and lower limits of $\phi(s)$ as a function of r is shown on the right for the pears-up-3 vesicles. The crosses correspond to the values of radii for which the vesicle shapes are shown.

is still narrow and well defined for pears-up-3 vesicle. As adhesion increases, the shape and the distribution of components change significantly and mixing of components is encouraged in the shapes corresponding to the pears-up-3 branch with a widening of it's upper end, which is in contrast to the shapes of the pears-up-2 branch. A mixed state is observed for the limiting structure at $r = 0.34$ of the pears-up-3 branch despite the shape asymmetry, and this can be confirmed from the concentration profile curve $\phi(s)$ in Fig. 6.13. The $max/min[\phi(s)]$ vs. r curves in Fig. 6.13 show the variation in the ϕ_B and ϕ_A values along the branch. There is a decay in the high curvature components from the domain rich in them, and this domain merges with the other domain to form a homogeneous one component system at the limiting structure. Our calculations thus suggest a possibility of a very interesting phenomenon where adhe-

sion can promote the complete mixing of components. This also makes pears-up-3 the only vesicles where due to a change in adhesion, the vesicle can go from a segregated state to a mixed state under adhesion. The energy difference (Fig. 6.2) between these two branches is very small and the vesicle can transition from the pears-up-2 branch to the pears-up-3 branch and vice versa with a discontinuous transition reflected in bending energy. The intersection point of these two branches at the adhesion radius $r = 0.118$ signifies two different shapes with different concentration profiles but having the same energy and thus an easy possibility of transition between them.

Prolate and pears-up-3 vesicles

We have shown the shapes of prolate branch in Fig. 6.14a and pears-up-3 branch in the Fig. 6.14b for comparison. The prolate branch starts as a mixed state at $r = 0$ which can be seen from Fig. 6.16, and then undergoes slight segregation under adhesion at the north pole with the rest of the vesicle still in a mixed state. The 2D shape profiles are shown in Fig. 6.15 where the transition between the shapes corresponding to the mixed and segregated distribution profile is marked. This segregation is not visible in the 3D prolate shapes but is clearly visible in the concentration profiles (Fig. 6.16). For $r = 0$, the vesicle has up-down symmetry and the distribution of the components is uniform. Breaking this up-down symmetry induces non-uniformity in the distribution of the components. This shows how sensitive the distribution of components can be, even to small changes in the shape. It is also interesting to note that at $r = 0.34$, the prolate and the pears-up-3 branches have similar overall shapes, but the difference in the concentration profiles and mean curvature at the north pole accounts for the large energy difference between them. This difference in mean curvature can be identified from Fig. 6.17.

We thus observe that the equally mixed configuration, which is only available for prolate-like shapes at $r = 0$ and $r = 0.01$ (of the prolate branch), can be stabilized under significant adhesion only at $r = 0.34$ (of the pears-up-3 branch). Thus for this reduced volume, v, there are only two configurations of a mixed state obtained under adhesion. Adhesion only weakly affects the distribution of components in the prolate vesicles, where an increase in adhesion promotes weak segregation, but leads to mixing in already segregated pears-up-3 vesicles.

Pears-up and pears down vesicles

Here we study vesicles composed of two approximately spherical parts of different sizes connected by a narrow neck. These vesicles have the lowest energy for small values of the adhesion radius, r, under the parameters that we have studied. We see

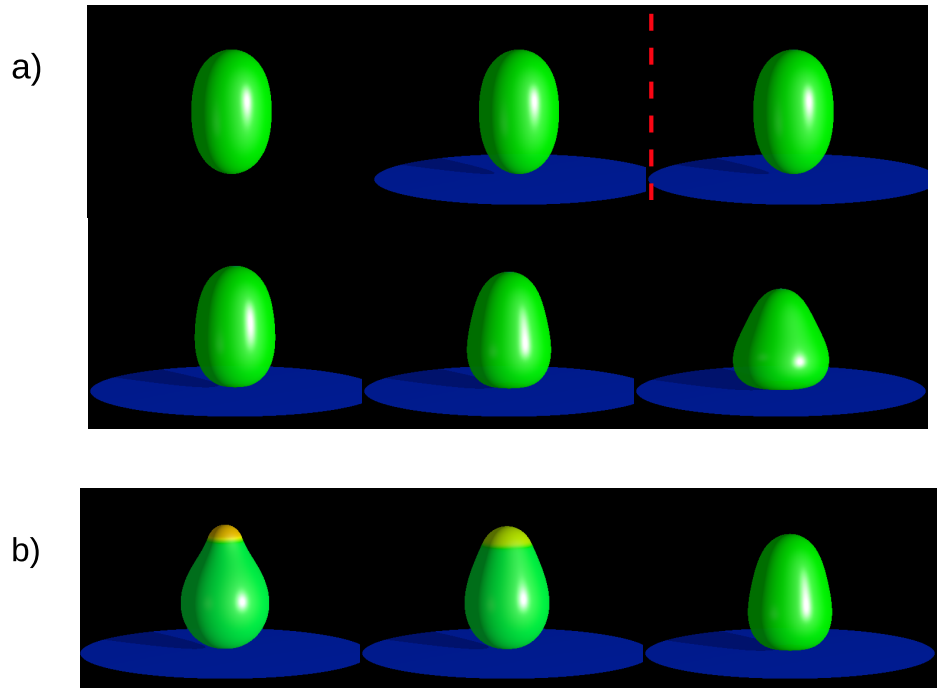

Figure 6.14: Row (a): Shapes of the prolate vesicles are shown for $r = 0, r = 0.01, r = 0.02, r = 0.20, r = 0.34, r = 0.53$. Row (b): Shapes of the pears-up-3 vesicles are shown for $r = 0.116, r = 0.15, r = 0.34$.

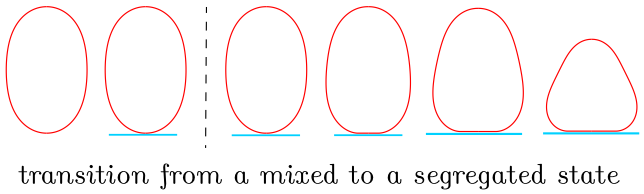

Figure 6.15: 2D shape profiles of the prolate vesicles are shown for $r = 0, r = 0.01, r = 0.02, r = 0.20, r = 0.34, r = 0.53$.

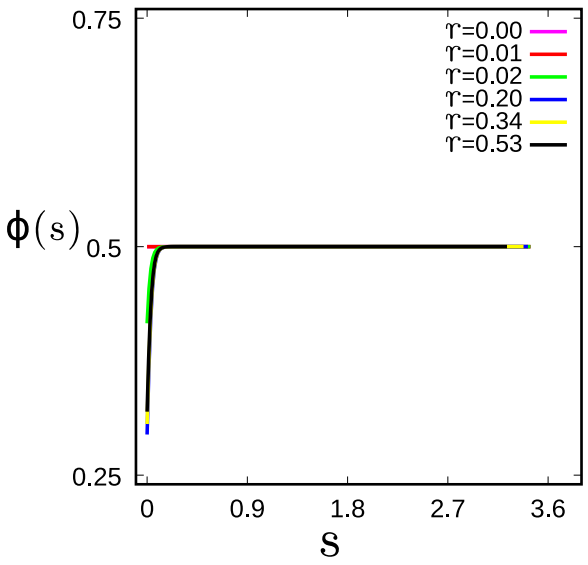

Figure 6.16: Local concentration profiles of component A, $\phi(s)$ over the total vesicle length are shown for the prolate vesicles for different values of reduced adhesion radii.

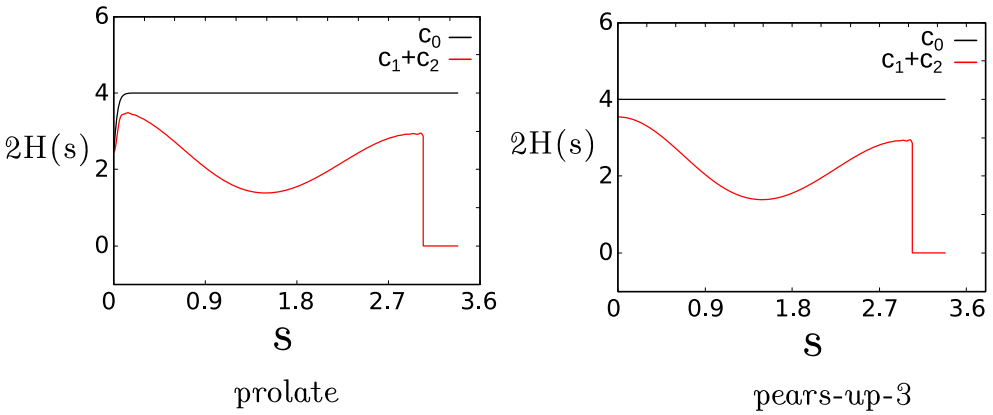

Figure 6.17: Overlay of $c_1 + c_2$ and c_0 profiles for prolate and pears-up-3 vesicles at $r = 0.34$.

that the component with the higher curvature is preferentially accumulated in the smaller spherical part of the vesicle and the components are uniformly distributed in both parts of the vesicle. The shapes and the 2D shape profiles of the pears branch with a larger bead and that of the pears branch with a smaller bead attached to the surface are shown in Fig. 6.18 and Fig. 6.20 respectively. Both these branches share the same origin in the bending energy diagram at $r = 0$. The pears-up branch exists for a reasonably large range up to $r = 0.44$ while the pears-down branch exists for a smaller range up to $r = 0.22$.

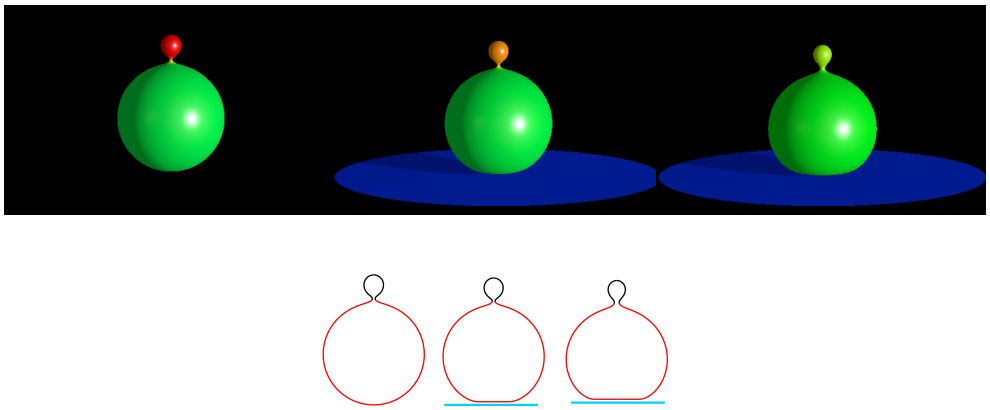

Figure 6.18: Shapes and 2D shape profiles for the pears-up vesicles are shown for $r = 0, r = 0.3, r = 0.44$. The regions in the 2D profile marked by different colours correspond to the two domains separated by an interface.

An already segregated pears-up shape at $r = 0$ undergoes mixing with an increase in adhesion as seen from the concentration profiles, $\phi(s)$ in the Fig. 6.19. Thus adhesion can overcome the segregation of components that can be encouraged by a shape change like budding as reported by ref. [56]. It is very interesting to note that adhesion can encourage mixing in a pears-up shape that has two different curvatures in it's two spheres. Interestingly, for these vesicles, the boundary between the high

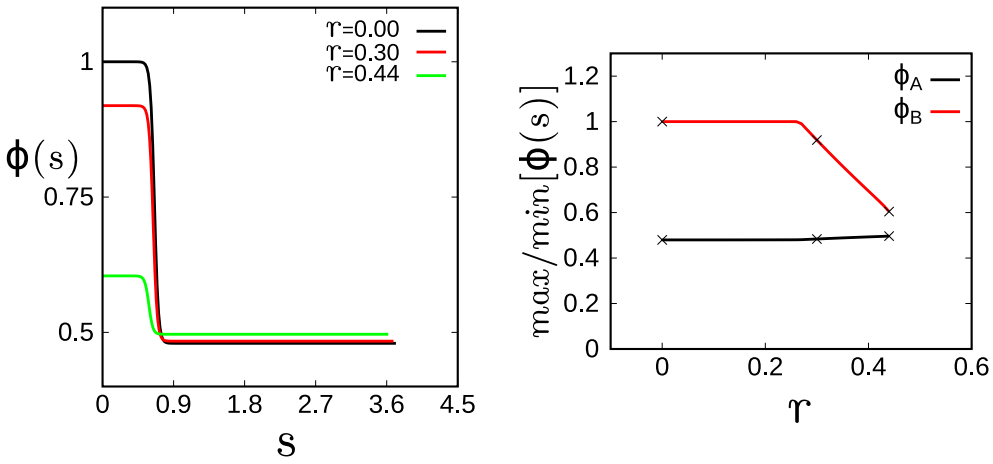

Figure 6.19: Local concentration profiles of component A, $\phi(s)$ over the total vesicle length for different values of reduced adhesion radii are shown on the left and the change in the upper and lower limits of concentration $\phi(s)$ as a function of r is shown on the right for the pears-up vesicles. The crosses correspond to the values of radii for which the vesicle shapes are shown.

and low concentration regions of the high curvature components is placed in the neck throughout the branch, and the concentration remains uniform in the two parts of the vesicle. Adhesion causes the smaller sphere to get smaller while the neck gets bigger. The change in the shape is however negligible for small adhesion radius, r. Initially, in the range of the adhesion radius, $0 \leq r \leq 0.26$, there is almost no change in the concentration profile. However, when the change of the shape due to the adhesion becomes sufficient, the concentration of the high curvature component in the smaller sphere decreases as seen in the $max/min[\phi(s)]$ vs. r curves of Fig. 6.19. This can be explained by the high mean curvature region formed at the rim of the adhered vesicle's surface. This causes the high spontaneous curvature components to move to the rim of the adhered vesicle from the small spherical part. With the increase in adhesion radius, this region of high mean curvature increases and attracts these high curvature components. In other words, we may suggest that an increase in adhesion likely promotes the migration of high spontaneous curvature components towards the base of the vesicle. Pears-up-2 are the only vesicle shapes which allow the high spontaneous curvature component to be present at the north pole of the vesicle with the increase in adhesion. However, this kind of vesicles are stable only up to small adhesion radius values.

Biologically, adhesion can be a useful mechanism to help the cell undergo mixing of components. This mechanism may be used by the cell to de-aggregate it's environment when a very high concentration of components can jam the cell and thereby make it unconducive to any chemical reactions [112].

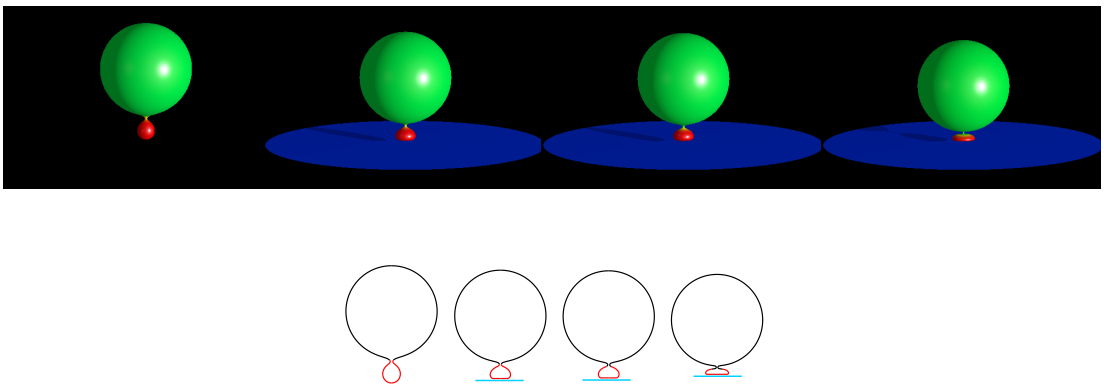

Figure 6.20: Shapes and 2D shape profiles for the pears-down vesicles are shown at $r = 0, r = 0.15, r = 0.16, r = 0.22$. The regions in the 2D profile marked by different colours correspond to the two domains separated by an interface.

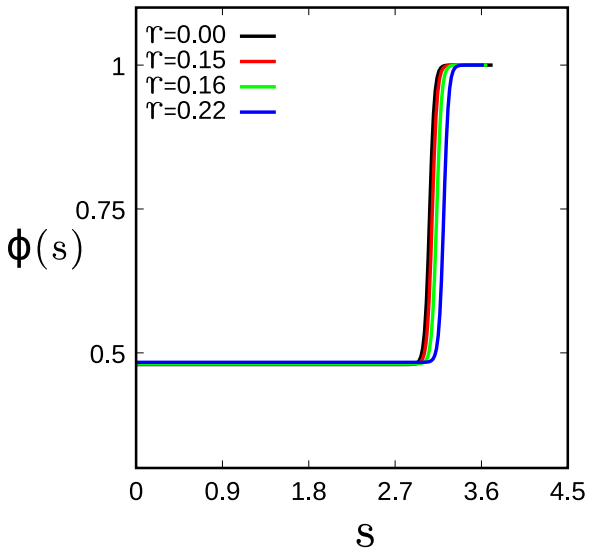

Figure 6.21: Local concentration profiles of component A, $\phi(s)$ over the total vesicle length are shown for the pears-down vesicles for different values of reduced adhesion radii.

The pears-down branch has the same origin as the pears-up branch at $r = 0$ in the bending energy diagram. Based on the shapes shown in Fig. 6.20, we can conclude that with the increase in adhesion, the components still prefer to be segregated. A negligible change is seen in the concentration profile of the components, and only the position of the boundary between the high and low concentration region of the high curvature components changes with the increase in adhesion, as seen from Fig. 6.21. We see that mainly the smaller spherical part of the vesicle attached to the surface changes it's shape. The larger upper spherical part separated by a narrow neck, remains unchanged, and the neck gets narrower when the radius of adhesion

increases. Such transformations result in an increase of energy. This is because the deformations lead to an increase in bending energy, and it's rise is not compensated by the adhesion energy since the size of the adhesion radius is constrained by the size of the smaller sphere attached to the substrate. It is also interesting to note that despite significant deformations in the small spherical part attached to the substrate, the distribution of components remains almost unchanged. These deformations cause the increase of the mean curvature at the rim of the adhered part of the vesicle and are restricted to a very small part of it. Thus, there isn't a sufficient driving force to induce the redistribution of the components due to adhesion. The concentration of the high curvature component at the substrate remains high for all values of the adhesion radius. Here, the increase in adhesion supports an overall segregation of components.

Thus, depending on whether a large or a small sphere is attached to the adhesion surface, the changes in the cell shape and the mixing/de-mixing mechanism are strongly dependent. The bending energy rise is rapid for the pears shape attached to the surface with a smaller spherical part as compared to the pears shape attached with the larger spherical part. The widening or narrowing of the neck can also be manipulated depending on whether a larger or a smaller spherical part of the vesicle is attached with the surface.

6.2 Summary and Conclusions

We may speculate that whenever a high curvature component is accumulated at the north pole of the vesicle, an increase in adhesion is likely to promote mixing and vice versa when the high curvature component is accumulated at the base of the vesicle, adhesion may likely promote segregation. Our calculations suggest that it may be likely to observe mixing of components in prolate-like shapes (including pears-up and pears-up-3) as compared to oblate-like shapes under adhesion. Interestingly, both budded (pears-up shapes) and non-budded (pears-up-3 shapes) shapes can encourage mixing of components, and non-budded oblate vesicles can encourage stronger segregation of components than the budded pears-like vesicles. We have shown that a vesicle with an initially segregated distribution of components can undergo mixing and vice versa with the increase in adhesion. It is interesting to observe such a complex behaviour for such a simple system at these parameter values.

In conclusion, we show that adhesion in particular can also promote the mixing of components in some, apart from the segregation of components in certain shapes. We have elucidated the close relationship between the shape and distribution of compo-

nents. Adhesion thus can be used as a tool to transition between different distributions of components with a change in shape. We hope these results can signify the role of adhesion as a mechanism for component redistribution in the cell systems.

Chapter 7

Summary and Conclusions

We have studied the adhesion of axisymmetric vesicles where the vesicle membrane is composed of either a single or two different kinds of membrane components. The vesicles were studied under the spontaneous curvature model. We focused on the shape transformations of vesicles caused by their adhesion to a flat surface. Different stable shapes of the adhered vesicles have been identified and the stability range of the different classes of vesicle shapes has been investigated. We have also investigated the coupling effect between the lateral distribution of membrane components and the shape of the adhered vesicles.

Main conclusions:

1) Shape transformations for different types of vesicles characterized by the reduced volume, v, and the reduced spontaneous curvature, c_0 have been investigated. It was found that adhesion can promote budding of vesicles, and that budding was more probable for vesicles with lower reduced volume than the vesicles with the larger reduced volume in their pinned adhesion state. In fact, the total energy calculations with fixed reduced adhesion strength, w as the parameter have shown that a very small change in adhesion strength can either induce or suppress budding without the change in spontaneous curvature.

2) It has been shown that there is a strong link between the local curvature of the adhered membrane surface and the ease of vesicle adhesion. Vesicles with the local curvature of the adhered membrane very close to the local curvature of the substrate can easily adhere to the substrate. Such a mechanism can be used for many biotechnological applications, for e.g., to collect nanoparticles just the way scavengers (leukocytes) do in our body.

3) It has been shown that the adhesion of concave oblate vesicles obtained at smaller reduced volumes is different than that of the convex oblate vesicles obtained for larger reduced volumes. Concave oblate vesicles can be easily stabilized for smaller adhesion strengths and large adhesion radii as they have more freedom to be deformed, whereas convex oblate vesicles are stabilized for larger adhesion strengths and smaller

adhesion radii as they have less freedom to be deformed.

4) The calculations done with the fixed reduced adhesion strength, w as a parameter have also shown that an increase in spontaneous curvature could enhance the adhesion of vesicles. The increase in the reduced spontaneous curvature, c_0 increases the stability range of adhered vesicles. The higher ease of adhesion can be related to a lower value of w_{min} (minimum adhesion strength required to obtain an adhered vesicle stable with respect to it's free state).

5) Oblate vesicles are found to be the most favoured and stable solutions for both zero and non-zero reduced spontaneous curvatures studied with the increase in adhesion strength – for the vesicles where the vesicle membrane is composed of a single kind of membrane component.

6) We have calculated the shapes and their corresponding distribution of components under adhesion. We have shown that adhesion can promote both mixing and lateral segregation of components depending on the shape of the adhered vesicle. The mixing and de-mixing of components can be induced by the change of adhesion radius. Non-budded structures like oblate vesicles were found to support segregation of components whereas budded structures like pears-up (pear structure attached to the surface with the larger sphere) vesicles could support mixing of components with the increase in adhesion radius. Complete mixing was observed for the limiting structure of the initially segregated pears-up-3 (pear-like vesicles with a wider upper end compared to pears-up-2 vesicles) branch under an increase in adhesion radius. This is the only vesicle shape to show complete mixing under significant adhesion.

7) It has been shown that an increase in adhesion radius is likely to promote migration of high curvature components towards the base of the vesicle – for the majority of shapes stabilized under the investigated set of parameters.

The additional conclusions of the thesis include:

1) New family of vesicle shapes called the "oblate-bead" (oblate-like vesicle attached to the surface with a spherical protrusion on it's free membrane part) shapes have been discovered for $v = 0.545$ and $c_0 = 0$. It is to be noted that a budded structure like oblate-bead could be stabilized under adhesion for zero spontaneous curvature which was not possible under free state at zero spontaneous curvature.

2) It was observed that a small change in reduced adhesion radius, r is necessary to change the distribution of components from the diffuse interface state of weak segregation to a sharp interface state corresponding to strong segregation. Thus, we may speculate that adhesion can be a mechanism by which cells can alternate between

strong and weak segregation in order to regulate the activation or de-activation of cell activities.

3) The complexity of the relation between the susceptibility to adhesion and the shape of the vesicle was found to depend upon the complexity of the vesicle shape. Even for simple shapes like oblates, it has been shown that the vesicles with larger reduced volumes are likely to have a high susceptibility to adhesion for small adhesion strengths, whereas, the vesicles with smaller reduced volumes (in comparison to the vesicles with larger reduced volumes) are likely to have a high susceptibility to adhesion at large adhesion strengths.

The results in the thesis elucidate the importance of cell adhesion as the mechanism responsible for cell shape transitions and various lateral distributions of components in cell membranes. Our results can be useful in biological scenarios, for e.g. in understanding the mechanism of cell/vesicle budding and transfer of membrane components between the daughter and the mother cell during such fission or fusion processes.

Appendix A

A.1 Gauss-Bonnet theorem

Gauss-Bonnet theorem [113,114] essentially connects the geometry of the surface (the curvature) to the topology (Euler characteristic) of the surface.

Let $R \subset S$ be a regular region of an oriented surface and let $C_1, ..., C_n$ be the piecewise regular curves that form the boundary ∂R of R. Then, let us suppose that each C_i is positively oriented and let $\theta_1, ..., \theta_p$ be the set of all external angles of the curves $C_1, ..., C_n$. Then we have,

$$\sum_{i=1}^{n} \int_{C_i} k_g(s) ds + \int \int_R K d\sigma + \sum_{i=1}^{p} \theta_i = 2\pi\chi(R) \tag{A.1.1}$$

where K is the Gaussian curvature, k_g is the geodesic curvature along the boundary curve C_i and $\chi(R)$ is the Euler characteristic of the surface. s is the arc-length of curve C_i.

Now, if the surface S is an orientable compact surface without a boundary, then we have,

$$\int \int_S K d\sigma = 2\pi\chi(S) \tag{A.1.2}$$

where, $\chi(S)$ is a topological invariant, which means as long as the topology does not change on deformation, the Euler characteristic of the surface remains constant. The above relation then suggests that even though the curvatures at individual points on the surface will change on deformation, but the total sum of all the Gaussian curvatures will remain constant under this deformation. The Euler characteristic becomes 2-2g for an orientable compact surface with no boundary, where 'g' is the genus or the measure of the number of holes of the surface.

Appendix B

B.1 Basics of differential geometry used to describe a surface

Biological surfaces have a very diverse molecular nature but at the first approximation, we can consider them to be homogeneous and smooth surfaces. We can therefore employ tools of differential geometry [94, 115, 116] to describe such smooth surfaces.

Let us consider an arbitrary point P on the surface and the position of this point with respect to the 3D Euclidean space is given by the position vector $\mathbf{r}(u, v)$ which is a function of the surface parameters u and v.

$$\mathbf{r}(u, v) = [x(u, v), y(u, v), z(u, v)] \tag{B.1.1}$$

The first and second order partial derivatives of the position vector $\mathbf{r}(u, v)$ along u and v,

$$\mathbf{r}_u = \partial\mathbf{r}/\partial u \tag{B.1.2}$$

$$\mathbf{r}_v = \partial\mathbf{r}/\partial v \tag{B.1.3}$$

$$\mathbf{r}_{uu} = \partial^2\mathbf{r}/\partial u^2 \tag{B.1.4}$$

$$\mathbf{r}_{vv} = \partial^2\mathbf{r}/\partial v^2 \tag{B.1.5}$$

$$\mathbf{r}_{uv} = \partial^2\mathbf{r}/\partial u\partial v \tag{B.1.6}$$

Then, the vector $d\mathbf{r}$ between two neighbouring points on the surface can be defined

as,

$$d\mathbf{r} = \mathbf{r}(u + du, v + dv) - \mathbf{r}(u, v) = \mathbf{r}_u du + \mathbf{r}_v dv \tag{B.1.7}$$

The length ds of this vector $d\mathbf{r}$ can now be calculated from,

$$I = ds^2 = d\mathbf{r} \cdot d\mathbf{r} = Edu^2 + 2Fdudv + Gdv^2 \tag{B.1.8}$$

where, $E = \mathbf{r}_u{}^2$, $F = \mathbf{r}_u \cdot \mathbf{r}_v$, $G = \mathbf{r}_v{}^2$.

The equation B.1.8 represents the first fundamental form which defines the surface metric. E, F and G represent the coefficients to this first fundamental form.

The length,

$$ds = \sqrt{(Edu^2 + 2Fdudv + Gdv^2)} = \sqrt{I} \tag{B.1.9}$$

Now, in order to define a curvature, let us again define the distance between two neighbouring points on the surface as,

$$d\mathbf{r} = \mathbf{r}(u + du, v + dv) - \mathbf{r}(u, v) = \mathbf{r}_u du + \mathbf{r}_v dv + \frac{1}{2}(\mathbf{r}_{uu} du^2 + 2\mathbf{r}_{uv} dudv + \mathbf{r}_{vv} dv^2) + ... \tag{B.1.10}$$

$$\mathbf{n} \cdot d\mathbf{r} = \frac{1}{2}(Ldu^2 + 2Mdudv + Ndv^2) \tag{B.1.11}$$

where, $L = \mathbf{n} \cdot \mathbf{r}_{uu}, M = \mathbf{n} \cdot \mathbf{r}_{uv}, N = \mathbf{n} \cdot \mathbf{r}_{vv}$.

Equation B.1.11 represents the second fundamental form which allows us to define the curvature of the surface at a point, and the coefficients L, M and N are the coefficients to this second fundamental form.

First, let us describe the curvature of a space curve at a given point s. We can introduce the following triple unit vectors as follows,

Tangent vector:

$$\mathbf{t}(s) = \frac{d\mathbf{r}(s)}{ds} \tag{B.1.12}$$

Main normal vector:

$$\mathbf{m}(s) = \frac{d^2\mathbf{r}(s)}{ds^2} \tag{B.1.13}$$

Bi-normal vector:

$$\mathbf{b}(s) = \mathbf{t}(s) \times \mathbf{m}(s) \tag{B.1.14}$$

These triple unit vectors constitute the Frenet frame at a point s on the space curve.

The curvature at a given point on the curve can then be described by the rate of

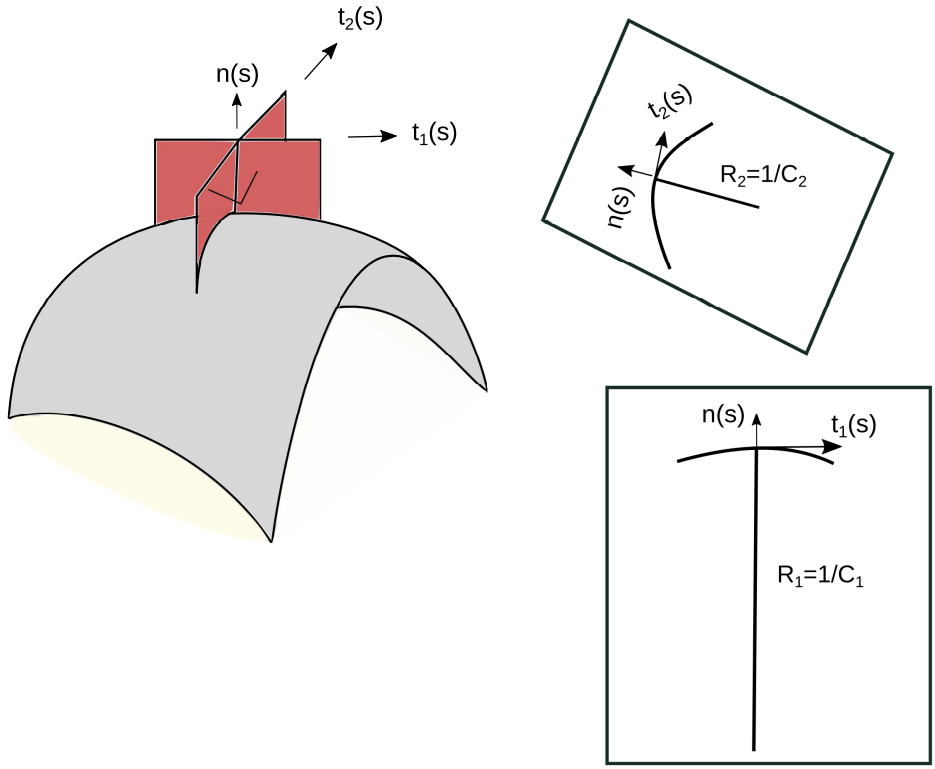

Figure B.1: The illustration of the principal curvatures C_1 and C_2 is shown at a given point s on the surface.

change of the tangent vector,

$$\mathbf{t}_s = \frac{d\mathbf{t}}{ds} = k(s)\mathbf{m} \tag{B.1.15}$$

and

$$\mathbf{t}(s) = \frac{d\mathbf{r}(s)}{ds} = \mathbf{r}_s \tag{B.1.16}$$

therefore we get,

$$\mathbf{t}_s = \frac{d^2\mathbf{r}(s)}{ds^2} = k(s)\mathbf{m} \tag{B.1.17}$$

where $k(s)$ is the curvature of the curve at a given point s.

Now, let the angle between the main normal $\mathbf{m}$ of the curve and the surface normal $\mathbf{n}$ be Θ.

We get,

$$\mathbf{n} \cdot \frac{d^2\mathbf{r}(s)}{ds^2} = k(s)\cos\Theta \tag{B.1.18}$$

but,

$$\mathbf{n} \cdot \frac{d^2\mathbf{r}(s)}{ds^2} = (\mathbf{n} \cdot \mathbf{r}_{uu})du^2 + 2(\mathbf{n} \cdot \mathbf{r}_{uv})dudv + (\mathbf{n} \cdot \mathbf{r}_{vv})dv^2 \tag{B.1.19}$$

therefore,

$$k_n(s) = k(s)\cos\Theta = \frac{Ldu^2 + 2Mdudv + Ndv^2}{Edu^2 + 2Fdudv + Gdv^2} \tag{B.1.20}$$

where, $k_n(s)$ is the normal curvature of the surface. The maximum and the minimum of the normal curvature correspond to the two principal curvatures C_1 and C_2 at each point on the surface.

The Mean curvature is defined as,

$$H = \frac{1}{2}(C_1 + C_2) \tag{B.1.21}$$

and the Gaussian curvature as,

$$K = C_1 C_2 \tag{B.1.22}$$

B.2 Derivation of the general form of bending energy

The general form [94, 117] of the bending energy is derived first and is then reduced to obtain the isotropic form of the bending energy in this section.

We have seen earlier that the isotropic form of bending energy (per unit area) describing isotropic thin films and membranes is given by,

$$F_b = \frac{\kappa}{2}(2H - C_0)^2 + \kappa_G K \tag{B.2.1}$$

where, $H = \frac{C_1+C_2}{2}$ is the mean curvature, C_0 is the spontaneous curvature, $K = C_1C_2$ is the Gaussian curvature, while κ and κ_G are the bending and Gaussian bending rigidities of the membrane respectively.

This expression of the isotropic bending energy can be generalized for the anisotropic membranes (using a continuum-mechanics approach) where the anisotropy may result from the tilt [79] or the in-plane orientational ordering [118] of the membrane components. We consider that in general, the 2D surface is anisotropic in two dimensions. This means that there is a possibility of two values of the principal curvatures and two values of the intrinsic (spontaneous) principal curvatures over the small area element dA. A lipid molecule is called anisotropic when the intrinsic principal curvatures are not identical, $C_{1m} \neq C_{2m}$. If, the principal curvatures C_1 and C_2 are equal to the intrinsic principal curvatures C_{1m} and C_{2m} and also if the orientations of the principal systems of the actual local membrane curvature tensor $\underline{C}$ and the intrinsic membrane curvature tensor $\underline{C}_m$ coincide, then the bending energy of that small area element becomes zero.

Thus, the elastic energy per unit area of a small area element dA of the thin plate can be defined as the mismatch between the intrinsic curvature of this surface element and it's actual local membrane curvature. In their respective principal systems, the curvature tensor matrices include only the diagonal elements.

$$\underline{C} = \begin{bmatrix} C_1 & 0 \\ 0 & C_2 \end{bmatrix} \tag{B.2.2}$$

$$\underline{C}_m = \begin{bmatrix} C_{1m} & 0 \\ 0 & C_{2m} \end{bmatrix} \tag{B.2.3}$$

In general, the principal systems of these two tensors ($\underline{C}_m$ and $\underline{C}$) make an angle ω with respect to each other in the tangent plane of the surface. This mismatch between the intrinsic membrane curvature and the actual local membrane curvature in the absence of any external forces can be represented by the tensor $\underline{M} = \underline{R}\underline{C}_m\underline{R}^{-1} - \underline{C}$, where

$$\underline{R} = \begin{bmatrix} \cos\omega & -\sin\omega \\ \sin\omega & \cos\omega \end{bmatrix} \tag{B.2.4}$$

is the rotation matrix.

Since the elastic energy per unit area (F_b) is a scalar quantity, i.e. it must be invariant with respect to all the transformations of the local coordinate system. We, therefore, consider only the invariants of the tensor $\underline{M}$ of the second order to define it.

Thus the elastic energy is represented as,

$$F_b = \frac{K_1}{2}(Tr\underline{M})^2 + K_2 Det\underline{M} \tag{B.2.5}$$

where K_1 and K_2 are the constants. On considering the equations from B.2.2 to B.2.5, the Eq. B.2.5 can be written as follows [119],

$$F_b = (2K_1 + K_2)(H - H_m)^2 - K_2(D^2 - 2DD_m\cos 2\omega + D_m^2) \tag{B.2.6}$$

where, $D = \frac{C_1 - C_2}{2}$ is the curvature deviator and it is the invariant of the curvature tensor ($D^2 = (Tr(\underline{C})/2)^2 - Det(\underline{C}) = H^2 - C_1C_2$), $D_m = (C_{1m} - C_{2m})/2$ is the intrinsic (spontaneous) curvature deviator and $H_m = (C_{1m} + C_{2m})/2$ is the intrinsic (spontaneous) mean curvature. H_m and D_m represent the anisotropic material properties of the membrane.

For the isotropic membranes (i.e. $D_m = 0$), the Eq. B.2.6 transforms (up to the constant terms independent of H and D) into the Helfrich expression as shown in Eq.

B.2.1, where $\kappa = K_1$ and $\kappa_G = K_2$ and

$$C_0 = (2K_1 + K_2)H_m/K_1 = (2\kappa + \kappa_G)H_m/\kappa \tag{B.2.7}$$

List of Publications

Publications related to the thesis:

[1] **J. Raval,** and W. T. Góźdź. Shape transformations of vesicles induced by their adhesion to flat surfaces. ACS omega, 5(26):16099-16105, 2020.

[2] **J. Raval,** A. Iglič, and W. T. Góźdź. Investigation of shape transformations of vesicles, induced by their adhesion to flat substrates characterized by different adhesion strength. International Journal of Molecular Sciences, 22(24):13406, 2021.

[3] **J. Raval,** A. Iglič, and W. T. Góźdź. Shape transformations of two-component vesicles, induced by their adhesion to flat surfaces.
(under preparation)

Other publications:

[1] N. Bibissidis, K. Betlem, G. Cordoyiannis, F. Prista-von Bonhorst, J. Goole, **J. Raval,** M. Daniel, W. T. Góźdź, A. Iglič and P. Losada-Pérez. Correlation between adhesion strength and phase behaviour in solid-supported lipid membranes. Journal of Molecular Liquids, 320:114492, 2020.

[2] **J. Raval,** E. Gongadze, M. Benčina, I. Junkar, N. Rawat, L. Mesarec, V. Kralj-Iglič, W. T. Góźdź, and A. Iglič. Mechanical and electrical interaction of biological membranes with nanoparticles and nanostructured surfaces. Membranes, 11(7):533, 2021.

Bibliography

[1] W. T. Góźdź, N. Bobrovska, and A. Ciach. Separation of components in lipid membranes induced by shape transformation. *The Journal of chemical physics*, 137(1):015101, 2012.

[2] U. Seifert and R. Lipowsky. Morphology of vesicles. *Handbook of biological physics*, 1:403–464, 1995.

[3] E. Sackmann, J. Käs, and J. Rädler. On shape transformations and shape fluctuations of cellular compartments and vesicles. *Physica Scripta*, 1993(T49A):111, 1993.

[4] G. M. Cooper. *The Cell: A Molecular Approach. 2nd edition.* Sinauer Associates, Sunderland (MA), 2000.

[5] T. P. Silverstein. The real reason why oil and water don't mix. *Journal of chemical education*, 75(1):116, 1998.

[6] D. Lombardo, M. A. Kiselev, S. Magazù, and P. Calandra. Amphiphiles self-assembly: basic concepts and future perspectives of supramolecular approaches. *Advances in Condensed Matter Physics*, 2015, 2015.

[7] M. Deserno. Fluid lipid membranes–a primer. *See http://www. cmu. edu/biolphys/deserno/pdf/membrane_ theory. pdf*, 2007.

[8] G. L. Mosley, C. D. Yamanishi, and D. T. Kamei. Mathematical modeling of vesicle drug delivery systems 1: vesicle formation and stability along with drug loading and release. *Journal of laboratory automation*, 18(1):34–45, 2013.

[9] J. N. Israelachvili, D. J. Mitchell, and B. W. Ninham. Theory of self-assembly of hydrocarbon amphiphiles into micelles and bilayers. *Journal of the Chemical Society, Faraday Transactions 2: Molecular and Chemical Physics*, 72:1525–1568, 1976.

[10] B. Alberts, A. Johnson, J. Lewis, and et al. *Molecular Biology of the Cell. 4th edition.* Garland Science, New York, 2002.

[11] A. Iglič, H. Hägerstrand, M. Bobrowska-Hägerstrand, V. Arrigler, and V. Kralj-Iglič. Possible role of phospholipid nanotubes in directed transport of membrane vesicles. *Physics Letters A*, 310(5-6):493–497, 2003.

[12] P. Chugh. Cells: why shape matters. *Science in School*, 46:8–13, 2019.

[13] O. M. Lancaster, M. Le Berre, A. Dimitracopoulos, D. Bonazzi, E. Zlotek-Zlotkiewicz, R. Picone, T. Duke, M. Piel, and B. Baum. Mitotic rounding alters cell geometry to ensure efficient bipolar spindle formation. *Developmental cell*, 25(3):270–283, 2013.

[14] O. Otto, P. Rosendahl, A. Mietke, S. Golfier, C. Herold, D. Klaue, S. Girardo, S. Pagliara, A. Ekpenyong, A. Jacobi, et al. Real-time deformability cytometry: on-the-fly cell mechanical phenotyping. *Nature methods*, 12(3):199–202, 2015.

[15] J. Käs and E. Sackmann. Shape transitions and shape stability of giant phospholipid vesicles in pure water induced by area-to-volume changes. *Biophysical journal*, 60(4):825–844, 1991.

[16] U. Seifert. Configurations of fluid membranes and vesicles. *Advances in physics*, 46(1):13–137, 1997.

[17] R. Lipowsky. Remodeling of membrane compartments: some consequences of membrane fluidity. *Biological chemistry*, 395(3):253–274, 2014.

[18] O. G. Mouritsen. The liquid-ordered state comes of age. *Biochimica et Biophysica Acta (BBA)-Biomembranes*, 1798(7):1286–1288, 2010.

[19] M. Cebecauer, M. Amaro, P. Jurkiewicz, M. J. Sarmento, R. Sachl, L. Cwiklik, and M. Hof. Membrane lipid nanodomains. *Chemical reviews*, 118(23):11259–11297, 2018.

[20] S. Komura and D. Andelman. Physical aspects of heterogeneities in multi-component lipid membranes. *Advances in colloid and interface science*, 208:34–46, 2014.

[21] D. Needham, T. J. McIntosh, and E. Evans. Thermomechanical and transition properties of dimyristoylphosphatidylcholine/cholesterol bilayers. *Biochemistry*, 27(13):4668–4673, 1988.

[22] U. Seifert. Fluid membranes – theory of vesicle conformations. *Habilitation theses Ludwig-Maximilians-Universitäat Müunchen*, 1994.

[23] Membrane Phase Transitions. *https://phys.libretexts.org/@go/page/1352*, mar 28 2021. Online.

[24] L. Mesarec, W. Góźdź, A. Iglič, V. Kralj-Iglič, E. G. Virga, and S. Kralj. Normal red blood cells' shape stabilized by membrane's in-plane ordering. *Scientific reports*, 9(1):1–11, 2019.

[25] S. Svetina and B. Žekš. Shape behavior of lipid vesicles as the basis of some cellular processes. *The Anatomical Record: An Official Publication of the American Association of Anatomists*, 268(3):215–225, 2002.

[26] B. Mavcic, B. Babnik, A. Iglic, M. Kanduser, T. Slivnik, and V. Kralj-Iglic. Shape transformation of giant phospholipid vesicles at high concentrations of c12e8. *Bioelectrochemistry*, 63(1):183–188, 2004.

[27] M. Drab, Ž. Pandur, S. Penič, A. Iglič, V. Kralj-Iglič, and D. Stopar. A monte carlo study of giant vesicle morphologies in nonequilibrium environments. *Biophysical Journal*, 120(20):4418–4428, 2021.

[28] W. Wintz, H. G. Döbereiner, and U. Seifert. Starfish vesicles. *EPL (Europhysics Letters)*, 33(5):403, 1996.

[29] A. Iglič, V. Kralj-Iglič, and J. Majhenc. Cylindrical shapes of closed lipid bilayer structures correspond to an extreme area difference between the two monolayers of the bilayer. *Journal of biomechanics*, 32(12):1343–1347, 1999.

[30] E. Farge and P. F. Devaux. Shape changes of giant liposomes induced by an asymmetric transmembrane distribution of phospholipids. *Biophysical journal*, 61(2):347–357, 1992.

[31] V. Kralj-Iglic. Stability of membranous nanostructures: a possible key mechanism in cancer progression. *International journal of nanomedicine*, 7:3579, 2012.

[32] L. A. Lasky, M. S. Singer, D. Dowbenko, Y. Imai, W. J. Henzel, C. Grimley, C. Fennie, N. Gillett, S. R. Watson, and S. D. Rosent. An endothelial ligand for l-selectin is a novel mucin-like molecule. *Cell*, 69(6):927–938, 1992.

[33] S. Huang and D. E. Ingber. The structural and mechanical complexity of cell-growth control. *Nature cell biology*, 1(5):E131–E138, 1999.

[34] H. Perinpanayagam, R. Zaharias, C. Stanford, R. Brand, J. Keller, and G. Schneider. Early cell adhesion events differ between osteoporotic and non-osteoporotic osteoblasts. *Journal of orthopaedic research*, 19(6):993–1000, 2001.

[35] C. N. Serhan and J. Savill. Resolution of inflammation: the beginning programs the end. *Nature immunology*, 6(12):1191–1197, 2005.

[36] A. A. Khalili and M. R. Ahmad. A review of cell adhesion studies for biomedical and biological applications. *International journal of molecular sciences*, 16(8):18149–18184, 2015.

[37] E. Paluch and C-P. Heisenberg. Biology and physics of cell shape changes in development. *Current Biology*, 19(17):R790–R799, 2009.

[38] E. A. Evans. Analysis of adhesion of large vesicles to surfaces. *Biophysical journal*, 31(3):425–431, 1980.

[39] U. Seifert and R. Lipowsky. Adhesion of vesicles. *Physical Review A*, 42(8):4768, 1990.

[40] A-S. Smith and U. Seifert. Vesicles as a model for controlled (de-) adhesion of cells: a thermodynamic approach. *Soft Matter*, 3(3):275–289, 2007.

[41] R. Lipowsky and U. Seifert. Adhesion of membranes: a theoretical perspective. *Langmuir*, 7(9):1867–1873, 1991.

[42] R. Lipowsky and U. Seifert. Adhesion of vesicles and membranes. *Molecular crystals and liquid crystals*, 202(1):17–25, 1991.

[43] S. Dasgupta, T. Auth, and G. Gompper. Wrapping of ellipsoidal nano-particles by fluid membranes. *Soft Matter*, 9(22):5473–5482, 2013.

[44] S. Cao, G. Wei, and J. Z. Y. Chen. Transformation of an oblate-shaped vesicle induced by an adhering spherical particle. *Physical Review E*, 84(5):050901, 2011.

[45] X. Yi and H. Gao. Budding of an adhesive elastic particle out of a lipid vesicle. *ACS Biomaterials Science & Engineering*, 3(11):2954–2961, 2017.

[46] T. Yue, Y. Xu, M. Sun, X. Zhang, and F. Huang. How tubular aggregates interact with biomembranes: wrapping, fusion and pearling. *Physical Chemistry Chemical Physics*, 18(2):1082–1091, 2016.

[47] M. Deserno and W. M. Gelbart. Adhesion and wrapping in colloid- vesicle complexes. *The Journal of Physical Chemistry B*, 106(21):5543–5552, 2002.

[48] J. Agudo-Canalejo and R. Lipowsky. Critical particle sizes for the engulfment of nanoparticles by membranes and vesicles with bilayer asymmetry. *ACS nano*, 9(4):3704–3720, 2015.

[49] W. T. Góźdź. Deformations of lipid vesicles induced by attached spherical particles. *Langmuir*, 23(10):5665–5669, 2007.

[50] K. A. Smith, D. Jasnow, and A. C. Balazs. Designing synthetic vesicles that engulf nanoscopic particles. *The Journal of chemical physics*, 127(8):08B612, 2007.

[51] M. Deserno. Elastic deformation of a fluid membrane upon colloid binding. *Physical Review E*, 69(3):031903, 2004.

[52] J. Agudo-Canalejo and R. Lipowsky. Stabilization of membrane necks by adhesive particles, substrate surfaces, and constriction forces. *Soft Matter*, 12(39):8155–8166, 2016.

[53] Z. Wu and X. Yi. Structures and mechanical behaviors of soft nanotubes confining adhesive single or multiple elastic nanoparticles. *Journal of the Mechanics and Physics of Solids*, 137:103867, 2020.

[54] Y. Zhao, S. Das, and Q. Du. Adhesion of multicomponent vesicle membranes. *Physical Review E*, 81(4):041919, 2010.

[55] T. R. Weikl and R. Lipowsky. Adhesion-induced phase behavior of multicomponent membranes. *Physical Review E*, 64(1):011903, 2001.

[56] U. Seifert. Curvature-induced lateral phase segregation in two-component vesicles. *Physical review letters*, 70(9):1335, 1993.

[57] K. Simons and E. Ikonen. Functional rafts in cell membranes. *nature*, 387(6633):569–572, 1997.

[58] E. Ikonen. Roles of lipid rafts in membrane transport. *Current opinion in cell biology*, 13(4):470–477, 2001.

[59] D. L. Parton, J. W. Klingelhoefer, and M. S. P. Sansom. Aggregation of model membrane proteins, modulated by hydrophobic mismatch, membrane curvature, and protein class. *Biophysical journal*, 101(3):691–699, 2011.

[60] K. A. Burke, E. A. Yates, and J. Legleiter. Biophysical insights into how surfaces, including lipid membranes, modulate protein aggregation related to neurodegeneration. *Frontiers in neurology*, 4:17, 2013.

[61] H. T. McMahon and J. L. Gallop. Membrane curvature and mechanisms of dynamic cell membrane remodelling. *Nature*, 438(7068):590–596, 2005.

[62] W. Helfrich. Elastic properties of lipid bilayers: theory and possible experiments. *Zeitschrift für Naturforschung C*, 28(11-12):693–703, 1973.

[63] T. Baumgart, S. T. Hess, and W. W. Webb. Imaging coexisting fluid domains in biomembrane models coupling curvature and line tension. *Nature*, 425(6960):821–824, 2003.

[64] T. Baumgart, S. Das, W. W. Webb, and J. T. Jenkins. Membrane elasticity in giant vesicles with fluid phase coexistence. *Biophysical journal*, 89(2):1067–1080, 2005.

[65] W. T. Góźdź. The interface width of separated two-component lipid membranes. *The Journal of Physical Chemistry B*, 110(43):21981–21986, 2006.

[66] B. J. Peter, H. M. Kent, I. G. Mills, Y. Vallis, P. J. G. Butler, P. R. Evans, and H. T. McMahon. Bar domains as sensors of membrane curvature: the amphiphysin bar structure. *Science*, 303(5657):495–499, 2004.

[67] A. Roux, D. Cuvelier, P. Nassoy, J. Prost, P. Bassereau, and B. Goud. Role of curvature and phase transition in lipid sorting and fission of membrane tubules. *The EMBO journal*, 24(8):1537–1545, 2005.

[68] M. C. Heinrich, B. R. Capraro, A. Tian, J. M. Isas, R. Langen, and T. Baumgart. Quantifying membrane curvature generation of drosophila amphiphysin n-bar domains. *The journal of physical chemistry letters*, 1(23):3401–3406, 2010.

[69] A. Callan-Jones, B. Sorre, and P. Bassereau. Curvature-driven lipid sorting in biomembranes. *Cold Spring Harbor perspectives in biology*, 3(2):a004648, 2011.

[70] S. Katz and S. Givli. Curvature-induced spatial ordering of composition in lipid membranes. *Computational and mathematical methods in medicine*, 2017, 2017.

[71] R. Parthasarathy, C-H. Yu, and J. T. Groves. Curvature-modulated phase separation in lipid bilayer membranes. *Langmuir*, 22(11):5095–5099, 2006.

[72] R. P. Rand and A. C. Burton. Mechanical properties of the red cell membrane: I. membrane stiffness and intracellular pressure. *Biophysical journal*, 4(2):115–135, 1964.

[73] Y. C. Fung. Theoretical considerations of the elasticity of red cells and small blood vessels. *Federation Proceedings*, 25(6):1761–1772, 1966.

[74] E. A. Evans. Bending resistance and chemically induced moments in membrane bilayers. *Biophysical journal*, 14(12):923–931, 1974.

[75] L. D. Landau and E. M. Lifshitz. *Theory of Elasticity. Vol. 7*. Pergamon press, Oxford (England), 1959 (1st ed.), 1970 (2nd ed.).

[76] P. B. Canham. The minimum energy of bending as a possible explanation of the biconcave shape of the human red blood cell. *Journal of theoretical biology*, 26(1):61–81, 1970.

[77] A. Iglič. A possible mechanism determining the stability of spiculated red blood cells. *Journal of biomechanics*, 30(1):35–40, 1997.

[78] M. Fošnarič, A. Iglič, and S. May. Influence of rigid inclusions on the bending elasticity of a lipid membrane. *Physical review E*, 74(5):051503, 2006.

[79] W. Helfrich and J. Prost. Intrinsic bending force in anisotropic membranes made of chiral molecules. *Physical Review A*, 38(6):3065, 1988.

[80] H. J. Deuling and W. Helfrich. The curvature elasticity of fluid membranes: a catalogue of vesicle shapes. *Journal de Physique*, 37(11):1335–1345, 1976.

[81] L. Miao, U. Seifert, M. Wortis, and H-G Döbereiner. Budding transitions of fluid-bilayer vesicles: the effect of area-difference elasticity. *Physical Review E*, 49(6):5389, 1994.

[82] E. A. Evans and Skalak R. *Mechanics and thermodynamics of biomembranes*. CRC press, Boca Raton, 1980.

[83] B. T. Stokke, A. Mikkelsen, and A. Elgsaeter. The human erythrocyte membrane skeleton may be an ionic gel. *European Biophysics Journal*, 13(4):203–218, 1986.

[84] W. Helfrich. Blocked lipid exchange in bilayers and its possible influence on the shape of vesicles. *Zeitschrift für Naturforschung C*, 29(9-10):510–515, 1974.

[85] E. A. Evans. Minimum energy analysis of membrane deformation applied to pipet aspiration and surface adhesion of red blood cells. *Biophysical journal*, 30(2):265–284, 1980.

[86] M. P. Sheetz and S. J. Singer. Biological membranes as bilayer couples. a molecular mechanism of drug-erythrocyte interactions. *Proceedings of the National Academy of Sciences*, 71(11):4457–4461, 1974.

[87] S. Svetina, A. Ottova-Leitmannová, and R. Glaser. Membrane bending energy in relation to bilayer couples concept of red blood cell shape transformations. *Journal of theoretical biology*, 94(1):13–23, 1982.

[88] R. M. Raphael and R. E. Waugh. Accelerated interleaflet transport of phosphatidylcholine molecules in membranes under deformation. *Biophysical Journal*, 71(3):1374–1388, 1996.

[89] J. Urbanija, B. Babnik, M. Frank, N. Tomšič, B. Rozman, V. Kralj-Iglič, and A. Iglič. Attachment of β 2-glycoprotein i to negatively charged liposomes may prevent the release of daughter vesicles from the parent membrane. *European Biophysics Journal*, 37(7):1085–1095, 2008.

[90] V. Kralj-Iglič, A. Iglič, H. Hägerstrand, and P. Peterlin. Stable tubular microexovesicles of the erythrocyte membrane induced by dimeric amphiphiles. *Physical Review E*, 61(4):4230, 2000.

[91] L. Miao, B. Fourcade, M. Rao, M. Wortis, and R. Zia. Equilibrium budding and vesiculation in the curvature model of fluid lipid vesicles. *Physical Review A*, 43(12):6843, 1991.

[92] U. Seifert, K. Berndl, and R. Lipowsky. Shape transformations of vesicles: Phase diagram for spontaneous-curvature and bilayer-coupling models. *Physical review A*, 44(2):1182, 1991.

[93] R. Mukhopadhyay, H. W. G. Lim, and M. Wortis. Echinocyte shapes: bending, stretching, and shear determine spicule shape and spacing. *Biophysical Journal*, 82(4):1756–1772, 2002.

[94] A. Iglič, D. Drobne, and V. Kralj-Iglic. *Nanostructures in biological systems: theory and applications*. CRC Press, 2015.

[95] W. C. Hwang and R. E. Waugh. Energy of dissociation of lipid bilayer from the membrane skeleton of red blood cells. *Biophysical journal*, 72(6):2669–2678, 1997.

[96] W. T. Góźdź. Influence of spontaneous curvature and microtubules on the conformations of lipid vesicles. *The Journal of Physical Chemistry B*, 109(44):21145–21149, 2005.

[97] J. Stoker. Differential geometry. volume XX of *Pure and Applied Mathematics*. Wiley, New York, 1969.

[98] W. T. Góźdź. Spontaneous curvature induced shape transformations of tubular polymersomes. *Langmuir*, 20(18):7385–7391, 2004.

[99] R. Lipowsky. Understanding giant vesicles: a theoretical perspective. In *The Giant Vesicle Book*, pages 73–168. CRC Press, 2019.

[100] G. I. Bell, M. Dembo, and P. Bongrand. Cell adhesion. competition between nonspecific repulsion and specific bonding. *Biophysical Journal*, 45:1051–1064, 1984.

[101] F. Brochard-Wyart and P. G. de Gennes. Adhesion induced by mobile binders: Dynamics. *Proceedings of the National Academy of Sciences*, 99(12):7854–7859, 2002.

[102] J. Steinkühler, J. Agudo-Canalejo, R. Lipowsky, and R. Dimova. Modulating vesicle adhesion by electric fields. *Biophysical journal*, 111(7):1454–1464, 2016.

[103] P. S. Swain and D. Andelman. The influence of substrate structure on membrane adhesion. *Langmuir*, 15(26):8902–8914, 1999.

[104] T. R. Weikl, M. Asfaw, H. Krobath, B. Różycki, and R. Lipowsky. Adhesion of membranes via receptor–ligand complexes: Domain formation, binding cooperativity, and active processes. *Soft Matter*, 5:3213–3224, 2009.

[105] J-Q. Lv, P-C. Chen, W. T. Góźdź, and Li. B. Mechanical adaptions of collective cells nearby free tissue boundaries. *Journal of Biomechanics*, 104:109763, 2020.

[106] J. Raval, E. Gongadze, M. Benčina, I. Junkar, N. Rawat, L. Mesarec, V. Kralj-Iglič, W. T. Góźdź, and A. Iglič. Mechanical and electrical interaction of biological membranes with nanoparticles and nanostructured surfaces. *Membranes*, 11(7), 2021.

[107] M. Benčina, N. Rawat, K. Lakota, S. Sodin-Šemrl, A. Iglič, and I. Junkar. Bioperformance of hydrothermally and plasma-treated titanium: The new generation of vascular stents. *International Journal of Molecular Sciences*, 22(21), 2021.

[108] T. Rouhiparkouhi, T. R. Weikl, D. E. Discher, and R. Lipowsky. Adhesion-induced phase behavior of two-component membranes and vesicles. *International journal of molecular sciences*, 14(1):2203–2229, 2013.

[109] A. Hategan, R. Law, S. Kahn, and D. E. Discher. Adhesively-tensed cell membranes: lysis kinetics and atomic force microscopy probing. *Biophysical journal*, 85(4):2746–2759, 2003.

[110] A. Hategan, K. Sengupta, S. Kahn, E. Sackmann, and D. E. Discher. Topographical pattern dynamics in passive adhesion of cell membranes. *Biophysical Journal*, 87(5):3547–3560, 2004.

[111] J. Raval, A. Iglič, and W. T. Góźdź. Investigation of shape transformations of vesicles, induced by their adhesion to flat substrates characterized by different adhesion strength. *International Journal of Molecular Sciences*, 22(24):13406, 2021.

[112] A. A. Hyman, C. A. Weber, and F. Jülicher. Liquid-liquid phase separation in biology. *Annual review of cell and developmental biology*, 30:39–58, 2014.

[113] K. Butt. The gauss-bonnet theorem. 2015.

[114] M. P. do Carmo. *Differential geometry of curves and surfaces: revised and updated second edition*. Courier Dover Publications, 2016.

[115] M. Voinova. Geometrical methods in the theory of lipid membranes' and cells' shapes. lectures 1-2. introduction to the differential geometry of surface.

[116] M. Deserno. Notes on differential geometry, 2004.

[117] A. Iglič, B. Babnik, U. Gimsa, and V. Kralj-Iglič. On the role of membrane anisotropy in the beading transition of undulated tubular membrane structures. *Journal of Physics A: Mathematical and General*, 38(40):8527, 2005.

[118] R. Oda, I. Huc, M. Schmutz, S. J. Candau, and F. C. MacKintosh. Tuning bilayer twist using chiral counterions. *Nature*, 399(6736):566–569, 1999.

[119] A. Iglič, M. Tzaphlidou, M. Remškar, B. Babnik, M. Daniel, and V. Kralj-Iglič. Stable shapes of thin anisotropic nano-strips. *Fullerenes, Nanotubes, and Carbon Nonstructures*, 13(3):183–192, 2005.